# Geophysical Analysis of the Salmon Peak Formation Near Amistad Reservoir Dam, Val Verde County, Texas, and Coahuila, Mexico, March 2006, to Aid in Piezometer Placement

By Gregory P. Stanton, Wade H. Kress, Andrew P. Teeple, Michael L. Greenslate, and Allan K. Clark

In cooperation with the U.S. Section, International Boundary and Water Commission

Scientific Investigations Report 2007–5143

**U.S. Department of the Interior**
**U.S. Geological Survey**

**U.S. Department of the Interior**
DIRK KEMPTHORNE, Secretary

**U.S. Geological Survey**
Mark D. Myers, Director

U.S. Geological Survey, Reston, Virginia: 2007

For product and ordering information:
World Wide Web: http://www.usgs.gov/pubprod
Telephone: 1-888-ASK-USGS

For more information on the USGS—the Federal source for science about the Earth, its natural and living resources, natural hazards, and the environment:
World Wide Web: http://www.usgs.gov
Telephone: 1-888-ASK-USGS



Suggested citation:
Stanton, G.P., Kress, W.H., Teeple, A.P., Greenslate, M.L., and Clark, A.K., 2007, Geophysical analysis of the Salmon Peak Formation near Amistad Reservoir dam, Val Verde County, Texas, and Coahuila, Mexico, March 2006, to aid in piezometer placement: U.S. Geological Survey Scientific Investigations Report 2007–5143, 70 p.

# Contents

## Figures

## Tables

# Conversion Factors and Datums

## SI to Inch/Pound

| Multiply | By | To obtain |
|---|---|---|
| | Length | |
| centimeter (cm) | 0.3937 | inch (in.) |
| millimeter (mm) | 0.03937 | inch (in.) |
| meter (m) | 3.281 | foot (ft) |
| kilometer (km) | 0.6214 | mile (mi) |
| | Area | |
| hectare (ha) | 2.471 | acre |
| square kilometer ($km^2$) | 0.3861 | square mile ($mi^2$) |
| | Volume | |
| cubic meter ($m^3$) | 264.2 | gallon (gal) |
| | Flow rate | |
| liter per second (L/s) | 15.85 | gallon per minute (gal/min) |

## Inch/Pound to SI

| Multiply | By | To obtain |
|---|---|---|
| | Length | |
| foot (ft) | 0.3048 | meter (m) |
| inch (in.) | 2.54 | centimeter (cm) |
| inch (in.) | 25.4 | millimeter (mm) |
| | Flow rate | |
| gallon per minute (gal/min) | 0.06309 | liter per second (L/s) |

Temperature in degrees Celsius (°C) may be converted to degrees Fahrenheit (°F) as follows:

°F=(1.8×°C)+32

Temperature in degrees Fahrenheit (°F) may be converted to degrees Celsius (°C) as follows:

°C=(°F-32)/1.8

Specific conductance is given in microsiemens per centimeter at 25 degrees Celsius (µS/cm at 25 °C).

Concentrations of chemical constituents in water are given either in milligrams per liter (mg/L) or micrograms per liter (µg/L).

## Datums

Vertical coordinate information is referenced to North American Vertical Datum of 1988 (NAVD 88).

Horizontal coordinate information is referenced to North American Datum of 1983 (NAD 83).

Altitude, as used in this report, refers to distance above the vertical datum.

# Geophysical Analysis of the Salmon Peak Formation Near Amistad Reservoir Dam, Val Verde County, Texas, and Coahuila, Mexico, March 2006, to Aid in Piezometer Placement

By Gregory P. Stanton, Wade H. Kress, Andrew P. Teeple, Michael L. Greenslate, and Allan K. Clark

## Abstract

Since 1992, numerous sinkholes have developed northwest of the Amistad Reservoir dam on the Rio Grande. Increases in the discharge of springs south of the dam, on the western side of the Rio Grande, in Coahuila, Mexico, have been documented. In 1995 the Mexico Section of the International Boundary and Water Commission (IBWC) completed a study of the western embankment (Coahuila, Mexico) of the dam that included surface geophysics, borehole geophysics, and installation of piezometers to learn more about subsurface conditions. As part of a 5-year safety inspection in 2005, technical advisors recommended that one line of similarly constructed piezometers be installed on the eastern embankment (Val Verde County, Texas) of the dam for comparison of water levels (potentiometric head) on both the western and eastern embankments of Amistad Reservoir dam. To provide technical assistance for the horizontal and vertical placement of piezometers on the eastern embankment of Amistad Reservoir dam, the U.S. Geological Survey, in cooperation with the U.S. Section of the IBWC, conducted a study along both the western and eastern embankments of Amistad Reservoir dam. The study involved an integrated approach using surface and borehole geophysical methods. In the western embankment investigation, geological and geophysical characteristics that indicate relatively large water-yielding properties of the Salmon Peak Formation were identified. The direct-current (DC) resistivity method was selected as the surface geophysical reconnaissance technique to correlate relatively large water-yielding properties of the Salmon Peak Formation, identified from analysis of borehole geophysical logs, with variations in subsurface resistivity. The dipole-dipole array and the reciprocal Schlumberger array were selected as the most applicable DC resistivity arrays. Two resistivity units were identified in both the dipole-dipole array data and the reciprocal Schlumberger array data along DC resistivity profiles on both embankments. Resistivity unit 1 generally is of relatively low resistivity, ranging from 45 to 150 ohm-meters compared with resistivity unit 2, which ranges from 120 to 345 ohm-meters (depending on the DC array type). The presence of mapped sinkholes in the reservoir north of the western embankment study area and the zone of increased water content (as indicated by zones of low neutron log count rates in nearby piezometers) leads to the conclusion that resistivity unit 1 is a preferential flow path where surface water from Amistad Reservoir is forced into the ground-water system (because of increased head from the reservoir). In the eastern embankment investigation, trends in the spatial distribution of sinkholes and the occurrence of weathered zones were identified from geologic descriptions of cores. The correlation of surface geophysical DC resistivity, historical lithologic data, and general trend of documented sinkholes along the eastern end of the eastern embankment profile were used to justify further exploration (drilling of piezometers) in the eastern expression of resistivity unit 1. The spatial location of the piezometers and the screened intervals were selected to best match the locations of the screened intervals of the western embankment piezometers. Six piezometers were installed on the eastern embankment and logged using borehole geophysical techniques. Surface DC resistivity sections superimposed on the resistivity logs for two piezometers indicate three discernible resistivity units that correlate with resistivity units 2, 1, and 2, respectively, identified in the western embankment study area. Resistivity units 1 and 2 in the DC resistivity profiles generally correspond with low and high resistivity zones, respectively, on the normal and lateral resistivity logs collected in the nearby piezometers at the time of installation.

## Introduction

Since 1992, numerous sinkholes have developed northwest of Amistad Reservoir dam, which impounds Amistad Reservoir (fig. 1) on the Rio Grande in Val Verde County, Tex., and Coahuila, Mexico. An increase in discharge of

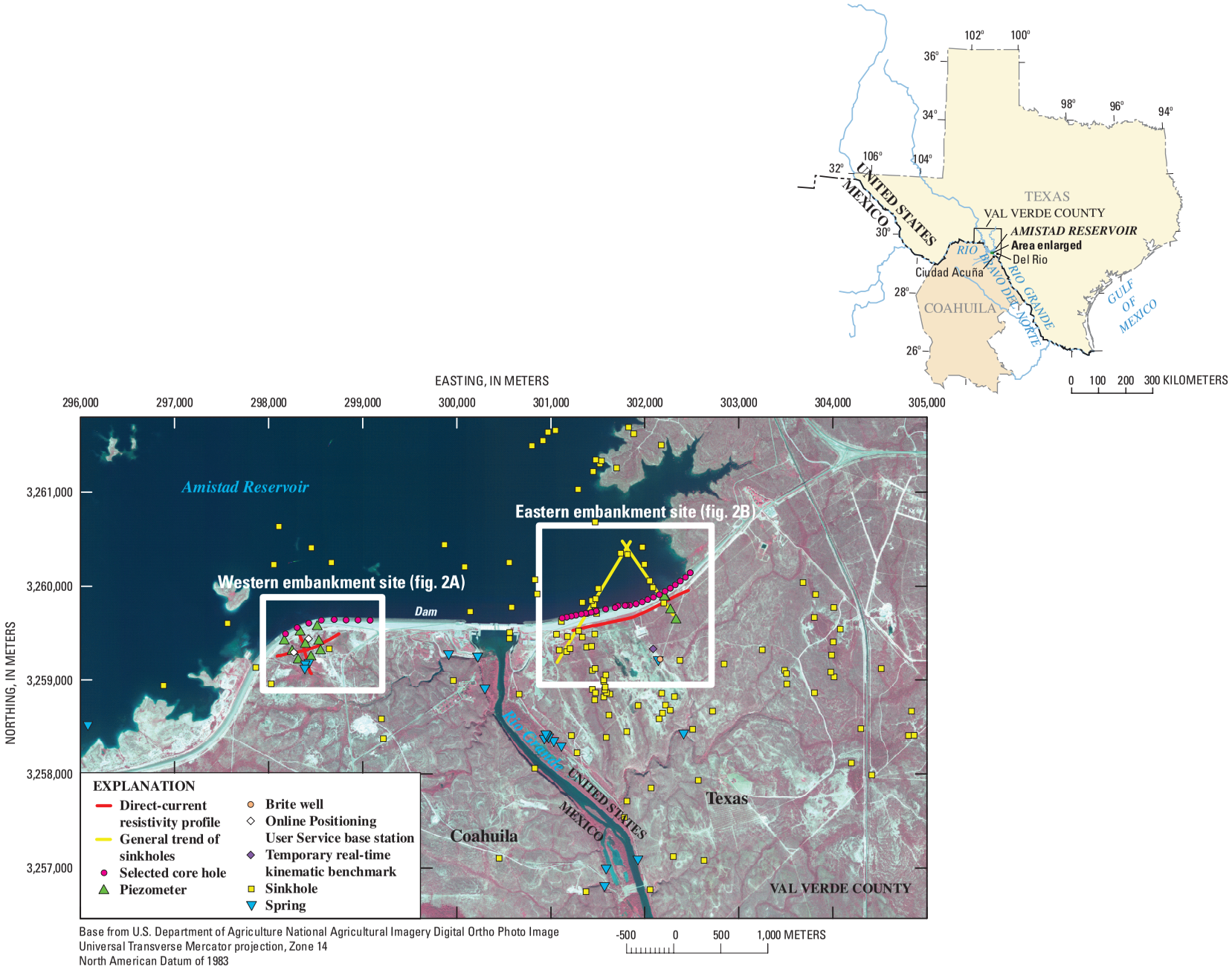


**Figure 1.** Location of Amistad Reservoir on the Rio Grande in Val Verde County, Texas; Coahuila, Mexico; and western and eastern embankment study sites.

springs south of the dam on the western side of the Rio Grande also has been documented by personnel at the International Boundary and Water Commission (IBWC) (Ken Breiton, U.S. Section, International Boundary and Water Commission, written commun., 2006). In 1995, the Mexico Section of the IBWC (MxIBWC) completed a study of the western embankment (Coahuila, Mexico) that included surface geophysics, borehole geophysics, and installation of piezometers to learn more about subsurface conditions. Piezometers were installed in three lines perpendicular to the centerline of the western embankment, with each line containing four piezometers (fig. 2A). After the 1995 study, the dam foundation along the centerline of a part of the western embankment was regrouted. As part of a 5-year safety inspection in 2005, technical advisors recommended that one line of piezometers be installed on the eastern embankment (Val Verde County, Tex.) of Amistad dam at identical land-surface altitudes and with depths similar to those on the western embankment. This recommendation is listed as task 13 in the Joint Report of the Technical Advisors of the International Boundary and Water Commission Regarding the Geotechnical, Electrical, Mechanical & Structural Safety of Amistad dam (Ken Breiton, U.S. Section, International Boundary and Water Commission, written commun., 2006). The purpose of the piezometers is to compare water

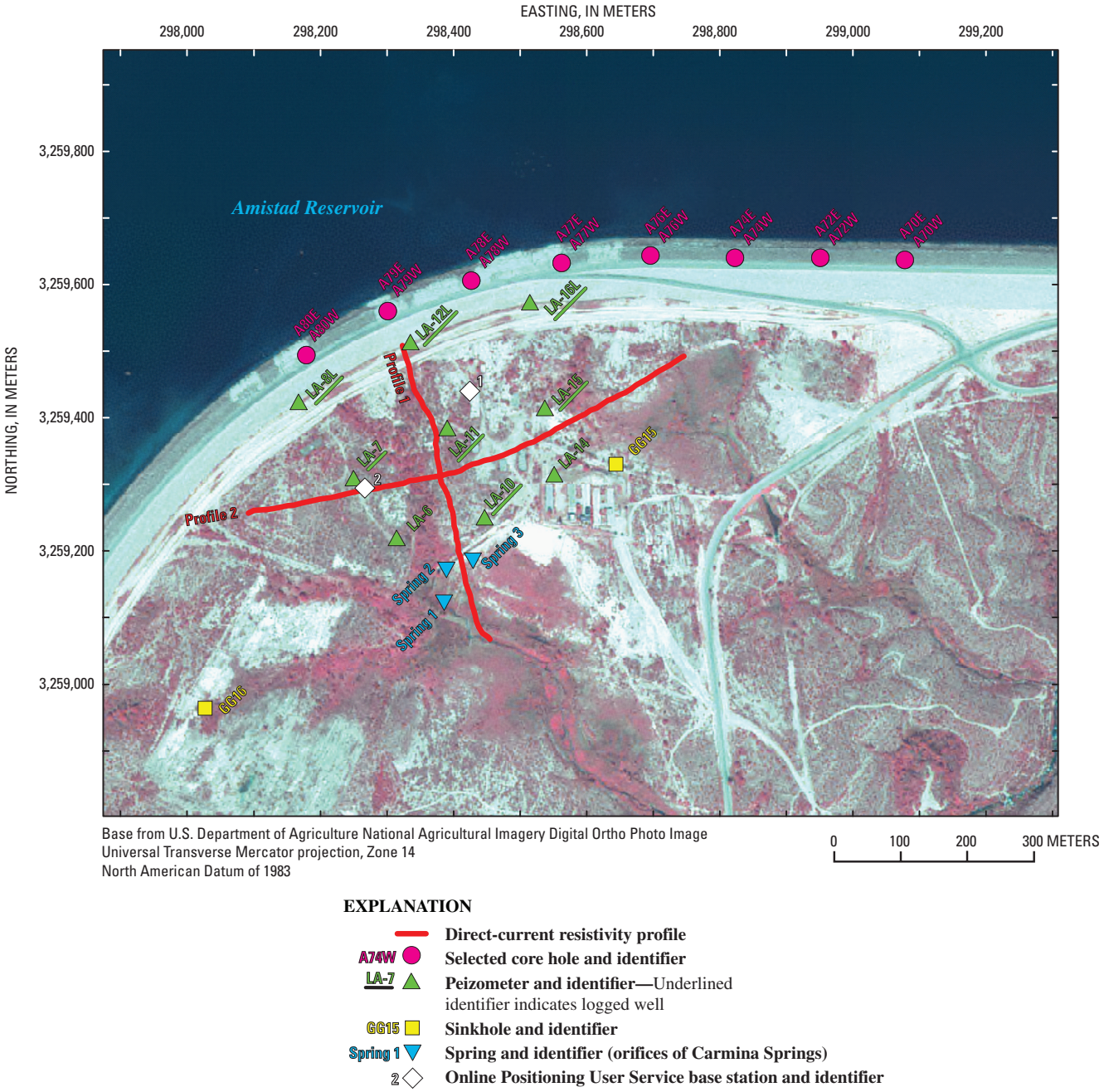


**Figure 2A.** Location of western embankment study site at Amistad Reservoir, Coahuila, Mexico.

levels (potentiometric head) on both the western and eastern embankments of Amistad Reservoir dam.

To provide technical assistance for the horizontal and vertical placement of piezometers on the eastern embankment of Amistad Reservoir dam, the U.S. Geological Survey (USGS) in cooperation with the U.S. Section, IBWC (USIBWC), conducted a study along both the western and eastern embankments of Amistad Reservoir dam. The study involved an integrated approach consisting of historical data review, geodatabase development, and surface and borehole geophysical investigations. The results of this approach were analyzed using the geodatabase to optimally locate piezometers along one line perpendicular to the centerline of the eastern embankment (fig. 2B) and install the piezometers using rotary drilling methods. Optimally located piezometers would allow objective comparison of water levels on the downgradient side (toe)

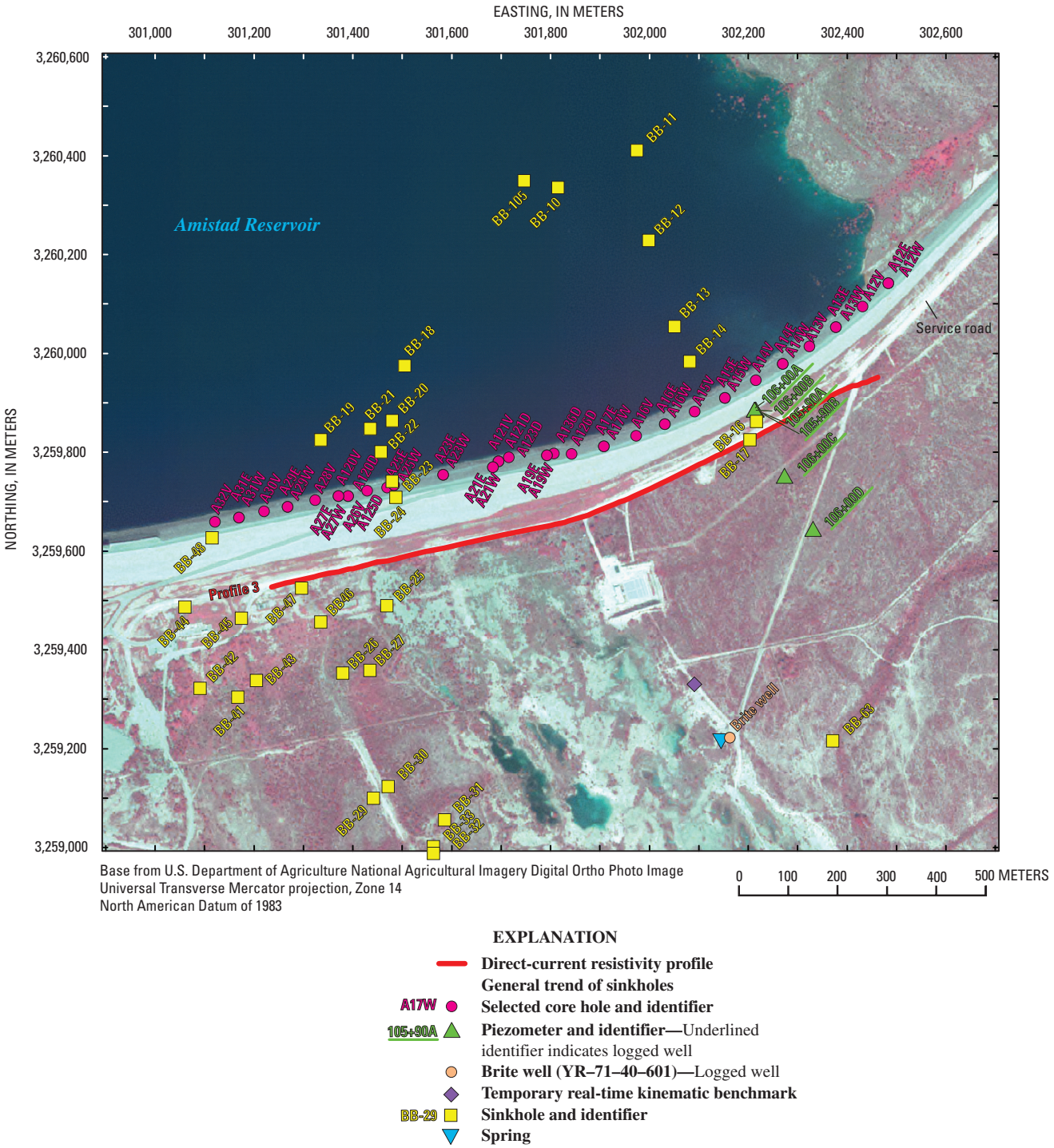


**Figure 2B.** Location of eastern embankment study site at Amistad Reservoir near Del Rio, Texas.

of both the western and eastern embankments to evaluate and compare leakage potential on both embankments. Hydrogeologic issues considered for this project included:

1. Complex karstic-limestone bedrock surface geology (as documented in core analysis done at the time of dam construction) that includes several mapped sinkholes and other surface expressions of dissolution.

2. Fluctuations in Amistad Reservoir pool elevation since the mid-1970s have caused variations in pressure head and moisture in the subsurface karst openings, many of which are clay-filled. There is concern that lower reservoir elevations could cause the clay to become unstable and possibly mobilize during future reservoir fluctuations (Jose Antonio Moza, Federal Electricity Commission, written commun., 1995).

3. Springs discharging downgradient from the dam on the western embankment are presumably caused by water flow beneath the dam. On the eastern embankment, the only indication of water flow beneath the dam is a flowing well several hundred meters downgradient from the dam.

Geologic, geophysical, and hydrologic data were collected along the western embankment to understand the physical setting and near-surface hydrogeology of existing piezometers and to aid the placement of piezometers on the eastern embankment for objective comparison of hydraulic activity. To accomplish these tasks, the following factors were considered:

1. The land-surface altitude at prospective sites such that piezometers on the eastern embankment would be at approximately the same altitude as the piezometers on the western embankment (as suggested in the Joint Report of the Technical Advisors of the International Boundary and Water Commission Regarding the Geotechnical, Electrical, Mechanical & Structural Safety of Amistad Dam (Ken Breiton, U.S. Section, International Boundary and Water Commission, written commun., 2005).

2. The local faults and disruptions in the continuity of the hydrogeologic units along the embankment and their effect on the ability to correlate correlation between study areas.

3. The potential for dissolution and development of secondary porosity, as detected through the use of geophysical methods, on both embankments.

## Purpose and Scope

This report presents the results of geophysical analysis from a reconnaissance-level study conducted on the eastern (Val Verde County, Tex.) and western (Coahuila, Mexico) embankments of Amistad Reservoir dam on the Rio Grande in March 2006 to characterize the near-surface hydrogeology. Piezometers on the eastern embankment were to be constructed at about the same land-surface altitudes and depths as those on the western embankment, and in similar lithology on the basis of geophysical data and core descriptions, for objective comparison of hydraulic heads at the toe of the dam. The purpose of this report is to document the technical approach that facilitated the optimum placement of the piezometers on the eastern embankment. The report documents an integrated borehole and surface geophysical approach. Geophysical data are used to identify and correlate subsurface features (lithology and water-yielding characteristics) between the western and eastern embankments so that eastern embankment piezometers could be placed to reflect subsurface conditions matching, to the extent possible, those of existing western embankment piezometers. Reporting water-level data monitored by the IBWC was not in the scope of the study. Because the project was a reconnaissance-level study, the report is not a comprehensive geologic or geophysical evaluation of the study area.

## Description of Amistad Reservoir and Dam

Amistad Reservoir is located about 21 kilometers north-northwest of Del Rio, Tex. on the Rio Grande between Val Verde County, Tex., and Coahuila, Mexico (fig. 1). The reservoir has a surface area of 26,300 hectares and has a volume of 3,886,578,000 cubic meters at conservation elevation of 340.46 meters above NAVD 88. The total contributing drainage area to the reservoir is 327,434 square kilometers in the United States and Mexico (Texas Water Development Board, 1971).

Amistad Reservoir dam was constructed for flood control and water conservation storage for the benefit of the United States and Mexico. The dam is operated and maintained jointly by the USIBWC and MxIBWC. Amistad Reservoir dam is the largest of the storage dams and reservoirs built on the international reach of the Rio Grande. The dam is 10 kilometers long, stands 77.4 meters above the riverbed, and consists of a concrete gravity spillway section in the river canyon flanked by earthen embankments. Dam construction began in December 1964, impoundment of water began May 31, 1968 (Texas Water Development Board, 1971), and construction was completed November 21, 1969.

## Area Hydrogeology

The near-surface karstic carbonate rocks of the area consist of five Lower Cretaceous, predominantly limestone formations (oldest to youngest): the West Nueces Formation, the McKnight Formation, the Salmon Peak Formation, the Del Rio Clay, and the Buda Limestone (table 1). This study focused on characterizing the Salmon Peak Formation. (All surface and borehole geophysical data were collected in the Salmon Peak Formation except for data at one well that also penetrates the upper unit of the McKnight Formation.)

Limestone typically has very low primary porosity and permeability with secondary porosity and permeability commonly occurring by solution enlargement of bedding planes,

**Table 1.** Summary of lithologic and hydrologic properties of near-surface geologic units in the area of Amistad Reservoir dam, Val Verde County, Texas, and Coahuila, Mexico.

[Groups, formations, and members modified from Greenwood (1956), Lozo and Smith (1964), Reeves and Small (1973), Humphreys (1984); lithology modified from Dunham (1962)]

| System | Group, formation, unit/member | | | Thickness (meters) | Lithology | Field identification | Cavern development | Porosity/ permeability |
|---|---|---|---|---|---|---|---|---|
| Lower Cretaceous | Washita Group | Buda Limestone | | 12–15 | Buff, light-gray, dense mudstone | Hard, porcellaneous and marly limestones | Minor | Low porosity/low permeability |
| | | Del Rio Clay | | 12–18 | Blue-green to yellow-brown clay | Blue-green to medium-brown shale; Ilymatogyra | None | Low porosity/low permeability |
| | | West prong beds of Del Rio Clay | | 0–15 | Yellowish-brown, argillaceous limestone with thin clay partings; Wacoensis waconella and Ilymatogyra areintina common | Yellowish-brown, argillaceous limestone; appears similar to Georgetown Formation on San Marcos Platform | Minor, associated with collapse from caverns developed in Salmon Peak Formation | High porosity/high permeability along fractures and areas of collapse, also some along bedding planes |
| | | Salmon Peak Formation | Upper unit | 0–9 | Wackestone to packstone, abundant echinoid fragments, calcispheres, foraminifera; glauconite, limonite and hematite | Light-gray mudstone, with abundant fossil fragments, stringers of shale; contains chert, nodules, and pyrite | Numerous, karst appear to develop in trends along fractures, also development along bedding planes | High porosity/high permeability associated with caverns and fractures |
| | | | Lower unit | 0–130 | Mudstone to wackestone; pelagic foraminifers, calcispheres, and scattered shell fragments, occasional organic matter and burrows | Massive, gray mudstone, stringers of shale; contains nodular and bedded chert, and pyrite | Numerous, karst appear to develop in trends along fractures, also development along bedding planes | High porosity/high permeability associated with caverns and fractures |
| | Fredericksburg Group | McKnight Formation | Upper unit | 0–36 | Anhydrites, dark-brown, fecal pellet packstone and organic-rich, laminated mudstone; fecal pellets, miliolids, shell fragments and globogerinids, oysters | Alternating light- to dark-grey, laminated and thin-bedded fecal pelleted mudstone to grainstone | Negligible | High porosity and permeability where evaporite dissolution has occurred |
| | | | Middle unit | 0–16 | Brown to black, laminated, organic rich mudstone; fecal-pellet packstone to grainstone, thin anhydrite and sulfur beds | Strong petroliferous odor, laminated mudstone; vegetative band on aerial photo | None | Low porosity/low permeability |
| | | | Lower unit | 0–35 | Anhydrite, alternating with laminated, black, shell fragment mudstone and wackestone; pelleted, shell fragmented, interclastic grainstone | Thin-bedded mudstone to grainstone | Negligible | Low to high porosity/low permeability |
| | | West Nueces Formation | Undivided | 0–91 | Gray, thick-bedded, burrowed, shell-fragment wackestone, packstone, and grainstone; dolomitic | Hard, massive, cherty, gray wackestone, some dolomite, miliolids, gastropods, and Texigryphaea | Minor, associated with fracture solutioning | Low porosity/low permeability |
| | | | Basal nodular member | 6–30 | Shaly, nodular limestone; mudstone and *miliolid* grainstone | Massive, nodular and mottled; abundant gastropods and Exogyra texana | Large lateral caves at surface | Porosity stratigraphically controlled/large conduit flow at surface; negligible permeability in subsurface |

fractures, and faults (Ford and Ewers, 1978). The intensity of these features is dependent on the intersection of faults or joints where dissolution can cause the local formation of caverns, sinkholes, and conduits for ground-water flow (Palmer, 1984). The rate at which dissolution features occur usually depends on the amount of water moving through the system, the pH of the water, the degree of calcium carbonate saturation (Fetter, 1994), and the availability of carbon dioxide in the water. Dissolution, as described above, has altered the permeability of the Salmon Peak Formation, which constitutes most of the bedrock beneath the Amistad Reservoir dam (Jose Antonio Moza, Federal Electricity Commission, written commun., 1995).

## Background of Amistad Reservoir

During design of the Amistad Reservoir in the early 1960s, dissolution features such as depressions, sinkholes, and caverns in the Rio Grande valley walls, river terraces and adjacent flood plains were documented (Jose Antonio Moza, Federal Electricity Commission, written commun., 1995). Preventative measures taken during construction (1964–65) to minimize dam seepage included the excavation of the dam foundation area (fig. 3A), filling of sinkholes in the reservoir impoundment area, excavation and concrete filling of caverns and elongated solution conduits in the ditch excavated for the curtain foundation (fig. 3B), and the construction of a grout curtain to a depth of about 50 meters in the bedrock foundation along the centerline of the dam (Jose Antonio Moza, Federal Electricity Commission, written commun., 1995).

As the reservoir began to fill in 1968, an increase in discharge of local springs was observed. Early discharge data were collected from orifices of Carmina Springs near the western embankment (fig. 2A), beginning in 1969 (Jose Antonio Moza, Federal Electricity Commission, written commun., 1995). By 1970 Amistad Reservoir pool elevation had reached approximately 322 meters above sea level, and Carmina Springs discharge was 0.4 cubic meter per second. Measurements in later years (table 2) indicate that there is a direct correlation (fig. 4) between the pool elevation and the discharge at Carmina Springs. Thus, despite efforts to minimize seepage, data indicate a substantial hydraulic connection between the reservoir and the shallow subsurface immediately downstream from the dam, which facilitates seepage.

**Table 2.** Elevation of Amistad Reservoir and discharge from Carmina Springs near Ciudad Acuna, Coahuila, Mexico, 1970–94 (modified from Jose Antonio Moza, Federal Electricity Commission, written commun., 1995).

| Year | Elevation, Amistad Reservoir (meters above sea level) | Discharge, Carmina Springs (cubic meters per second) |
|---|---|---|
| 1970 | 322 | 0.4 |
| 1971 | 328 | .9 |
| 1973 | 343 | 2.0 |
| 1974 | 346 | 2.1 |
| 1984 | 334 | 1.5 |
| 1986 | 329 | .8 |
| 1990 | 332 | 1.6 |
| 1994 | 331 | 1.1 |

## Approach

The approach was designed to facilitate the optimum placement of piezometers that were to be constructed on the eastern embankment at the same land-surface altitude and depth as those on the western embankment and in similar lithology on the basis of geophysical data and core descriptions. These piezometers were to be used for the objective comparison of hydraulic heads at the toe of the dam. Specifically, the approach involved the following steps:

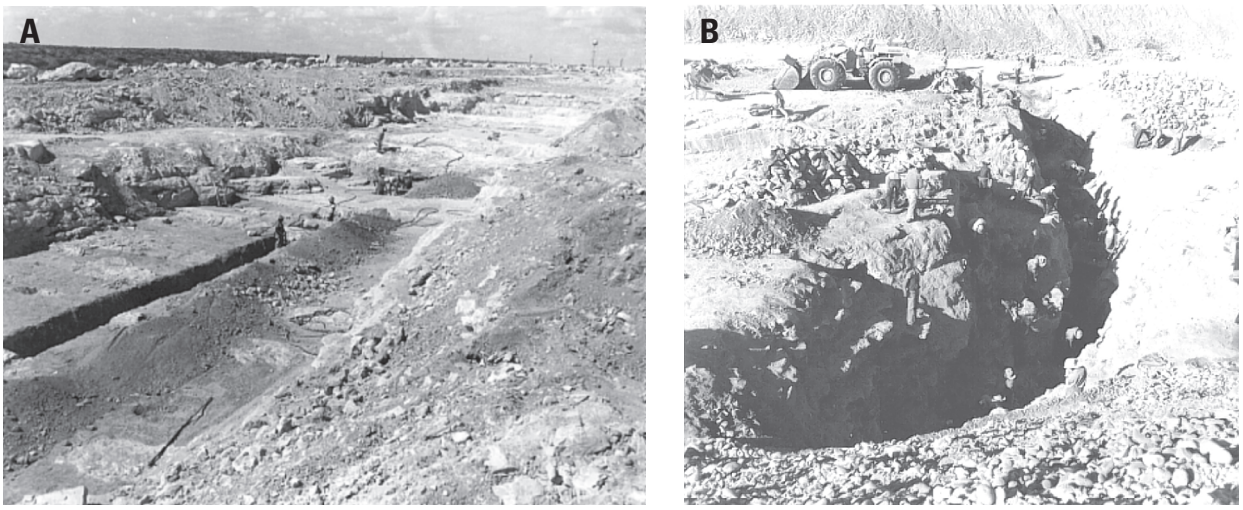


**Figure 3.** Amistad Reservoir dam construction, 1965: (A) excavation of dam foundation area along eastern embankment, and (B) excavation of ditch for curtain foundation along western embankment.

1. Review existing literature to create a geodatabase containing geologic, geotechnical, and geophysical data that could be used for analysis and interpretation.
2. Document geologic and hydrogeologic characteristics of the Salmon Peak Formation near the western embankment piezometers.
3. Collect and analyze new and existing surface and borehole geophysical data along the western embankment.
    a. Develop preliminary borehole geophysical interpretations to identify the geologic and hydrogeologic characteristics contributing to the hydraulic connection between the reservoir and the shallow subsurface immediately downstream from the dam.
    b. Correlate surface geophysical data with preliminary interpretations of borehole geophysical data from the western embankment to identify subsurface features that could be used to correlate data collected from the eastern embankment.
4. Analyze the geodatabase to determine the best starting point for surface geophysical survey.
5. Collect, continuously process, and analyze surface geophysical data collected from the eastern embankment to identify a location for one piezometer transect.
6. Present preliminary data, interpretations, and the location identified for the installation of the eastern embankment piezometer transect to USIBWC staff.
7. Guide the drilling and installation of the transect of piezometers along the eastern embankment.
8. Obtain and log drill cuttings and borehole geophysical data for each new piezometer. Evaluate borehole geophysical logs to determine optimum vertical placement of well screens for each piezometer.

## Western Embankment Investigation

Geologic and geophysical characteristics that indicate relatively large water-yielding properties of the Salmon Peak Formation were identified. Borehole geophysical logs (natural gamma, gamma-gamma, caliper, and neutron) were collected during the installation of the western embankment piezometer transects in 1995 (Paul Gibson, U.S. Section, International Boundary and Water Commission, written commun., 2006). The direct-current (DC) resistivity method (Zohdy and others, 1974) was selected for the reconnaissance study as the surface geophysical technique to correlate relatively large water-yielding properties of the Salmon Peak Formation, identified from analysis of existing borehole geophysical logs, with variations in subsurface resistivity. To aid in the correlation

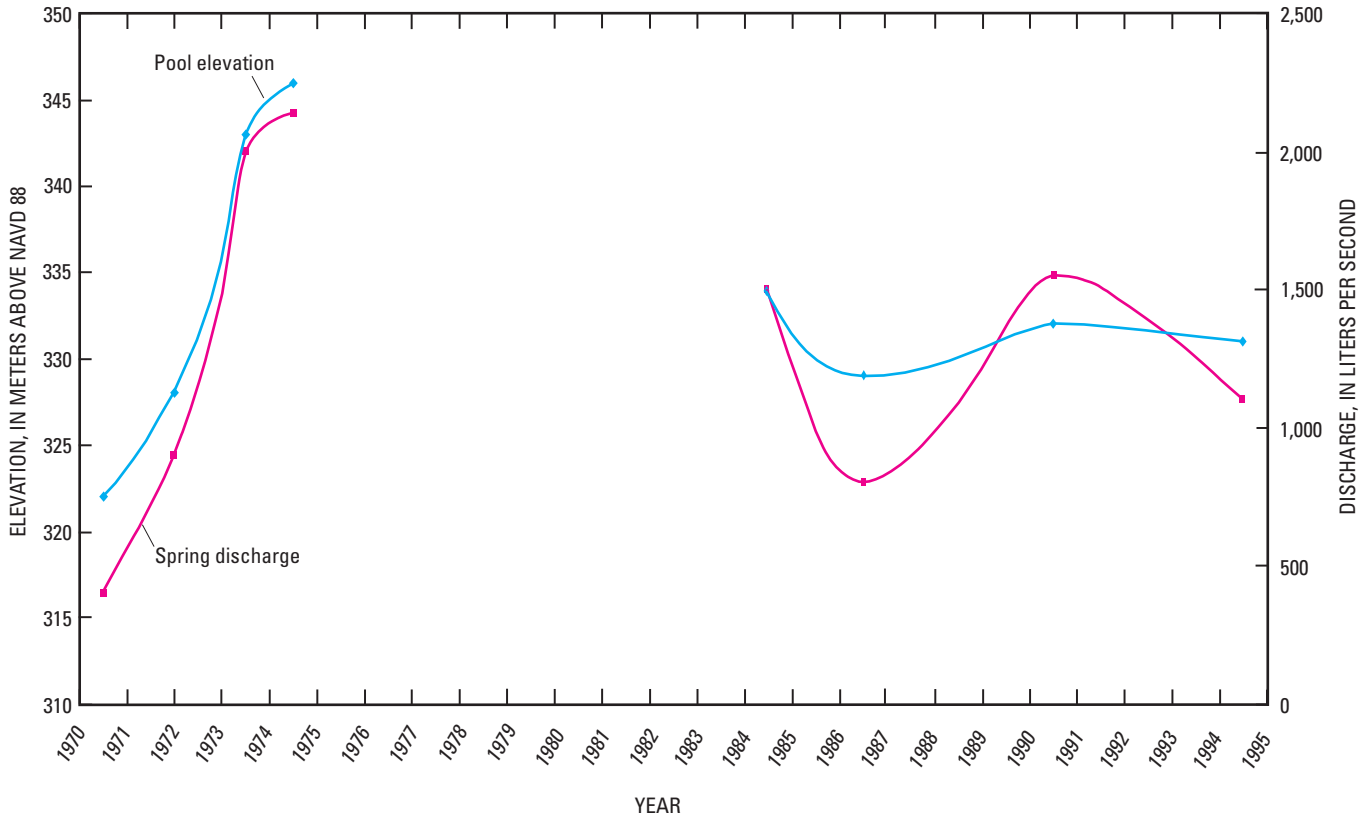


**Figure 4.** Elevation of Amistad Reservoir and discharge from Carmina Springs near Ciudad Acuna, Coahuila, 1970–94 (modified from Jose Antonio Moza, Federal Electricity Commission, written commun., 1995).

between surface and borehole geophysical data, borehole induction resistivity logs, as well as natural gamma and fluid conductivity logs, were collected. Borehole resistivity logs were collected to relate geophysical variations in gamma, caliper, and neutron logs, identified as changes in water-yielding properties, to changes in the electrical stratigraphy of the subsurface along DC resistivity profiles.

### Eastern Embankment Investigation

Historical data from the USIBWC were analyzed to identify trends in the spatial distribution of sinkholes near the eastern embankment and the occurrence of weathered zones identified from geologic descriptions of cores collected by the IBWC along the eastern embankment. By evaluating the occurrence of these features, an area was selected for further exploration using DC resistivity. DC resistivity data collected along the eastern embankment were continuously processed and inverted. Inversion involves estimation of subsurface physical properties from measured geophysical field data using computer-modeling software. Inversion results in the form of images representing sections of subsurface resistivity produced from the DC resistivity data were evaluated to identify subsurface electrical signatures similar to those obtained from the data collected along the western embankment. Similar signatures were identified and correlated with geologic properties from the geodatabase to select potential sites for piezometer installation. As the piezometers were installed, drill cuttings were used to construct geologic logs to complement and refine borehole geophysical logs. The resistivity data used to site the new piezometers were compared to geologic and geophysical log data collected after installation of the piezometers to verify similarities to lithologies at piezometers on the western embankment.

## Methods

The combination of historical data, applied geophysics, and ground-truthing methods can be used to contribute to the solution of most geotechnical engineering and environmental problems (U.S. Army Corps of Engineers, 1995). Most geophysical techniques do not measure the physical properties needed to solve the problem under consideration; however, most geophysical techniques can measure contrasts in the physical properties that can be used to infer contrasts in geology or hydrogeology. The correlation of measured geophysical contrasts that reflect changes in geology or hydrology of the subsurface primarily is empirical and depends on the quality of the results. There is no substitute for specific geologic or engineering observations (such as borings, test pits, and trenches) to aid in the empirical correlation. Borings or other tests are used to validate and calibrate geophysical results and ultimately to improve the accuracy of the interpretation.

Surface and borehole geophysical methods are used to measure the physical properties of the subsurface, such as electrical conductivity or resistivity, dielectric permittivity, magnetic permeability, density, or acoustic velocity (American Society for Testing and Materials, 1999). Such methods provide a relatively quick and inexpensive means to characterize the subsurface. The results (measurements) can be influenced by chemical and physical properties of soils, rocks, and pore fluids. Interpretations from these measurements can be used to image the distribution of physical properties in the subsurface (American Society for Testing and Materials, 1999). Surface and borehole geophysical methods and their application to ground-water and environmental investigations are described in detail in Zohdy and others (1974), Keys (1990), and U.S. Army Corps of Engineers (1995). The geophysical surveys used in this investigation were conducted in accordance to applicable American Society for Testing and Materials (ASTM) guides (1999; 2001; 2004a, b, c).

Drilling in karstic limestone can be challenging because of the high potential for intersecting permeable dissolution cavities, which can cause circulation loss and lack of returned drill cuttings. Drilling methods used to complete the boreholes in this investigation were a combination of tri-cone air-rotary and down-hole pneumatic hammer, which have several advantages: (1) ability to drill in partly consolidated and consolidated geologic materials, (2) cuttings returned in air stream for accurate correlation, (3) drilling is rapid and readily accomplished, and (4) facilitates geophysical logging of the borehole (Lapham and others, 1997). Some disadvantages include the potential for circulation loss in fractured or karstified rock and the potential for altering the formation near the borehole by causing or opening new fractures. Well construction and completion was performed in accordance with ASTM standards (American Society for Testing and Materials, 2004d),

### Geodatabase

A geodatabase was developed to consolidate geological, geotechnical, and geophysical data collected during previous (early 1960s to 1995) and current (2006) investigations in a comprehensive temporal and spatial database (Shah and Quigley, 2005). The geodatabase was developed using Oasis montaj (Geosoft Inc., 2006). (Oasis montaj is the software used to create, manage, and visualize the geodatabase.) The geodatabase includes geologic-log data from foundation test borings along the centerline of Amistad Reservoir dam; geologist descriptions of borings from piezometers installed along the western embankment; borehole geophysical natural gamma, resistivity, and neutron logs; and DC resistivity data. These data were entered into the geodatabase in an American Standard Code for Information Interchange (ASCII) format. In addition, data collected during construction of the piezometers also were archived in the geodatabase. Existing borehole geophysical logs for the western embankment piezometers were digitized and imported into the geodatabase. The raw geophysical data that were collected also were modified to an ASCII format and archived in the geodatabase. Surface information, such as sinkhole and spring locations, also was obtained and

entered into the geodatabase. The geodatabase was used during fieldwork to produce lithologic and resistivity sections and to perform various types of spatial analyses useful to understand and visualize the subsurface and to aid in placement of the new eastern embankment piezometers.

## Borehole Geophysics

Thirteen piezometers (seven on the western embankment and six on the eastern embankment) and one existing open hole (Brite well) were logged using borehole geophysical methods. The seven piezometers (fig. 2A; LA–12L, LA–11, LA–10, LA–16L, LA–15, LA–8L, LA–7) on the western embankment, owned by the MxIBWC, are located below the western end of the dam. These piezometers were logged with electromagnetic (EM) induction conductivity, natural gamma, and fluid resistivity tools. The selected piezometers on the western embankment are completed with polyvinyl chloride (PVC) casing, which prevented the collection of some additional logs. The six eastern embankment piezometers (fig. 2B; 105+90B, 105+90A, 106+00B, 106+00A, 106+00C, 106+00D) and one existing open hole (Brite well) owned by the USIBWC were logged using the previously mentioned methods and also with open-hole tools such as caliper and casing collar locator. In wells with sufficient static water level, normal resistivity logs, spontaneous potential (SP) logs, acoustic televiewer (ATV) logs, acoustic velocity logs, full-waveform sonic variable intensity logs (VIL), and EM flowmeter logs also were collected if possible.

Pertinent information for wells such as spatial location, elevation, well identifier, total depth, and casing and well-construction record was provided by the MxIBWC. In addition to the logs collected for this study, the MxIBWC piezometers were logged by a contractor in 1995 at the time of drilling. The logs collected at that time were neutron, density, caliper, and natural gamma. These previously collected logs were digitized for use in this study because only photocopies of the logs were available formatted with compressed depth scales and very little detail. This study included the collection of EM induction conductivity logs to correlate borehole geophysical data with surface geophysical resistivity data. All geophysical probes interfaced to either a Mount Sopris MGXII or Century System VI log-acquisition system in the logging truck by way of 0.25-inch- (6-millimeter-) diameter four-conductor wireline. Individual borehole geophysical methods are described in appendix 1; logs are described in appendix 2; and logs are contained in appendix 3.

## Surface Geophysics

Three profiles, (two on the western embankment and one on the eastern embankment) were surveyed using DC resistivity methods. The two profiles surveyed on the western embankment (fig. 2A) were done to determine the effectiveness of using DC resistivity profiling methods to image changes in subsurface resistivity that correlate with increases in the water-yielding properties of the Salmon Peak Formation.

### Direct-Current Resistivity

Electrical surface geophysical methods can be used to detect changes in the electrical properties of the subsurface (Zohdy and others, 1974). The electrical properties of soils and rocks are determined by water content, mineralogical clay content, salinity, porosity, and the presence of metallic minerals. Typically the resistivity of the water has a large effect on the bulk resistivity. One of the most commonly used methods for measuring earth resistivity is the DC resistivity method (Keller and Frischknecht, 1966). Generally the DC resistivity method uses two electrodes as a transmitter connected to a source of electric current to create a current field. An electrical potential field is created that is measured by a pair of potential electrodes, used as a receiver. On the basis of the configuration of the electrodes (known as an array), the amount of current applied through the transmitter, and the measured potential across the receiver, the apparent resistivity can be determined. The underlying physical principle used to calculate resistivity for the DC resistivity method is embodied in Ohm's law. According to Ohm's law, the resistance (R) of earth material can be determined by

$$R = \Delta V/I, \quad (1)$$

where $\Delta V$ is the potential difference (voltage drop) measured by the receiver, and I is the current (amperes) applied by the transmitter. The resistance calculated from DC resistivity measurements is a specific measurement of the ability of earth material to transmit electrical current that is directly dependent on the geometry and electrode spacing of the array used to obtain that measurement. To obtain a measurement that is independent of the geometry and electrode spacing resistance, R measurements are multiplied by a geometric factor (K), unitless, to calculate apparent resistivity ($\rho_a$) represented in the following equation:

$$\rho_a = K \Delta V/I. \quad (2)$$

Apparent resistivity represents the resistivity of completely uniform (homogenous and isotropic) earth material (Keller and Frischknecht, 1966). To determine the resistivity of nonuniform earth material, inverse modeling software is used. A description of the DC resistivity method as well as electrical tables of the properties of earth materials can be found in Zohdy and others (1974), Sumner (1976), and Sharma (1997).

Apparent resistivity data were collected along three profiles (fig. 2A–B) at the Amistad study site using an IRIS Syscal Pro 10-channel 96-electrode resistivity meter (fig. 5A). The IRIS Syscal Pro was configured with eight sets of

multi-conductor cables, each cable having 12 electrode terminals with 5-meter spacing. Stainless steel electrodes were installed in the ground and connected to electrode terminals built into the multi-conductor cables (fig. 5B). After the initial section of resistivity data was collected, the first two cables of 24 electrodes were moved ahead of the survey line. A partial section of data then was collected using the previous 72 electrodes (electrodes 25–96) and the 24 electrodes (electrodes 97–120) just moved. This process, known as the roll-along technique, was continued until all data along the desired line length were collected. The data from the roll-alongs can be combined into a single apparent-resistivity data set during processing or processed individually. Appropriate quality assurance/quality control procedures such as testing contact resistance before data collection was performed for each segment of each profile. Contact resistance measures the resistance to current flow at electrodes caused by imperfect electrical contact with the earth (Boyd, 2006). Poor data quality or anomalous data can result from high or highly variable electrode contact resistances along a profile. To decrease the effect of contact resistances along each profile, a saltwater solution was applied using a backpack sprayer (fig. 6A) to each electrode (fig. 6B) before the contact resistance test was performed. If upon testing, contact resistance was anomalously high, saltwater was reapplied; if the problem persisted then the electrodes were moved slightly, saltwater was reapplied, and then contact resistance was remeasured until acceptable values were obtained. The final contact resistance values

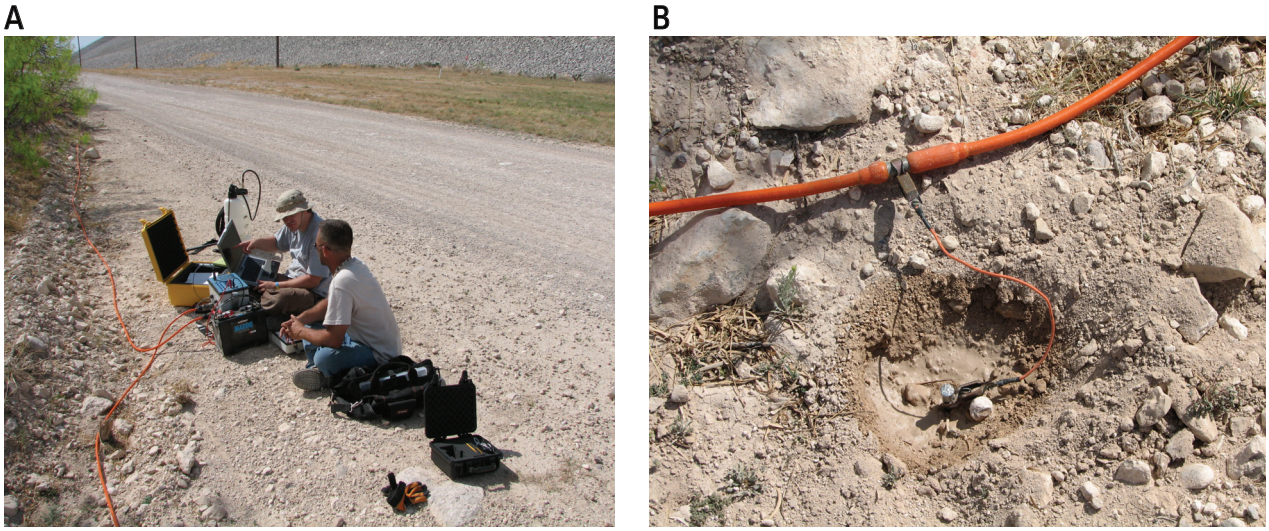


**Figure 5.** Near Amistad Reservoir dam, March 2006, along direct-current resistivity profile 3: (A) IRIS Syscal Pro resistivity meter connected to multi-conductor cables, and (B) stainless steel electrode connected to electrode takeout built into multi-conductor cable.

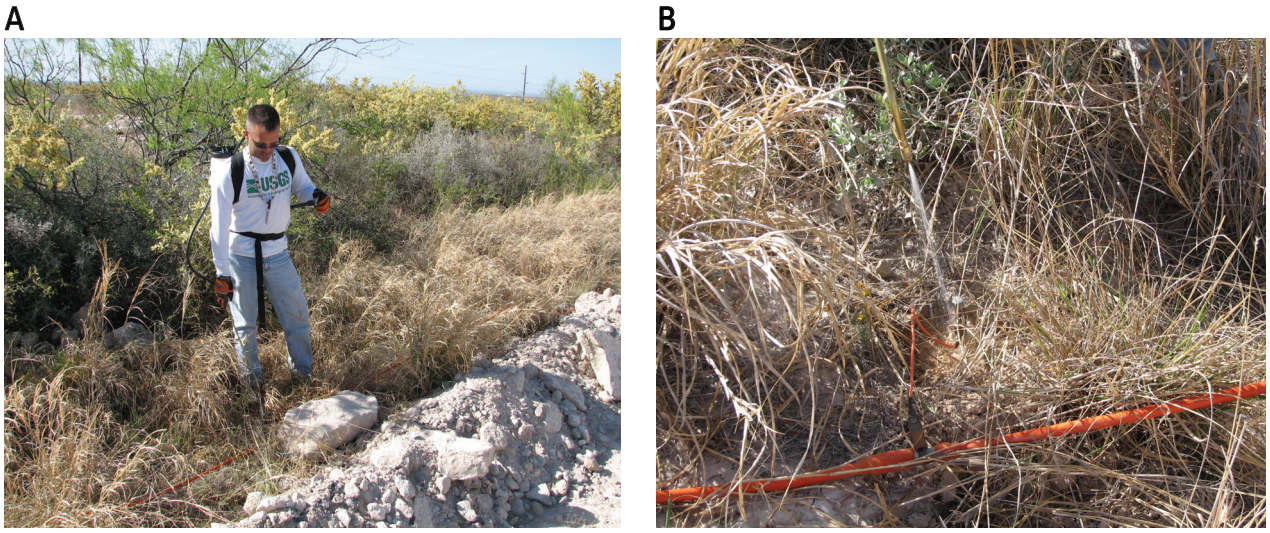


**Figure 6.** Near Amistad Reservoir dam, March 2006, along direct-current resistivity profile 3, application of a saltwater solution (A) using a backpack sprayer, and (B) to an electrode to decrease the effect of contact resistances.

collected using the dipole-dipole array configuration prior to apparent resistivity data collection for each profile is on file at the Texas Water Science Center, West Texas Program Office, San Angelo.

Trimble 5800 Global Positioning System (GPS) units were used to establish two temporary GPS survey benchmarks referred to as Online Positioning User Service (OPUS) (National Oceanic and Atmospheric Administration, 2006) base stations in the western embankment study site (fig. 2A). The GPS units collected static GPS observations at base stations 1 and 2 for approximately 3 and 4 hours, respectively. The GPS static observations were processed using OPUS, provided by the National Geodetic Survey, to derive geographic and elevation coordinates for each base station. The OPUS solutions for each base station are provided in appendix 4. Three Trimble 5800 GPS units, one configured as a base station (fig. 7A) and two configured as rovers (fig. 7B), were used in real-time kinematic (RTK) mode to survey electrode locations along each profile to derive geographic and elevation coordinates. A GPS base station was set up on OPUS base station 1 using the OPUS-derived solution to establish the geographic and elevation coordinate for that point. The GPS at base station 1 was used to collect GPS observations and determine corrections, then radio these corrections to the rover GPS units for real-time corrections. To verify the proper set-up of base station 1 and each rover GPS, both rovers were set up on base station 2 to collect RTK GPS data. The RTK solution for each rover was compared to the results of the OPUS solution to verify that the GPS units were configured correctly. The RTK-GPS derived elevations were incorporated in the apparent-resistivity data sets during post-processing to allow for topographic corrections during inverse modeling. Geographic coordinates were input into the geodatabase to geospatially reference each DC resistivity profile and the eastern embankment piezometers. To extend data collection into the eastern embankment study site a temporary RTK benchmark (fig. 2B) was established, then the base station was relocated to the temporary RTK benchmark and used to survey the DC resistivity profile along the eastern embankment.

Two DC resistivity profiles (fig. 2A) were collected along the western embankment to image the subsurface resistivity near the three transects of piezometers. DC resistivity profile 1 trending north to south was collected so that the profile data could be compared to hydrogeologic and borehole geophysical data from piezometer transect 1 (LA–8L, LA–7, LA–6; fig. 2A) and transect 2 (LA–12L, LA–11, LA–10; fig. 2A ) and to image the subsurface resistivity between the toe of the dam and the springs. DC resistivity profile 2 trends west to east intersecting piezometer transects 1–3 perpendicularly south of piezometers LA–7, LA–11, and LA–15. DC resistivity profile 2 was collected to image the subsurface resistivity semi-parallel to the toe of the dam and to collect data between piezometer transects 1–3. DC resistivity profile 3 was collected traversing west to east along the eastern embankment (fig. 2B). Apparent resistivity data were inverted in the field to identify resistivity features similar to the features characterized along DC resistivity profiles 1 and 2.

Two arrays, the dipole-dipole (fig. 8A) and a modification of the Schlumberger array (fig. 8B), the reciprocal Schlumberger array (fig. 8C), were used to collect DC resistivity data for each profile (Zohdy and others, 1974). The dipole-dipole and reciprocal Schlumberger arrays were chosen because they can be easily optimized to allow for the maximum number of potential pairs (channels) to be measured with a single current injection. The dipole-dipole array is good for mapping vertical structures such as dikes or cavities but relatively poor for mapping horizontal structures (Loke, 2004); whereas the Schlumberger array is superior in distinguishing lateral from vertical variations in resistivity (U.S. Army Corps of Engineers, 1995). The theorem of reciprocity states that no change will be observed in the measured voltage if the positions of the potential electrodes and of the current electrodes are interchanged; therefore the reciprocal Schlumberger array should have similar lateral and vertical resolution capabilities (Keller and Frischknecht, 1966). One disadvantage to using the dipole-dipole array is a decrease in signal strength for large values of “n” spacings (transmitter and receiver separations) making it more susceptible to environmental noise than the reciprocal Schlumberger array (Loke, 2004).

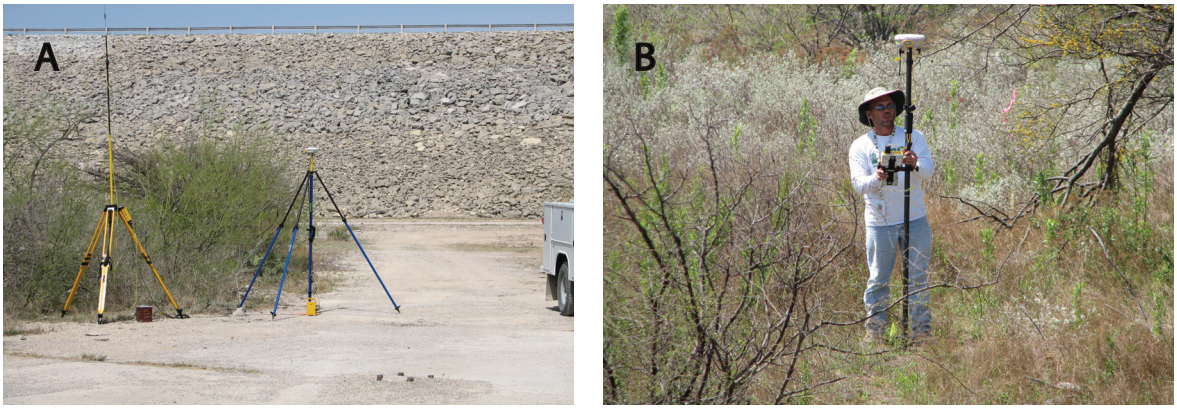


**Figure 7.** Near Amistad Reservoir dam, March 2006, along direct-current resistivity profile 2: (A) real-time kinematic (RTK) Global Positioning System base station, and (B) RTK rover used to survey electrode locations.

## Inverse Modeling of Direct-Current Resistivity Data

Apparent resistivity, as calculated from the field measurements, is the electrical resistivity of an equivalent electrically homogeneous and isotropic subsurface and is used to represent the average resistivity of the heterogeneous subsurface (Grant and West, 1965). To estimate the true subsurface resistivity, an inverse modeling program develops a model consisting of rectangular blocks of individual resistivities (Loke, 2004). The inversion program calculates the system response of that model to produce synthetic calculated apparent resistivity data. The calculated data are compared to the collected field data. The root mean square (RMS) difference between the measured and calculated apparent resistivities is used to determine the accuracy of the model. The inversion program attempts to reduce the RMS difference by altering the model resistivity values and recalculating the calculated apparent resistivity; this alteration and recalculation of resistivities is known as an iteration. When the RMS difference between the calculated and measured apparent resistivity no longer improves appreciably between iterations (more than 1 percent between iterations), a solution is reached. This final model represents a non-unique estimate of the true distribution of subsurface resistivity. The inverse modeling process is described in detail by Loke (2004) and Advanced Geosciences, Inc. (2006).

All apparent resistivity data were inverted using AGI EarthImager 2D version 2.1.2 Resistivity and Induced Polarization Inversion Software (Advanced Geosciences, Inc., 2006). After analysis of apparent resistivities and the evaluation of both smooth and blocky (robust) inversion methods it was determined that the robust inverse modeling method best modeled the apparent resistivity data because of sharp contrast in the apparent resistivity data. The smooth inversion method gives better results where there are gradual changes in subsurface resistivity, whereas the robust method produces substantially better results where the subsurface geology consists of a number of regions that are almost homogeneous but with sharp boundaries between the different regions (Loke and others, 2003). A robust model inversion, based on the assumption of an exponential distribution of data errors (Burkardt, 2005; Advanced Geosciences, Inc., 2006), minimizes the integral of the absolute value of the difference between the measured and the calculated apparent resistivity.

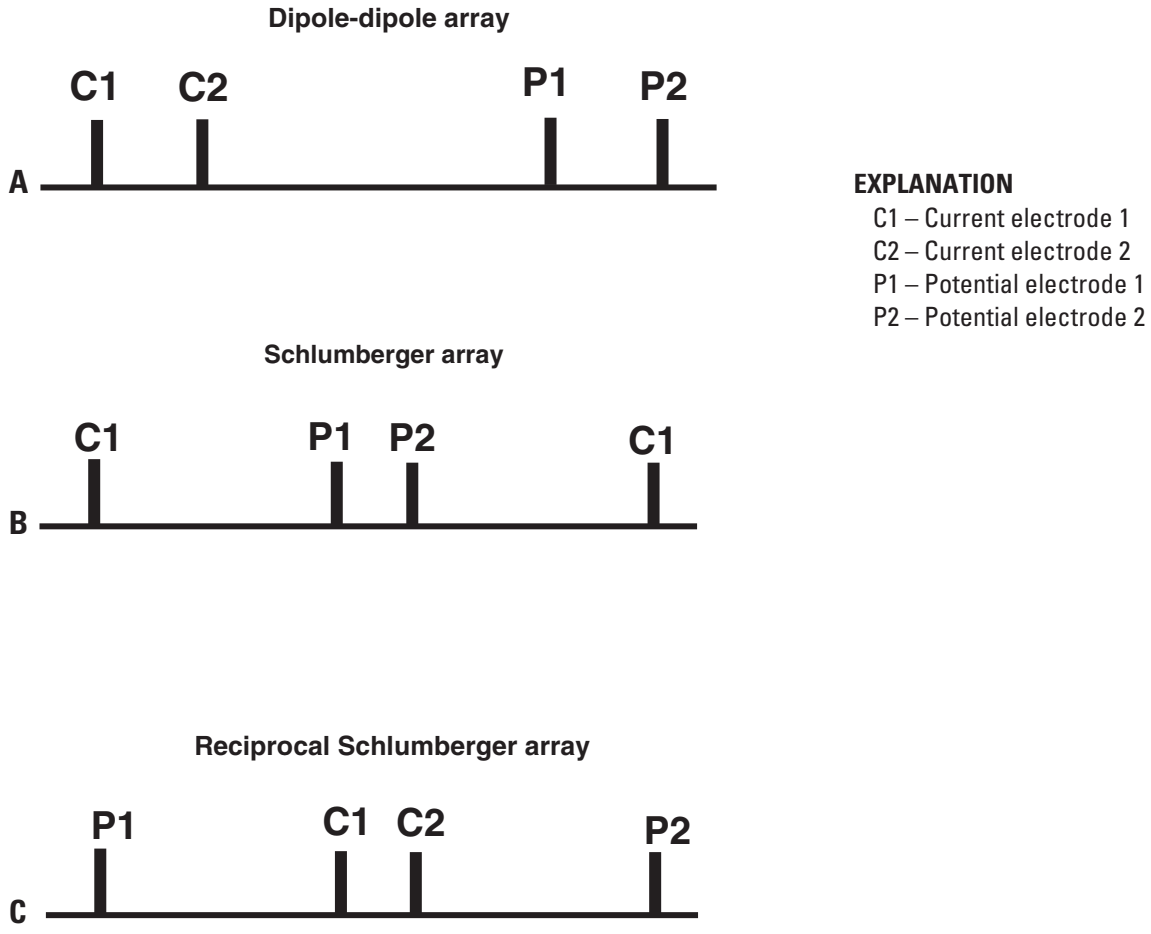


**Figure 8.** Configuration of current (C1 and C2) and potential (P1 and P2) electrodes used to collect direct-current resistivity data for (A) dipole-dipole array, (B) Schlumberger array, and (C) reciprocal Schlumberger array.

Model inversion parameters are settings that are applied to a model inversion to control certain criteria throughout the inversion process. All apparent-resistivity data were inverted using a maximum eight-iteration inversion. An inversion can be stopped prior to the eighth iteration when any of the stop criteria in the model inversion parameters are met. All data sets were first inverted without using any criteria for data removal. Model inversion parameters then were optimized for data processing and inverse modeling of the apparent resistivity data collected along the three profiles. Raw apparent-resistivity data initially were filtered using the criteria for data removal (appendix 5) to remove poor-quality data points. Data also were filtered during the inversion process on the basis of the resistivity inversion parameters (appendix 5). Because the three apparent resistivity profiles used to collect both dipole-dipole and reciprocal Schlumberger arrays yielded dense apparent-resistivity data sets, the data sets were processed as individual roll-alongs (subsections). By subsectioning large data sets and calculating model inversions for each subsection, data and model-convergence can be evaluated appropriately to address specific problem areas in a large profile.

## Borehole Drilling and Piezometer Installation

Borehole drilling was done with a Gardner-Denver model 17W direct rotary drill rig owned and operated by the USGS. A combination of tri-cone air-rotary and down-hole pneumatic hammer methods was used to complete the boreholes. In these drilling methods a large compressor forces high pressure air through the drill pipe and through ports in the bit. The high pressure forces the cuttings up through the annulus between the drill pipe and the borehole walls, thus providing a constant means of cuttings removal and air circulation to cool the bit. When using tri-cone bits, the combination of downward pressure exerted by the drill rig and the rotating action of the steel or carbide-studded rollers grinds the rock. During pneumatic hammer drilling, the bottom of the bit acts as a jackhammer, fracturing and pulverizing the rock for removal. In both methods, the cuttings are either ground or pulverized to a size sufficient to be removed by the up-hole air velocity and collected at land surface.

If during the drilling process, adequate ground water was not encountered, water from a potable source well at the IBWC Amistad Reservoir dam Project Office was injected into the boreholes to minimize the amount of dust generated and to assist in the cooling and lubrication of the drill bit.

A 250-millimeter tri-cone bit was used to drill the boreholes from land surface to a depth of about 1 meter. A 146-millimeter pneumatic hammer was then used to drill a pilot hole from 1 to about 4.5 meters. The 250-millimeter rotary bit was then re-attached and used to enlarge or “ream” the pilot hole to a diameter that would accept the surface casing and Portland cement seal. After the borehole was at a depth of about 4.5 meters, a 5-meter length of 168-millimeter outside diameter steel casing with a wall thickness of 5 millimeters was lowered into and centered in the hole. A type I/II Portland cement slurry was mixed and hand-poured into the annulus to form a surface seal from a depth of 4.5 to 1 meter below land surface. The remaining annulus was back-filled to land surface with bentonite chips or pellets, or both, and approximately 24 hours was allowed for the Portland cement to solidify. The 146-millimeter pneumatic hammer was lowered through the surface casing and used to drill from 4.5 meters below land surface to the completion depth of each borehole.

The piezometers were constructed to ATSM standards for design and installation of monitoring wells (American Society for Testing and Materials, 2004d), hereinafter referred to as ASTM D 5092–04. The piezometers were constructed subsequent to drilling and geophysical logging. A 0.3-meter layer of 8- to 16-mesh sand pack was piped to the bottom of the hole prior to setting the casing and screen. The piezometers were cased with 63.5-millimeter schedule 40 PVC casing and screen. The PVC casing sections were threaded together and lowered to the top of the 0.3-meter sand pack. A sand pack was piped to 0.6 meter above the screened interval. Next, 3.6 meters of bentonite pellets were placed on top of the sand pack. Bentonite grout was then mixed and piped to within 0.3 meter of land surface. Bentonite chips were used to fill the annulus between the PVC and steel surface casings from a depth of 0.3 meter to land surface.

One of the study objectives was to design and construct the piezometers in a similar fashion as the existing piezometers on the western embankment. Because some materials of the type used in the existing wells were unavailable, some design modifications were necessary. These modifications were discussed with USIBWC personnel and approved prior to construction. Design changes include the substitution of 0.040-inch (1-millimeter) (number 40) slot-size screen (horizontally slotted) for the 0.25-inch (6-millimeter) screen and 8- to 16-mesh sand pack for the 0.50-inch (13-millimeter) gravel pack used in the western embankment piezometers. According to ASTM D 5092-04, it is recommended that an 8- to 12-mesh sand pack be used in conjunction with a number 40 slot-size screen. The 8- to 16-mesh sand used in this project was factory-washed and sieved to a nominal particle size of 0.0469 to 0.0937 inch (1 to 2 millimeters), which correspond to respective mesh numbers of 18 and 8. Because the sand available was slightly smaller than is generally recommended, a sediment sump was placed below the screen in each well to catch any fine particles that might pass through the screen openings.

The piezometers on the western embankment were constructed using 2-meter screen lengths. Screens in metric lengths were not readily available, and it was not possible to cut the screens to 2 meters because of threaded joints; therefore screens in 10-foot (3.0-meter) lengths were used.

In addition to the screen and sand pack design modifications, the 2-meter cement plug used in the western embankment piezometers was omitted because of the likelihood of the cement filtering down through the lower bentonite seal and contaminating the sand pack prior to its solidifying.

# Geophysical Analysis

To efficiently compile, store, and compare geologic and geophysical data, a geodatabase was created at the beginning of the project and used throughout the project. Data were added to the geodatabase as the project progressed. Borehole geophysical logs, both existing and newly acquired, were compiled and merged into multiple-property logs for comparison and analysis. These logs are contained in appendix 3 and are described briefly in the sections below. Many borehole geophysical properties were recorded and used to obtain information on the geologic, lithologic, and water-yielding properties that lead to possible explanations of differences in resistivity of the rocks in the formations. Geophysical differences among layers were delineated and integrated with surface geophysical DC resistivity in two-dimensional (2D) and three-dimensional (3D) visualizations.

Each subsection of inverted DC resistivity was exported from AGI EarthImager 2D in an ASCII format. Subsequently, each subsection for a single profile was imported into a spreadsheet format and inputted into Oasis montaj using an array format that uses the distance as a reference point. An array format consists of multiple values for any given variable. In this case, there are multiple depths and resistivities for a given distance; therefore each depth and resistivity for a given distance would be placed into a new column. These data were imported into the geodatabase through the Oasis montaj Data Import Wizard, specifying the array columns.

Overlap present in the DC resistivity data from the roll-alongs for profiles 2 and 3 caused multiple resistivities for a given depth and distance. To combine these overlapping data points, a nonlinear filter operation was performed along the array channel using a filter width of two data points. This nonlinear filter analyzes each individual point resistivity and determines the validity of the data point using an algorithm based on the width of data features and the relation of these features to a local background (Geosoft Inc., 2006; Help Topic NLFILT GX). The number of data points specifies the filter width. If the data point is determined to be noise, it is replaced by an estimated value on the basis of interpolation from surrounding data-point values. These filtered values were then gridded using an array-channel section grid. The profiles were gridded using a minimum-curvature gridding method with a 0.25-meter grid-cell size.

All lithologic and geophysical data were plotted together on lithologic and resistivity sections for 2- and 3-D visualizations. The color scale for the DC resistivity profiles then was determined by matching the color zones in the DC resistivity profile with the lateral resistivity log for piezometer 106+00B (appendix 3). The color scale then was compared to the general geology throughout the profile to see if the highly resistive zones closely matched the zones of unweathered limestone. This process was repeated until a uniform color scale was obtained. Because of various resistivity changes between the dipole-dipole array and the reciprocal Schlumberger array, a unique color resistivity scale was determined for each.

## Analysis of Geologic Data and Geophysical Log Descriptions

On March 8, 10–12, and 19–22, 2006, geophysical logs were collected from individual wells below the Amistad Reservoir dam. All piezometers were completed in the Salmon Peak Formation except for the Brite well, which also penetrates the upper McKnight Formation. All geophysical log responses are discussed in relation to lithologic descriptions and possible anomalous features in the subsurface. All wells were logged using at minimum, the geophysical methods of natural gamma and induction conductivity, which can be collected in open holes or PVC-cased piezometers. The existing piezometers on the western embankment were LA–12L, LA–11, LA–10, LA–16L, LA–15, LA–8L, and LA–7 (fig. 2A). The piezometers drilled by USGS and logged on the eastern embankment were 105+90B, 105+90A, 106+00B, 106+00A, 106+00C, and 106+00D (fig. 2B). The Brite well also was logged. In addition to the previously mentioned minimum suite of logs, open-hole logging techniques were used on the eastern embankment (where applicable) including electric long (64N) and short (16N) normal resistivity, SP, fluid conductivity, temperature, acoustic velocity, full-waveform sonic VIL, ATV, and EM flowmeter, caliper, and casing collar locator. For various reasons, not all geophysical methods were used on all wells. For example, some wells did not contain a static fluid column over the total length of the borehole at the time of logging, which inhibits the collection of flowmeter, acoustic, and electric logs. The descriptions contained in this section mostly will pertain to geophysical variations that relate to effects on resistivity such as the water-yielding properties of the rocks and do not constitute a complete analysis of every geophysical response. All depths are in meters below land surface datum (LSD). The borehole geophysical logs are contained in appendix 3.

## Western Embankment Investigation

### Analysis of Hydrogeologic Data

The geodatabase was used to create two 2D sections (fig. 9, at end of report) of lithologic data along DC resistivity profiles 1 and 2 on the western embankment. The lithologic sections were created by projecting lithologic data in the geodatabase 200 meters west or east of a line centered along DC resistivity profile 1 (fig. 9A). A second section was created by projecting all available geologic data 200 meters north and south of profile 2 (fig. 9B). The sections were used to identify the depth and extent of the alluvium, the weathered features in limestone, and the argillaceous fossiliferous zone along each DC resistivity profile.

Geologist descriptions of the borings along DC resistivity profile 1 (fig. 9A) indicate a concentration of weathered features in the Salmon Peak Formation extending from about

295 meters above NAVD 88 to a few meters below land surface, except for boring (LA–12), which indicates a second zone of weathered features ranging from about 278 to 285 meters above NAVD 88. Borings south of the toe of the dam (fig. 9A) are shallow and do not identify the total depth of weathered features in the Salmon Peak Formation. Borings indicate an argillaceous fossiliferous zone in the Salmon Peak Formation that ranges from about 280 to 290 meters above NAVD 88. The argillaceous fossiliferous zone was identified consistently in borings from Amistad Reservoir prior to dam construction and serves as a distinct geologic marker throughout the study area. The top of this feature was identified along sections of lithologic data (fig. 9A–B) to visualize its vertical displacement, which can be used as an indicator of faulting throughout the study area. The lithologic section along DC resistivity profile 1 shows a continuous surficial alluvial layer ranging from about 2 to 5 meters thick.

The thickness of the zone of weathered features varies along the section ranging in thickness from about 18 to 40 meters, and the top of the zone ranges in elevation from 332 to 324 meters above NAVD 88. Two borings, LA–12L and LA–16L, indicate a secondary weathered zone; however, the total thickness of that zone was not identified. The alluvial layer along profile 2 is a continuous layer extending from a depth of about 320 meters above NAVD 88 to land surface and ranging from about 2 to 7 meters thick.

## Borehole Geophysical Log Analysis

Seven piezometers along the western embankment (LA–12L, LA–11, LA–10, LA–16L, LA–15, LA–8L, and LA–7) were logged through casing using borehole geophysical methods in March 2006. The open boreholes were logged at the time of drilling in June 1995 by MxIBWC. Selected logs run in open boreholes in 1995 were digitized from photocopies for inclusion in this report (appendix 3). A detailed log analysis is provided in appendix 2 that includes discussion of the individual logs (appendix 3) for each piezometer starting with the deepest piezometer LA–12L and continuing along that transect to the shallowest piezometer (LA–10). A brief discussion of the geophysical properties related to the water-yielding properties of the formation or other information, or both, that could relate to resistivity follows.

Piezometer LA–12L, near the toe at of the dam on the western embankment, extends about 50 meters below LSD (fig. 2A; appendix 3). The neutron log is an indicator of the presence of hydrogen (Keys, 1990), which absorbs neutrons and reduces the neutron count rate. Decreased count rates are shown on the neutron log at 3–6, 7.5–8.5 and 18.5 meters below LSD because of shale beds at those depths. The neutron log for piezometer LA–12L shows relatively low count rates from 20 meters to the bottom of the borehole compared with the upper part of the borehole. Compared to the other boreholes, this zone shows the lowest neutron count rate, possibly indicating the greatest water content of the all western embankment borehole logs. However, slightly increased count rates are at 27–28, 29.5–32, 37–42, and 44.5–48.5 meters below LSD, zones which also are coincident with zones of lower natural gamma responses, indicating relatively pure limestone, with little shale or clay, at those depths. Possible zones of increased water content in the formation are at 24–27, 32–36.5 and 41–44 meters below LSD.

Piezometer LA–11 is about 141 meters southeast of piezometer LA–12L on the western embankment and extends about 20 meters below LSD (fig. 2A, appendix 3). The natural gamma log peaks from piezometer LA–11 generally correlate with shale and clay on the lithology log provided by MxIBWC (Paul Gibson, U.S. Section, International Boundary and Water Commission, written commun., 2006); the natural gamma log shows excellent correlation with the induction resistivity and conductivity logs and neutron log at 3.5–8 and 14.3–15.3 meters below LSD as related to clay or shale layers. Interpretations of decreased neutron count rate and decreased natural gamma count rate indicate possible zones of increased water content in the formation at 8–9, 12–13, and 16.8–17.8 meters below LSD.

Piezometer LA–10 is about 286 meters southeast of piezometer LA–12L on the western embankment and extends about 15 meters below LSD (fig. 2A; appendix 3). The natural gamma log from piezometer LA–10 shows two zones of increased count rate at 2.8–3.4 and 10.5–11 meters below LSD that correspond to interbedded shale beds in the lithologic descriptions and zones of decreased count rates on the neutron log. Somewhat decreased count rates also are at 3.5–4.5 and 12.7–14 meters below LSD, zones which correspond to weathered limestone zones with decreased gamma count rates; such zones appear to contain higher amounts of hydrogen (Keys, 1990) and are assumed to be water-yielding zones in the limestone. The induction resistivity log shows very little variation in resistivity and mostly greater than 100 ohm-meters, except for the interbedded shale zone at 2.5–3.5 meters below LSD where the resistivity decreases to less than 100 ohm-meters.

Piezometer LA–16L is about 189 meters east-northeast of piezometer LA–12L on the western embankment and extends about 47.5 meters below LSD (fig. 2A, appendix 3). Piezometer LA–16L logs indicate that beneath a shale layer at 15.5–16.5 meters below LSD the neutron count rate decreased at 21–28 and 28.5–30.5 meters below LSD, which indicates increased water content in the weathered limestone.

Piezometer LA–15 is about 225 meters south-southeast of piezometer LA–16L on the western embankment and extends about 20 meters below LSD (fig. 2A, appendix 3). The natural gamma log of piezometer LA–15 shows increased count rates at 1.75–4.5 and 11.3–12.3 meters below LSD, zones that correspond with shale layers on the lithology log (Paul Gibson, U.S. Section, International Boundary and Water Commission, written commun., 2006) and with zones of increased conductivity and decreased resistivity per those logs. The neutron log shows decreased count rates in the shale layers noted above. Below the shale layer at 11.3–12.3 meters below LSD, the neutron count rate decreased, indicating increased water content in the weathered limestone.

Piezometer LA–8L is about 191 meters west-southwest of piezometer LA–12L on the western embankment and extends about 46.5 meters below LSD (fig. 2A, appendix 3). The natural gamma log for piezometer LA–8L shows increased count rates at 10–12, 14–15.5, and 37.5–40 meters below LSD. The zone at 10–12 meters below LSD corresponds with a shale layer on the lithology log (Paul Gibson, U.S. Section, International Boundary and Water Commission, written commun., 2006). Other zones of increased natural gamma count rate do not correspond with a shale layer on the lithology log (Paul Gibson, U.S. Section, International Boundary and Water Commission, written commun., 2006) and possibly could be caused by a clay-filled void (at 14–15.5 meters below LSD). A zone of increased induction conductivity and decreased resistivity at 5–9 meters correlates with gravel, clay, and shale, and interbedded shale layers along with a zone of decreased neutron count rate. Other zones of decreased neutron count rate are at 16.5–17.5, 22.4–23.5, 24.2–25.4, 28.8, and 31 meters below LSD; all occur in weathered limestone (Paul Gibson, U.S. Section, International Boundary and Water Commission, written commun., 2006) indicating possible water-yielding zones at these depths.

Piezometer LA–7 is about 223 meters south-southeast of piezometer LA–8L on the western embankment and extends about 20 meters below LSD (fig. 2A, appendix 3). The natural gamma log shows increased count rates at 5–6, 7.7–8.6, and 13.2–14.5 meters below LSD, zones that correspond with shale layers on the lithology log (Paul Gibson, U.S. Section, International Boundary and Water Commission, written commun., 2006) and with zones of increased conductivity and decreased resistivity per these logs. The caliper log shows increased borehole diameter at 3.5–6 and 16 meters below LSD, and large- and small-diameter responses at 16.9–17.6 meters below LSD. These zones are probably related to karst openings or fractures in the weathered limestone. The zone at 16.9–17.6 meters below LSD is unique in that it shows an increase in borehole diameter above and below a 0.5-meter zone of the borehole that is smaller than bit size. This smaller-diameter zone possibly indicates a swelling clay layer in a karst opening. The neutron log count rate decreased drastically in this zone, also indicating clay or water-yielding media, or both.

## Analysis of Resistivity Profiles 1 and 2

Two identifiable resistivity units are in both the dipole-dipole array data and reciprocal Schlumberger array data along DC resistivity profile 1 (fig. 10, at end of report). Resistivity unit 1, a near-surface, low-resistivity unit, generally ranges in resistivity from less than 45 to greater than 120 ohm-meters in the dipole-dipole array and from less than 75 to greater than 150 ohm-meters in the reciprocal Schlumberger array. The deeper, more resistive unit, resistivity unit 2, generally ranges in resistivity from about 120 to greater than 345 ohm-meters in the dipole-dipole array and from about 150 to greater than 365 ohm-meters in the reciprocal Schlumberger array. In both resistivity arrays, a vertical high-low resistivity boundary between resistivity unit 1 and resistivity unit 2 is observed at a horizontal distance of about 285 meters in the profile. The resistivities south of this boundary are relatively low except for two features in the dipole-dipole array and one feature in the reciprocal Schlumberger array.

DC resistivity profile 2 shows a similar two-unit electrical structure—a continuous, near-surface low-resistivity unit, resistivity unit 1, ranging from about 20 to less than 10 meters thick in the reciprocal Schlumberger array; and resistivity unit 2, a relatively high-resistivity zone that is well defined in the reciprocal Schlumberger array (fig. 10D), but becomes less so in the dipole-dipole array (fig.10C). Resistivity unit 2 in the dipole-dipole array is less well defined (distorted) from the beginning of the profile to about 475 meters. This distortion is attributed to poor-quality data, of which about 40 percent was removed in the inversion process. A low-resistivity feature is observed at about 250 meters along the profile in both arrays in about the lowermost 50 meters of the profile.

## Integration of Results

The upper extent of major lithologic features identified in lithologic sections (fig. 9A–B) were superimposed on DC resistivity profiles 1 and 2 (fig. 11, at end of report) to conduct an assessment of the hydrogeologic characteristics of the Salmon Peak Formation along the western embankment. The lithologic section along DC resistivity profile 1 shows a concentration of weathered features extending to about 295 meters above NAVD 88 except for boring LA–12, which indicates a second zone of concentrated weathered features ranging from about 278 to 285 meters above NAVD 88. These zones of weathering generally correlate with the thickness and extent of resistivity unit 1 (low resistivity) near the toe of the dam. Although the total thickness of resistivity unit 1 was not completely ground-truthed by the geologist descriptions, borings from LA–12 and LA–16 do indicate that a deeper secondary weathered zone is present; however the total depth was not identified. Neutron logs from LA–12 and LA–16 identify possible zones of increased water content in the formation occurring from the bottom of the boring to about 20 meters below LSD. Compared to the other boreholes, LA–12 shows the lowest neutron count rate in this zone possibly indicating the greatest water content of all western embankment borehole logs. The presence of mapped sinkholes (fig. 1) in the reservoir north of the western embankment study area and the zone of increased water content in LA–12 indicated by the neutron log leads to the conclusion that resistivity unit 1 (fig. 10A–B) is a preferential flow path where surface water from Amistad Reservoir is forced into the ground-water system (because of increased head from the reservoir). The increased occurrence of weathered limestone along this profile indicates a potential conduit for ground-water movement along resistivity unit 1 identified in profile 1 (fig. 10A–B).

A vertical high-low resistivity boundary, at about 285 meters along profile 1 (fig. 10A–B), was identified in both

arrays. Borings along the south end of this profile are shallow and do not identify the total depth of weathered features (low resistivity). The high resistivity side of the boundary in profile 1 is evident in profile 2 because profile 2 intersects profile 1 at about 257 meters. This high-resistivity zone (2) along profile 1 (fig. 11A–B) begins to increase in elevation from about 850 meters along the profile (fig. 11C) to the end of the profile. This increase in elevation of resistivity unit 2 at about 850 meters correlates to the location of springs 1, 2, and 3 (fig. 11A–B), which suggests that water moves through the preferential flow path (resistivity unit 1) and discharges to the surface through the springs because of the presence of more resistive, less weathered (less permeable) limestone.

Comparison of the inverse modeling results of DC resistivity profiles 1 and 2 to the lithologic sections, together with interpretations of borehole geophysical neutron logs, leads to the conclusion that the low-resistivity unit (1) in profiles 1 and 2 are zones of increased weathering in the Salmon Peak Formation which is indicative of a preferential flow path for ground-water movement. This electrical contrast of high and low resistivity was used in the evaluation of DC resistivity data collected in the eastern embankment study area. To provide an alternative and complimentary presentation of the geologist descriptions of borings, available neutron logs, and DC resistivity profiles 1 and 2, a 3D section map was produced (figs. 12–13, at end of report). 3D visualization allows a comprehensive view of selected data that were used to interpret the preferential flow path in the western embankment study area. An important consideration regarding the 3D images is that they are constructed from the 2D inversion results with each line independent of one another (McDougal and others, 2004). The data have been interpreted by a 2D inversion that contains no information of other profiles and, therefore, is not constrained by the adjacent data set. This can result in disagreement of resistivity values where the profiles cross (McDougal and others, 2004).

## Eastern Embankment Investigation

The service road along the southern toe of the eastern embankment was selected for DC resistivity profile 3 (fig. 2B). (The service road has little traffic and a shoulder that was clear of brush, thus facilitating the collection of the DC resistivity data. Data collection in a westerly direction was limited because of the intersection of another service road where heavy equipment was transported for quarrying operations.) The starting point along the service road for DC resistivity profile 3 was determined by (1) examining the spatial trend of documented sinkholes (fig. 2B) and (2) visually analyzing the thickness and extent of the weathered zones in the Salmon Peak Formation. A line of sinkholes has formed along each of two zones semi-perpendicular to the eastern embankment (figs. 1, 2B). The first zone occurs between borings A32V and A23E and the second is between borings A15V and A15E. Analysis of the lithologic section indicated that profile 3 should start in the first zone of sinkholes and extend east through the second zone of sinkholes.

### Analysis of Lithologic Data

To assess the hydrogeologic characteristics of the Salmon Peak Formation along the eastern embankment, a 2D section of available lithologic data (fig. 14, at end of report) was developed from all data 200 meters north or south of a line centered between the historical borings and the service road. Analysis of the lithologic section indicates that the weathered zone is thickest along the east end of the section; thus the second zone of sinkholes subsequently was given priority over the first zone with regard to geophysical analysis for piezometer siting (see “Eastern Embankment Piezometer Placement” section).

### Analysis of DC Resistivity Profile 3

In both the dipole-dipole array and the reciprocal Schlumberger array, resistivity unit 1 is separated into three different parts by resistivity unit 2 (fig. 15, at end of report). The profiles can be divided into vertical sections for detailed analysis and are designated in the analysis by meters along the profile. The first part of resistivity unit 1 is from the beginning of the profile (0) to about 280 meters (western expression) along the profile. Resistivity unit 2 starts to decline in elevation from the surface at about 380 meters along the profile (central expression). From that point, resistivity unit 1 continues until resistivity unit 2 rises back to the surface at about 750 meters along the profile. The last part of resistivity unit 1 (eastern expression) appears again at about 990 meters along the profile and continues to the end of the profile. The base elevation of resistivity unit 1 decreases gradually from the beginning (west) of the profile to the end (east). At the beginning of the profile, the base elevation of resistivity unit 1 is about 315 meters above NAVD 88, and at the end of the profile, the elevation is about 295 meters above NAVD 88. The last 330 meters along the profile of resistivity unit 1 is difficult to distinguish because of the multiple resistive features in the unit. These resistive features show a similarity to the features in profile 1 at the western embankment study site (fig. 10). In profile 1, a sharp vertical boundary occurs between resistivity unit 1 and resistivity unit 2. Resistivity unit 1 becomes appreciably thicker at that boundary. A vertical boundary between resistivity unit 1 and resistivity unit 2 occurs at about 990 meters along profile 3 where resistivity unit 1 becomes thicker. The thickness of resistivity unit 1 from 990 meters along the profile to the end of the profile is more than double the average thickness of resistivity unit 1 from the beginning of the profile to 750 meters along the profile.

The western and eastern expressions of resistivity unit 1 correlate with the general trend of sinkholes (fig. 2B) documented by the USIBWC in the eastern embankment study area. To assess the hydrogeologic characteristics of the Salmon

Peak Formation in the eastern embankment study area along DC resistivity profile 3, the upper extent of major lithologic features (fig. 14) were superimposed on DC resistivity profile 3 (fig. 16, at end of report). The thickness and extent of weathered zones do not correlate with the thickness and extent of the western expression of resistivity unit 1. There is, however, a substantial increase in the thickness of weathered zones in the limestone west of DC resistivity profile 3 shown by the first two geologist descriptions of borings (fig. 16B).

Lithologic data show that the thickness of resistivity unit 1, along its central and eastern expressions, corresponds generally with the extent and thickness of weathered zones in the limestone (fig. 16); however, there is an increase in the thickness of alluvial deposits (fig. 14) along the central expression of resistivity unit 1. Because alluvium tends to be less resistive than limestone (Loke, 2004), it is possible that the decrease in resistivity along the central expression of resistivity unit 1 is predominantly influenced by the increased thickness of alluvium more so than the underlying weathered limestone.

Because of the lack of lithologic correlation along the western expression and the increased thickness of alluvium along the central expression, these features were not chosen for further exploration. The zone of concentrated weathered features on the eastern end of DC resistivity profile 3 is thickest and extends to a greater depth along the eastern end of the section. The correlation of surface geophysical DC resistivity, historical lithologic data, and general trend of documented sinkholes along the eastern end of profile 3 were used to justify further exploration (drilling of piezometers) in the eastern expression of resistivity unit 1.

## Borehole Geophysical Log Analysis

Geophysical logging occurred immediately after drilling was completed, before casing was set on all but one well logged on the eastern embankment. A detailed log analysis provided in appendix 2 includes discussion of the individual logs (appendix 3) for each piezometer from the deepest piezometers (105+90B and 106+00B) to the shallowest piezometer (105+90A). A brief discussion of the geophysical properties related to the water-yielding properties of the formation or other information, or both, that could relate to resistivity follows.

Piezometer 105+90B is the deepest of the 105+90 pair of piezometers, extending to about 36 meters below LSD (fig. 2B, appendix 3). Several zones of enlarged borehole diameter are evident on the caliper log, probably related to karstification or fracture openings in the limestone. These zones are centered at 6, 8, 12.2, 22.5, 24.5, 27.3, 27.8, and 30.5 meters below LSD. The natural gamma log shows increased count rates in all of these enlarged zones. Increased count rates probably are caused by clay commonly contained in karst openings. Visible in the borehole televiewer image are some indications of open dissolution voids and bedding planes or low-angle fractures, many of which correspond with caliper enlargements. Some easily identifiable voids occur at 7.5–8.5, 12.2, 14.2–14.5, 15, 22.5, 24.5, 25, 27–28.7, and 30.3–30.8 meters below LSD. The fluid conductivity curve indicates a slightly lower-conductivity (fresher) fluid at the bottom of the hole, which probably is aquifer water entering the hole at the bottom and displacing slightly higher-conductivity fluid that was left in the hole from drilling. The temperature curve has a trend similar to that of the fluid conductivity and shows a slightly lower temperature near the bottom of the borehole.

Piezometer 105+90A extends to about 10.7 meters below LSD and is a shallow companion to piezometer 105+90B, which is 3.5 meters southeast (fig. 2B, appendix 3). The caliper log shows zones similar to those of 105+90B, increased borehole diameter at 6 and 8 meters below LSD, which indicates possible laterally continuous openings at those depths between piezometers 105+90A and 105+90B. The coincidence of natural gamma peaks and caliper anomalies indicates clay is in the karst openings as was indicated in 105+90B. An anomaly of decreased fluid conductivity at about 9 meters below LSD could indicate relatively fresh inflow into the borehole from the aquifer.

Piezometer 106+00B is the deepest of the 106+00 pair of piezometers and the deepest of the USGS-drilled wells, extending to about 48 meters below LSD (fig. 2B, appendix 3). The zone at 16.5–21 meters below LSD shows a smaller decrease in resistivity (but shows a similar trend) compared to that for piezometer 105+90B, which is 3 meters from piezometer 106+00B. The geologist description of this zone in piezometer 106+00B does not note limey shale as does the description of the less resistive zone in piezometer 105+90B but does note hard clay layers and a decrease in clay content with depth. A few zones of enlarged borehole diameter evident on the caliper log probably are related to dissolution or fracture openings in the limestone. Two large openings occur at 6.5–8.5 meters below LSD (referred to as the upper void) and 10.5–12 meters below LSD (referred to as the lower void) with diameters of 30 centimeters in the upper void and greater than 45 centimeters in the lower void. At the time of logging, the water level in the borehole was about 8.4 meters below LSD, which corresponds to the bottom of the upper void. This indicates that water could be exiting the borehole at this point. The natural gamma log shows increased count rates on both of these borehole enlargements. Increased counts probably are caused by the presence of clay that commonly is contained in karst openings. Elsewhere in piezometer 106+00B, natural gamma peaks coincide with small enlargements at 14.8, 24.3, 30.7, 34, and 37.5 meters below LSD, which probably are associated with dissolution-enhanced bedding-plane- or fracture-related openings. The ATV image and acoustic delta-T fluctuations (or cycle-skips) also indicate fracture or bedding-plane-related anomalies at these depths.

A computer generated virtual core analysis of piezometer 106+00B using the caliper and ATV data of zones not showing natural gamma peaks indicates several additional zones of fractures or dissolution openings at 15–16, 19.7,

21–21.5, 22.5, 27.25, 34.5–35.5, 38–39, and 45.5–48 meters below LSD. The horizontal features intersecting the borehole at 22.5, 24.3, and 30.6 meters below LSD appear to produce discontinuities for acoustic wave-energy propagation along the borehole, creating a diagonal effect on the full-waveform sonic VIL near these depths.

Piezometer 106+00A extends about 26 meters below LSD and is a shallow companion to piezometer 106+00B, which is 3.5 meters southeast (fig. 2B, appendix 3). Resistivity logs, including induction, normal, and lateral logs, all show some variation in resistivity, especially the zones at 10–12.5 meters below LSD (similar to 106+00B) and 17–18 meters below LSD. The 64N resistivity log, which measures deeper into the formation (with less resolution) than the 16N decreases only slightly at 17–18 meters and actually reads higher than the 16N and lateral logs at the 10–12.5-meter zone, which indicates that the 16N and lateral logs probably are being influenced by borehole fluid in the area of the formation closest to the borehole wall; this also was the case in piezometer 106+00B. Both zones show erratic acoustic delta-T readings (cycle-skips) because of irregular borehole diameter, or fractures, or both. The horizontal features intersecting the borehole at 12, 15, 17.5, 20, 22.5, and 24.5 meters below LSD appear to produce discontinuities for acoustic wave-energy propagation along the borehole, creating a diagonal effect on the full-waveform sonic VIL near these depths. At about 12 meters below LSD, the caliper indicates a 10-centimeter diameter increase, and the ATV image indicates a large void; a similar feature is at 17.5 meters below LSD. Both features appear to be karst openings that are transmitting water. The EM flowmeter shows upward flow that originates below 24 meters below LSD and decreases at about 16 meters below LSD. The water level continuously declined as the logging was in progress and became stable at about 12 meters below surface, at the same depth as the upper karst opening.

Piezometer 106+00C is about 24 meters below LSD and is the third piezometer in the 106+00 transect. The piezometer was placed 137 meters south of piezometers 106+00A and 106+00B, which are near the toe of the dam (fig. 2B, appendix 3). The geophysical logs for piezometer 106+00C indicate a decrease in induction resistivity and an increase in natural gamma count rate at 10–12.5 meters below LSD, probably in response to the large borehole diameter that is likely the result of a dissolution cavity. The cavity appears to be about 2 meters high on the basis of the caliper log response. The increase in natural gamma count rate at 10.5–12.5 meters probably is caused by the abundance of clay in the cavity, as described in the geologist description. This cavity also was the likely exit point of some water added to the borehole. The ATV shows an excellent image of the trace of the bottom of this cavity at 12.5 meters below LSD. Similar sets of responses occur at 13–13.5 meters below LSD at a much smaller scale. At 13.5–16 meters below LSD the increase in resistivity, as shown on the 16N, 64N, and lateral logs, probably is the result of unsaturated, dense limestone (as given in the geologist description). Immediately below the relatively high-resistivity zone at 16–16.4 meters below LSD, a natural gamma count rate increase appears to correspond to a dark trace on the ATV that is probably a horizontal opening containing clay. This horizontal feature intersecting the borehole appears to produce discontinuities for acoustic wave-energy propagation along the borehole, creating a diagonal effect on the full-waveform sonic VIL at 15.7–16.4 meters below LSD.

Piezometer 106+00D is about 21.6 meters below LSD and is the fourth piezometer in the 106+00 transect. The piezometer was placed 275 meters south of piezometers 106+00A and 106+00B, which are near the toe of the dam (fig. 2B; appendix 3). Resistivity logs, including induction, normal, and lateral logs, all show some variation in resistivity, with a decrease (in induction resistivity) at 10–12 meters below LSD and an increase (in 16N, 64N, and lateral log resistivity) at 15–17 meters below LSD. The log responses from this piezometer are very similar to those of piezometer 106+00C. The zones mentioned above correlate with similar responses in piezometer 106+00C on the induction resistivity, 16N/64N/lateral log resistivity, natural gamma, caliper, ATV image, and VIL.

The Brite well is located 662 meters southwest of piezometer 106+00A and extends about 133 meters below LSD (fig. 2B, appendix 3). On March 11, 2006, at the time of logging, the well flowed at about 2.8 liters per second from the casing at land surface. The well log indicates an interval of variable and irregularly increased borehole diameter, probably associated with karst- or fracture-related openings. This interval occurs in the McKnight Formation below 119 meters below LSD. Consequently, most of the flow that is moving up the borehole originates from the McKnight Formation as evident in the ambient EM flowmeter measurements, increasing from about 0.2 liter per second (upward) at 126 and 128 meters below LSD to greater than 3 liters per second (upward) at 121.5 meters below LSD. Also, the fluid conductivity shows greater variation of fluid conductivity in the McKnight Formation than in the Salmon Peak Formation; fluid conductivity ranges from about 1,160 to about 1,190 microseimens per centimeter, possibly indicating a mixing of various sources of water in the borehole.

## Integration of Results

Comprehensive evaluation of surface geophysical DC resistivity data, borehole geophysical data, and lithologic data were used to establish a relation between low-resistivity features identified in the surface geophysical resistivity data and zones of increased weathering in the Salmon Peak Formation at the western embankment study site. By evaluating the general trend of sinkholes and sections of lithologic data using a geodatabase, an area was selected for DC resistivity data collection along the eastern embankment. The results of the DC resistivity survey were used to identify three expressions of resistivity unit 1 (low-resistivity unit) showing similar characteristics to those identified at the western embankment study site. The eastern expression of resistivity unit 1 was

selected for further exploration and piezometric head monitoring. The piezometer 106+00 transect intersects profile 3 at about 1,140 meters along the profile. Although borehole geophysical logs provide highly detailed information proximal to the boring, and surface geophysical data provide continuous big-picture information, the results of the dipole-dipole array and reciprocal Schlumberger array data collected along profile 3 have been superimposed on the borehole geophysical logs for piezometers 105+90B, 105+90A, 106+00B, and 106+00A for comparison. Combining the two data sets allows the geophysical analyst to identify general log characteristics to better understand the hydrogeologic characteristic most controlling the changes in resistivity shown in the surface geophysical DC resistivity data.

Included in the piezometer 105+90B log is a 6-meter section of surface DC resistivity for the dipole-dipole array and for the reciprocal Schlumberger array. The surface DC resistivity sections are superimposed on the resistivity logs and indicate three discernible resistivity units. These three resistivity units can be observed in the dipole-dipole array and in the borehole resistivity logs and correlate with resistivity units 2, 1, and 2, respectively, identified in the western embankment study area (appendix 3). These three resistivity units are observed in their entirety in the reciprocal Schlumberger array for this piezometer even though there appears to be only a slight increase in resistivity near the bottom of the well. In the dipole-dipole array, the uppermost expression of resistivity unit 2 decreases in resistivity at about 7.5 meters below LSD; in the reciprocal Schlumberger array, the decrease in resistivity begins at about 6.5 meters below LSD. This decrease in resistivity is the expression of the upper extent of resistivity unit 1 and continues downward to the base of resistivity unit 1 at 34 meters below LSD where resistivity unit 2 appears again. The expression of resistivity unit 2 at 34 meters below LSD is more evident in the dipole-dipole array as a sharp resistivity increase but appears only as a slight increase in resistivity as shown in the reciprocal Schumberger array. The delineation of resistivity unit 1 is at 7.5–34 meters below LSD in the dipole-dipole array and at 6.5–34 meters below LSD in the reciprocal Schlumberger array. The lowest DC resistivity values in resistivity unit 1 appear at about 18–22 meters below LSD in the dipole-dipole array and at about 15–23.5 meters below LSD in the reciprocal Schlumberger array. These lowest values of DC resistivity correspond with the zone of lowest resistivity on the normal and lateral resistivity logs at 17–22 meters below LSD.

Included in the piezometer 105+90A log is a 6-meter section of surface DC resistivity for the dipole-dipole array and for the reciprocal Schlumberger array. Both arrays indicate a single resistive layer (resistivity unit 2) near this piezometer.

The surface DC resistivity sections superimposed on the piezometer 106+00B resistivity logs indicate three discernible resistivity units. These three resistivity units, observed in the dipole-dipole array and in the borehole resistivity logs, correlate with resistivity units 2, 1, and 2, respectively, identified in the western embankment study area (appendix 3). The dipole-dipole and reciprocal Schlumberger arrays for the surface DC resistivity indicate three resistivity units near this piezometer. The three resistivity units consist of resistivity unit 2 at the top and bottom of the well and a conductive resistivity unit 1 in the middle. In both arrays, the uppermost expression of resistivity unit 2 decreases in resistivity at about 11 meters below LSD and continues downward to the base of resistivity unit 1 at 35 meters below LSD, where resistivity unit 2 appears again. In the dipole-dipole array, this decrease in resistivity is the expression of the upper extent of resistivity unit 1 and continues to about 35 meters below LSD, becoming very resistive at about 46 meters below LSD. The expression of resistivity unit 2 at 35 meters below LSD is more evident in the dipole-dipole array as a sharp resistivity increase but appears only as a slight increase in resistivity in the reciprocal Schumberger array. The delineation of resistivity unit 1 is at 11–35 meters below LSD in the dipole-dipole array and at 11–38 meters below LSD in the reciprocal Schlumberger array. The lowest DC resistivity values in resistivity unit 1 appear at about 18–23.5 meters below LSD in the dipole-dipole array and at about 15–23.5 meters below LSD in the reciprocal Schlumberger array. These lowest values of DC resistivity correspond with the zone of lowest resistivity on the normal and lateral resistivity logs at 17–23 meters below LSD, except for the lower void at 10.5–12 meters below LSD.

Included in the piezometer 106+00A log is a 6-meter section of the surface DC resistivity profile for the dipole-dipole array and for the reciprocal Schlumberger array. Both arrays indicate two resistivity units near this piezometer. These two resistivity units consist of resistivity unit 2 directly above a more conductive resistivity unit 1. In the dipole-dipole array, the uppermost expression of resistivity unit 2 decreases in resistivity at about 12 meters below LSD and contains a highly resistive zone at about 4–7 meters below LSD. The uppermost expression of resistivity unit 2 in the reciprocal Schlumberger array decreases in resistivity at about 12.5 meters below LSD. The lowest DC resistivity values in resistivity unit 1 appear at about 21.5–24 meters below LSD in the dipole-dipole array and from about 21 meters below LSD to below the bottom of the piezometer in the reciprocal Schlumberger array. These lowest values of DC resistivity do not correspond well to the lowest values on the normal resistivity logs nor do the highest values of DC resistivity. A possible reason for this lack of agreement is that water was added to the borehole just prior to logging, thus the rock and clay surrounding the borehole probably were not saturated at the time of logging. The water level was declining as water exited the borehole during logging at the void at 12 meters below LSD and then became stable. Another explanation might be that the karst system is nonhomogeneous or that the DC resistivity data were collected 20–30 meters south of the piezometer.

The surface DC resistivity sections superimposed on the resistivity logs for piezometers 105+90B and 106+00B indicate three discernible resistivity units that can be observed in the dipole-dipole array and in the borehole resistivity logs. These three resistivity units correlate with resistivity units 2, 1, and 2, respectively, identified in the western embankment

**Table 3.** Locations and construction information for observation wells near Amistad Reservoir dam, Val Verde County, Texas, and Coahuila, Mexico.

[LSD, land surface datum; --, not applicable]

| Embankment | Piezometer identifier | Latitude | Longitude | Altitude of LSD (meters above NGVD 88) | Altitude of top of casing (meters above NGVD 88) | Altitude of top of screened interval (meters above NGVD 88) | Distance from LSD to top of screened interval (meters) | Altitude of bottom of screened interval (meters above NGVD 88) | Altitude of bottom of completed well (meters above NGVD 88) | Length of screened interval (meters) | Total drilled depth below LSD (meters) |
|---|---|---|---|---|---|---|---|---|---|---|---|
| Western | LA–12L | 29 26.928 | 101 04.758 | 333.344 | -- | 289.34 | 44 | 287.34 | 283.34 | 2 | 50 |
| Western | LA–11 | 29 26.859 | 101 04.721 | 331.143 | -- | 315.14 | 16 | 313.14 | 311.14 | 2 | 20 |
| Western | LA–10 | 29 26.786 | 101 04.686 | 328.942 | -- | 316.94 | 12 | 314.94 | 313.94 | 2 | 15 |
| Western | LA–16L | 29 26.963 | 101 04.647 | 334.734 | -- | 296.48 | 38.25 | 293.73 | 287.18 | 2 | 47.5 |
| Western | LA–15 | 29 26.877 | 101 04.632 | 331.886 | -- | 317.88 | 14 | 315.88 | 311.88 | 2 | 20 |
| Western | LA–8L | 29 26.877 | 101 04.861 | 334.355 | -- | 294.35 | 40 | 292.35 | 284.35 | 2 | 46.5 |
| Western | LA–7 | 29 26.816 | 101 04.808 | 332.296 | -- | 317.79 | 14.5 | 315.79 | 312.29 | 2 | 20 |
| Eastern | 105+90B | 29 27.160 | 101 02.363 | [1]335.149 | 334.13 | 304.91 | 30.23 | 301.86 | 299.14 | 3.05 | 36 |
| Eastern | 105+90A | 29 27.160 | 101 02.363 | [1]335.149 | 334.80 | 328.16 | 6.98 | 325.14 | 324.34 | 3.02 | 10.7 |
| Eastern | 106+00B | 29 27.160 | 101 02.363 | [1]335.149 | 335.36 | 290.89 | 44.25 | 287.84 | 286.84 | 3.05 | 48.2 |
| Eastern | 106+00A | 29 27.167 | 101 02.365 | [1]335.149 | 335.25 | 314.26 | 20.88 | 311.21 | 309.14 | 3.05 | 26 |
| Eastern | 106+00C | 29 27.096 | 101 02.325 | [2]334.573 | 335.35 | 318.25 | 16.32 | 315.20 | 310.57 | 3.05 | 24 |
| Eastern | 106+00D | 29 27.037 | 101 02.288 | [2]333.875 | 335.36 | 319.61 | 14.26 | 316.56 | 311.87 | 3.05 | 21.6 |
| Eastern | Brite well | 29 26.810 | 101 02.387 | 324 | -- | 314 | 10 | 194 | 276.45 | 120 | 133 |

[1] Same altitude used for 105+90B, 105+90A, 106+00B, and 106+00A (Paul Gibson, U.S. Section, International Boundary and Water Commission, written commun., 2006).

[2] From Paul Gibson (U.S. Section, International Boundary and Water Commission, written commun., 2006).

study area. The delineation of resistivity units 1 and 2 in the DC resistivity profiles generally corresponds with low and high resistivity zones, respectively, on the normal and lateral resistivity logs collected in the nearby piezometers at the time of installation. The surface DC resistivity sections superimposed on the resistivity logs for piezometer 106+00A indicate two discernible resistivity units that can be observed in the dipole-dipole array and that correlate with resistivity units 2 and 1, respectively; however, these units are not discernible on the resistivity logs for piezometer 106+00A. Piezometer 105+00A was not deep enough to observe both resistivity units.

A geologic characteristic that generally controls changes in resistivity is clay that commonly occurs in karst openings. This clay often is removed as variable lake levels force water through the karst openings at varying pressure heads.

## Eastern Embankment Piezometer Placement

The piezometer monitoring network along the eastern embankment was designed to function similarly to the western embankment network. The spatial location of the piezometers and the screened intervals were selected using the various 2D- and 3D-visualizations of lithologic data, borehole geophysical logs, and the inversion results of DC resistivity data to best match the locations of the screened interval of the western embankment piezometers and best satisfy the recommendations of Joint Report of the Technical Advisors of the International Boundary and Water Commission Regarding the Geotechnical, Electrical, Mechanical & Structural Safety of Amistad dam (Ken Breiton, U.S. Section, International Boundary and Water Commission, written commun, 2005).

Three piezometer nests (LA–8, LA–12, and LA–16) on the western embankment each consist of three separate piezometers open to zones that reflect deep, medium, and shallow hydraulic heads. These nests are at the toe of the dam and mark the northernmost piezometers in the three western embankment transects (fig. 2A). The piezometer transect constructed on the eastern embankment was designed to match the LA–12/LA–11/LA–10 transect on the western embankment in regard to hydrogeologic setting, lithologic zones, and similar elevations.

The horizontal location of the eastern embankment piezometers was determined by comparing the DC resistivity profiles for the two embankments (figs. 10–16). The locations of the screened intervals were duplicated by constructing the intervals at similar altitudes in some piezometers and similar lithologies in others (using core data and geophysical logs). Five piezometers were constructed on the eastern embankment to match the piezometers in that transect with the following piezometer numbers and screened interval rationale:

106+00B—similar screen elevation as LA–12L
105+90B—similar screen elevation as LA–12M
106+00A—same lithologic unit as LA–12L
105+90A—same lithologic unit as LA–12M
106+00C—same lithologic unit as LA–11
106+00D—similar elevation as LA–10 (because same lithologic unit is not present)

Piezometer LA–12M is a nearby shallow piezometer (depth of 34 meters and screened interval of 30 to 32 meters below LSD) paired with the deep piezometer LA–12L. Piezometer LA–12M was not logged for the reconnaissance study, but lithologies determined for piezometer LA–12L are considered similar to those in piezometer LA–12M.

Both USGS and USIBWC personnel agreed upon the horizontal and vertical placement of the eastern embankment piezometers. Table 3 shows the locations and construction information of the piezometers and wells used in the study. Schematic drawings of piezometer construction detail are included on the geophysical logs in appendix 3.

The results of the eastern embankment DC resistivity survey were used to identify three expressions of low-resistivity (resistivity unit 1) units showing characteristics similar to those identified and characterized as weathered limestone at the western embankment study site. This information was used to select vertical placement of well screens in the new piezometers (table 3).

## Summary

Amistad Reservoir dam, which impounds Amistad Reservoir on the Rio Grande in Val Verde County, Texas, and Coahuila, Mexico, was constructed in the late 1960s for flood control and water conservation storage for the benefit of the United States and Mexico. Impoundment of water began May 31, 1968. The dam is operated and maintained jointly by the U.S. and Mexico Sections of the International Boundary Water Commission (IBWC). Since 1992, numerous sinkholes have developed northwest of Amistad Reservoir dam. Increases in the discharge of springs south of the dam on the western side of the Rio Grande, in Coahuila, Mexico, have been documented. In 1995 the Mexico Section of the IBWC completed a study of the western embankment (Coahuila, Mexico) of the dam that included surface geophysics, borehole geophysics, and installation of piezometers to learn more about subsurface conditions. Piezometers were installed in three lines perpendicular to the centerline of the western embankment, with each line containing four piezometers. After the 1995 study, the centerline of a part of the western embankment was regrouted. As part of a 5-year safety inspection in 2005, technical advisors recommended that one line of piezometers be installed on the eastern embankment (Val Verde County, Tex.) of the dam at identical land-surface altitudes and with depths similar to those on the western embankment. The purpose of the piezometers is to compare water levels (potentiometric head) on both

the western and eastern embankments of Amistad Reservoir dam.

To provide technical assistance for the horizontal and vertical placement of piezometers on the eastern embankment of Amistad Reservoir dam, the U.S. Geological Survey, in cooperation with the U.S. Section of the IBWC, conducted a study along the western and eastern embankments of Amistad Reservoir dam. The study involved an integrated approach consisting of historical data review, geodatabase development, and borehole and surface geophysical investigations. To efficiently compile, store, and compare geologic and geophysical data, a geodatabase was created at the beginning of the project and used throughout the project. Data were added to the geodatabase as the project progressed. Borehole geophysical logs, both existing and newly acquired, were compiled and merged into multiple-property logs for comparison and analysis. The results of this approach were analyzed using the geodatabase to optimally locate piezometers along one line perpendicular to the centerline of the eastern embankment. This report presents the geophysical analysis from a reconnaissance-level study conducted on the eastern and western embankments of Amistad Reservoir dam on the Rio Grande in March 2006 to characterize the near-surface hydrogeology in the Salmon Peak Formation to facilitate optimum placement of piezometers along the eastern embankment.

In the western embankment investigation, geologic and geophysical characteristics that indicate relatively large water-yielding properties of the Salmon Peak Formation were identified. The direct-current (DC) resistivity method was selected as the surface geophysical reconnaissance technique to correlate relatively large water-yielding properties of the Salmon Peak Formation, identified from analysis of borehole geophysical logs, with variations in subsurface resistivity. The reciprocal Schlumberger array and the dipole-dipole array were selected as the most applicable DC resistivity arrays. Two identifiable resistivity units are present in both the dipole-dipole array data and reciprocal Schlumberger array data along DC resistivity profiles on both embankments. These resistivity units were first identified in profile 1 on the western embankment. Resistivity unit 1, a near-surface, low-resistivity unit, generally ranges in resistivity from less than 75 to greater than 150 ohm-meters in the reciprocal Schlumberger array and from less than 45 to greater than 120 ohm-meters in the dipole-dipole array. The deeper, more resistive unit, resistivity unit 2, generally ranges in resistivity from about 150 to greater than 365 ohm-meters in the reciprocal Schlumberger array and from about 120 to greater than 345 ohm-meters in the dipole-dipole array. In both resistivity arrays, a vertical high-low resistivity boundary between resistivity unit 1 and resistivity unit 2 is observed. The presence of mapped sinkholes in the reservoir north of the western embankment study area and the zone of increased water content, as indicated by the lowest neutron log count rates in piezometer LA–12, leads to the conclusion that resistivity unit 1 is a preferential flow path where surface water from Amistad Reservoir is forced into the ground-water system (because of increased head from the reservoir). The increased occurrence of weathered limestone along this profile also indicates a potential conduit for ground-water movement along resistivity unit 1 identified in profile 1. Borehole resistivity logs were collected to relate geophysical variations in existing gamma, caliper, and neutron logs, identified as changes in water-yielding properties, to changes in the electrical stratigraphy of the subsurface along the DC resistivity profiles as resistivity units 1 and 2.

Resistivity units 1 and 2, as identified on the western embankment, were identified as present on the eastern embankment by geophysical correlation. On the eastern embankment in both the dipole-dipole array and the reciprocal Schlumberger array, resistivity unit 1 is separated into three different parts by resistivity unit 2 in profile 3. These resistive features show a similarity to the features in profile 1 on the western embankment. In western embankment profile 1, a sharp vertical boundary occurs between resistivity unit 1 and resistivity unit 2; resistivity unit 1 becomes appreciably thicker at that boundary. In eastern embankment profile 3, a vertical boundary also occurs between resistivity unit 1 and resistivity unit 2, and resistivity unit 1 becomes thicker at that boundary.

In the eastern embankment investigation, trends in the spatial distribution of sinkholes were identified by analyzing historical data from the IBWC and the occurrence of weathered zones identified in geologic descriptions of cores collected by the IBWC along the eastern embankment. The western and eastern expressions of resistivity unit 1 correlate with the general trend of sinkholes documented by IBWC in the eastern embankment study area. To assess the hydrogeologic characteristics of the Salmon Peak Formation in the eastern embankment study area along DC resistivity profile 3, the upper extent of major lithologic features were superimposed on DC resistivity profile 3. The thickness and extent of weathered zones do not correlate with the thickness and extent of the western expression of resistivity unit 1. There is, however, a substantial increase in the thickness of weathered zones in the limestone west of DC resistivity profile 3 shown by geologist descriptions of borings.

Lithologic data show that the thickness of resistivity unit 1, along its central and eastern expressions on the eastern embankment, corresponds generally with the extent and thickness of weathered zones in the limestone; however, the thickness of alluvial deposits increases along the central expression of resistivity unit 1. Because alluvium tends to be less resistive than limestone, it is possible that the decrease in resistivity along the central expression of resistivity unit 1 is predominantly influenced by the increased thickness of alluvium more so than the underlying weathered limestone. Because of the lack of lithologic correlation along the western expression and the increased thickness of alluvium along the central expression, these features were not chosen for further exploration. The zone of concentrated weathered features on the eastern end of DC resistivity profile 3 is thickest and extends to a greater depth along the eastern end of the section. The correlation of surface geophysical DC resistivity, historical lithologic data, and general trend of documented sinkholes

along the eastern end of profile 3 were used to justify further exploration (drilling of piezometers) in the eastern expression of resistivity unit 1.

The piezometer monitoring network along the eastern embankment was designed to function similarly to the western embankment network. The spatial location of the piezometers and the screened intervals were selected using the various two- and three-dimensional visualizations of lithologic data, borehole geophysical logs, and inversion results of DC resistivity data to best match the locations of the screened intervals of the western embankment piezometers and to best satisfy the recommendations of Joint Report of the Technical Advisors of the International Boundary and Water Commission. Six piezometers were installed on the eastern embankment and logged using borehole geophysical techniques including electric long (64-inch) and short (16-inch) normal resistivity, spontaneous potential, fluid conductivity, temperature, acoustic velocity, full-waveform sonic, acoustic televiewer, electromagnetic flowmeter, caliper, and casing collar locator. Borehole geophysical logs provide highly detailed information proximal to the boring, and surface geophysical data provide continuous big-picture information. Combining the borehole and surface geophysical results allows the geophysical analyst to identify general log characteristics to better understand the hydrogeologic characteristic most controlling the changes in resistivity shown in the surface geophysical DC resistivity data.

The surface DC resistivity sections superimposed on the resistivity logs for piezometers 105+90B and 106+00B indicate three discernible resistivity units in the dipole-dipole array and in the borehole resistivity logs. These three resistivity units correlate with resistivity units 2, 1, and 2, respectively, as identified in the western embankment study area. Resistivity units 1 and 2 in the DC resistivity profiles generally correspond with low- and high-resistivity zones, respectively, on the normal and lateral resistivity logs collected in the nearby piezometers at the time of installation. The surface DC resistivity sections superimposed on the resistivity logs for piezometer 106+00A indicate two discernible resistivity units that can be observed in the dipole-dipole array and that correlate with resistivity units 2 and 1, respectively; however, these units are not discernible on the resistivity logs for piezometer 106+00A.

## References Cited


Advanced Geosciences, Inc., 2006, Instruction manual for EarthImager 2D version 2.1.0—Resistivity and IP inversion software: Austin, Tex., accessed November 1, 2006, at *http://www.agiusa.com/files/pub/softwareproducts.shtml*

American Society for Testing and Materials, 1999, Standard guide for using the direct current resistivity method for subsurface investigation: ASTM D 6431–99, 14 p.

American Society for Testing and Materials, 2001, Standard guide for conducting borehole geophysical logging—electromagnetic induction: ASTM standard D 6726–01, 7 p.

American Society for Testing and Materials, 2004a, Standard guide for conducting borehole geophysical logging—Gamma: ASTM D 6274–98, 11 p.

American Society for Testing and Materials, 2004b, Standard guide for conducting borehole geophysical logging—Mechanical caliper: ASTM D 6167–97, 6 p.

American Society for Testing and Materials, 2004c, Standard guide for use of the metal detection method for subsurface investigation: ASTM D 7046–04, 7 p.

American Society for Testing and Materials, 2004d, Standard practice for design and installation of ground water monitoring wells: ASTM D 5092–04, 16 p.

Biot, M.A., 1952, Propagation of elastic waves in a cylindrical bore containing a fluid: Journal of Applied Geophysics, v. 23, p. 997–1,005.

Boyd, T.M., Introduction to geophysical exploration, DC resistivity notes—Resistivity guess, accessed November 3, 2006, at *http://galitzin.mines.edu/INTROGP/notes_template.jsp?url=RES%2FNOTES%2F1estres.html&page=DC%20Resistivity%3A%20Notes%3A%20Resistivity%20Guess*

Burkardt, John, 2005, MATH2070, numerical methods in scientific computing I—LAB #7, accessed January 24, 2007, at *http://www.scs.fsu.edu/~burkardt/math2070/lab_07.html*

Century Geophysical Corp., 2006, accessed August 24, 2006, at *http:// www.century-geo.com*

Dunham, R.J., 1962, Classification of carbonate rocks according to depositional texture, in Classification of Carbonate Rocks Symposium: American Association of Petroleum Geologists Memoir 1, p. 108–121.

Fetter, C.W., 1994, Applied hydrogeology (3d ed.): Prentice-Hall, Inc., 691 p.

Ford, D.C., and Ewers, R.O., 1978, The development of limestone cave systems in the dimensions of length and depth: The Canadian Journal of Earth Sciences, v. 15, p. 1,783–1,798.

Geonics Limited, 1992, Geonics EM39 borehole conductivity logger operating manual: Mississauga, Ontario, Canada, Geonics Limited.

Geosoft Inc., 2006, Mapping and processing system help topics: Oasis montaj MAPS version 6.3.

Grant, F.S., and West, G.F., 1965, Interpretation theory in applied geophysics—Part 3, Electrical conduction and electromagnetic induction methods: New York, McGraw-Hill, p. 384–572.

Greenwood, Robert, 1956, Submarine volcanic mudflows and limestone dikes in the Grayson Formation (Cretaceous) of central Texas: Gulf Coast Association of Geological Societies Transactions, v. 6, p. 167–177.

Hearst, J.R., Nelson, P.H., and Paillet, F.L., 2000, Well logging for physical properties—A handbook for geophysicists, geologists, and engineers (2d ed.): John Wiley, 483 p.

Humphreys, C.H., 1984, Stratigraphy of the Lower Cretaceous (Albian) Salmon Peak Formation of the Maverick Basin, south Texas, *in* Miller, B.C., Smith, C.I., Rose, P.R., Humphreys, C.H., and Webster, R.E., eds., Stratigraphy and structure of the Maverick Basin and Devils River Trend, Lower Cretaceous, southwest Texas: San Antonio Geological Society Guidebook, p. 34–59.

Keller, G.V., and Frischknecht, F.C., 1966, Electrical methods in geophysical prospecting: Oxford, United Kingdom, Pergamon Press, Inc., 519 p.

Keys, W.S., 1990, Borehole geophysics applied to groundwater investigations: U.S. Geological Survey Techniques of Water-Resources Investigations, book 2, chap. E2, 150 p.

Keys, W.S., 1997, A practical guide to borehole geophysics in environmental investigations: CRC-Lewis Publishers, 176 p.

Lapham, W.W., Wilde, F.D., and Koterba, M.T., 1997, Guidelines and standard procedures for studies of ground-water quality—Selection and installation of wells, and supporting documentation: U.S. Geological Survey Water-Resources Investigations Report 96–4233, 110 p.

Loke, M.H., 2004, Tutorial—2-D and 3-D electrical imaging surveys: Geotomo Software, accessed November 1, 2006, at *http://www.geoelectrical.com*

Loke, M.H., Acworth, Ian, and Dahlin, Torleif, 2003, A comparison of smooth and blocky inversion methods in 2D electrical imaging surveys: Exploration Geophysics, v. 34, p. 182–187.

Lozo, F.E., Jr., and Smith, C.I., 1964, Revision of Comanche Cretaceous stratigraphic nomenclature, southern Edwards Plateau, southwest Texas: Gulf Coast Association of Geological Societies Transactions, v. 14, p. 285–306.

McDougal, R.R., Abraham, J.D., and Bisdorf, R.J., 2004, Results of electrical resistivity data collected near the town of Guernsey, Platte County, Wyoming: U.S. Geological Survey Open-File Report 2004–1095, 7 p.

National Oceanic and Atmospheric Administration, 2006, Online Positioning User Service, accessed November 3, 2006, at *http://www.ngs.noaa.gov/OPUS/*.

Paillet, F.L., 1991, Qualitative and quantitative interpretation of fracture permeability using acoustic full-waveform logs: The Log Analyst, v. 32, no. 3, p. 256–270.

Palmer, A.N., 1984, Geomorphic interpretation of karst features, *in* LaFleur, R.G., ed., Groundwater as a geomorphic agent: London, Allen & Unwin, p. 173–209.

Raymer, L.L., Hunt, E.R., and Gardner, J.S., 1980, An improved sonic transit time to porosity transform, *in* Transactions, Society of Professional Well Log Analysts 21st Annual Logging Symposium: Houston, Tex., 12 p.

Reeves, R.D., and Small, T.A., 1973, Ground-water resources of Val Verde County, Texas: Texas Water Development Board Report 172, 144 p.

Shah, S.D., and Quigley, S.M., 2005, Geodatabase of environmental information for Air Force Plant 4 and Naval Air Station-Joint Reserve Base Carswell Field, Fort Worth, Texas, 1990–2004: U.S. Geological Survey Open-File Report 2005–1041, 1 CD.

Sharma, P.V., 1997, Environmental and engineering geophysics: Cambridge, United Kingdom, Cambridge University Press.

Sumner, J.S., 1976, Principles of induced polarization for geophysical exploration: Elsevier, 277 p.

Texas Water Development Board, 1971, Engineering data on dams and reservoirs in Texas—Part III: Texas Water Development Board Report 126.

U.S. Army Corps of Engineers, 1995, Geophysical exploration for engineering and environmental investigations: Engineering Manual 1110-1-1802, chap. 4, 57 p.

Wylie, M.R.J., 1963, The fundamentals of well log interpretation: New York, Academic Press, 238 p.

Zohdy, A.A.R., Eaton, G.P., and Mabey, D.R., 1974, Application of surface geophysics to ground-water investigations: U.S. Geological Survey Techniques of Water-Resources Investigations, book 2, chap. D1, 116 p.

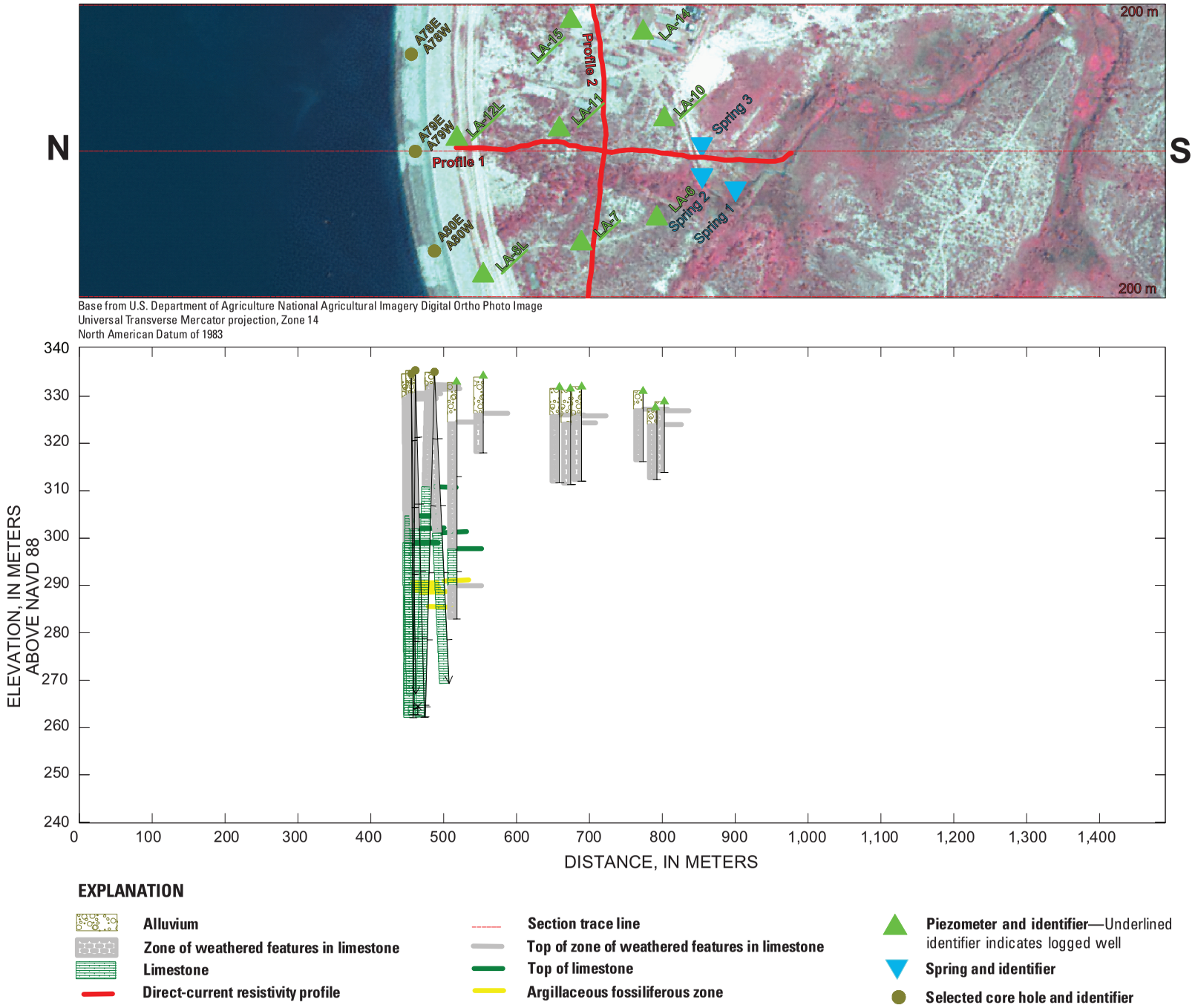


**Figure 9A.** Section showing available lithologic data near direct-current resistivity profile 1.

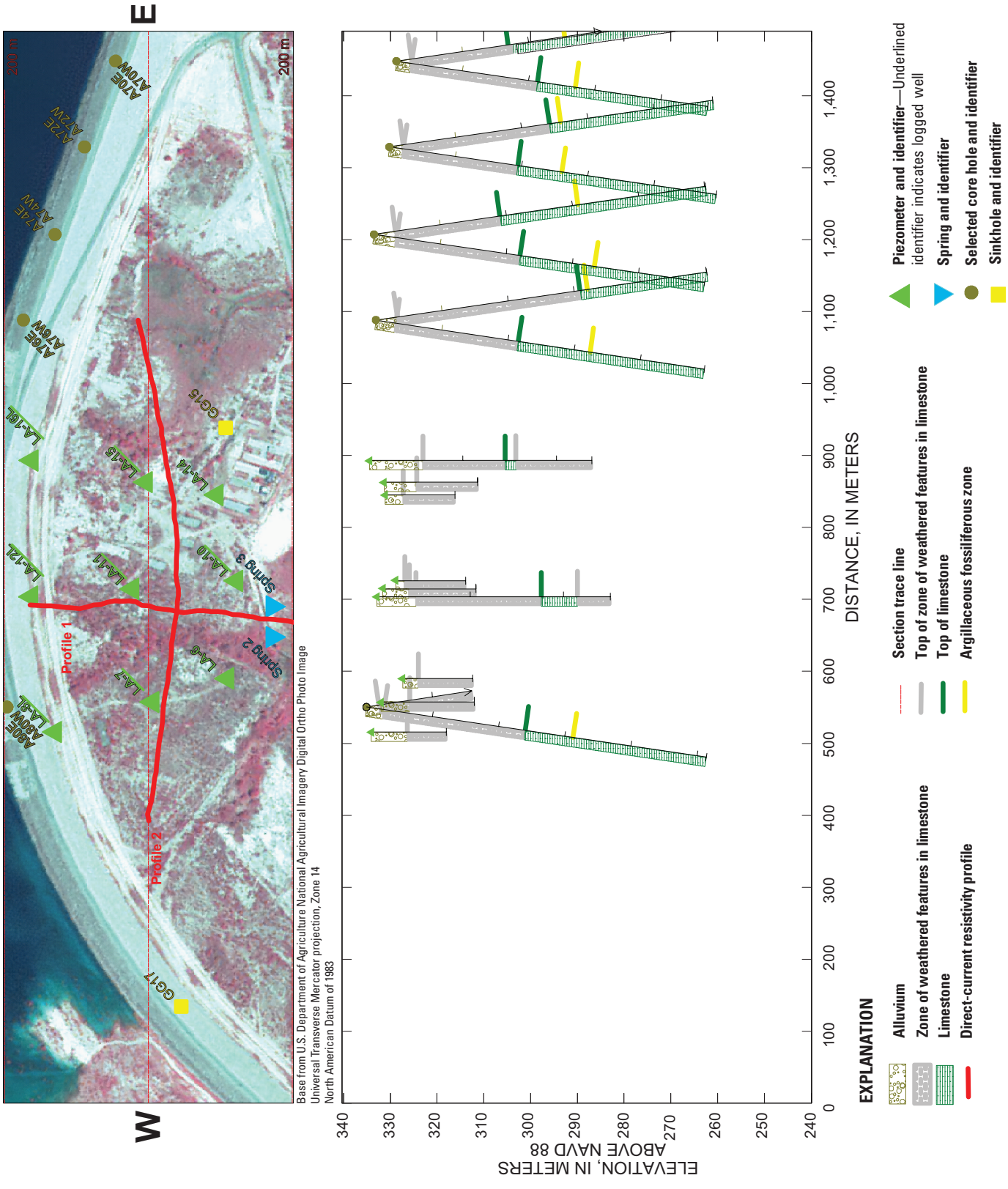


**Figure 9B.** Section showing available lithologic data near direct-current resistivity profile 2.

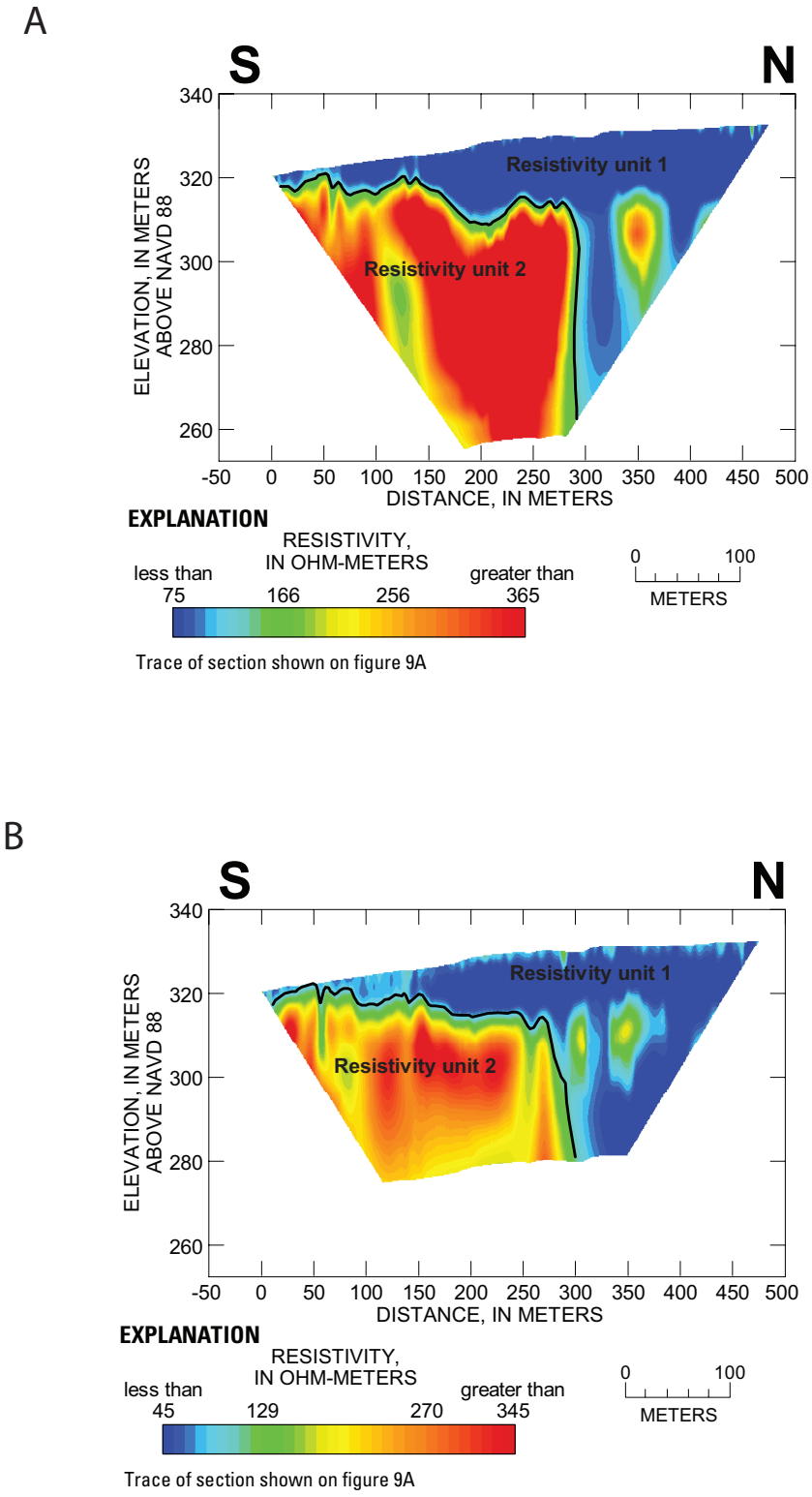


**Figure 10.** Robust inverse model results of direct-current resistivity profile 1 (A) reciprocal Schlumberger array and (B) dipole-dipole array; and profile 2 (C) reciprocal Schlumberger array (D) and dipole-dipole array.

C

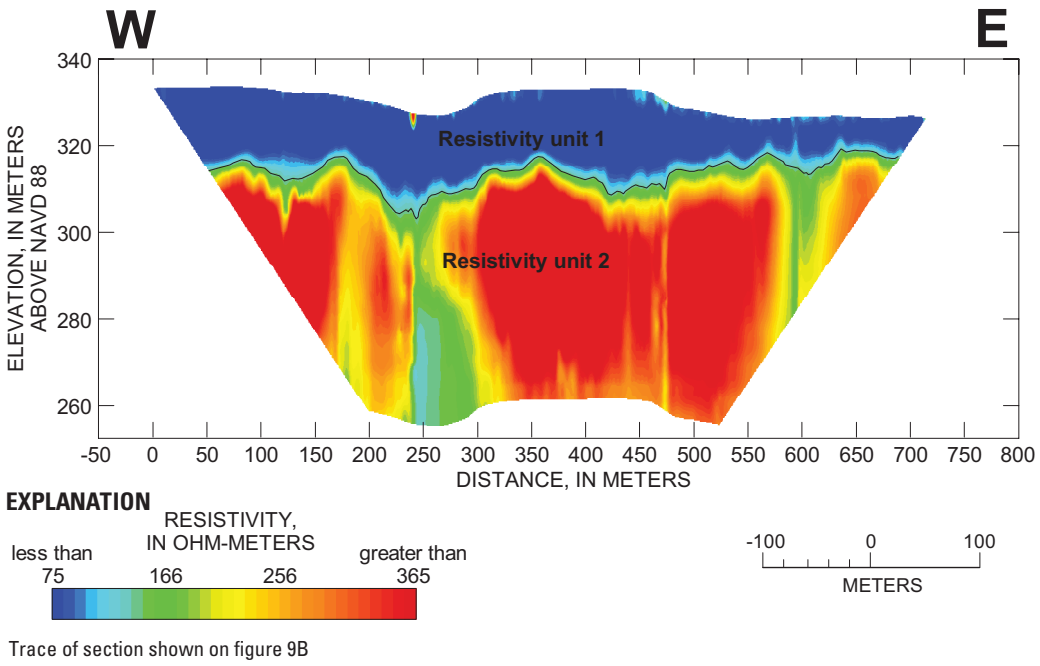


D

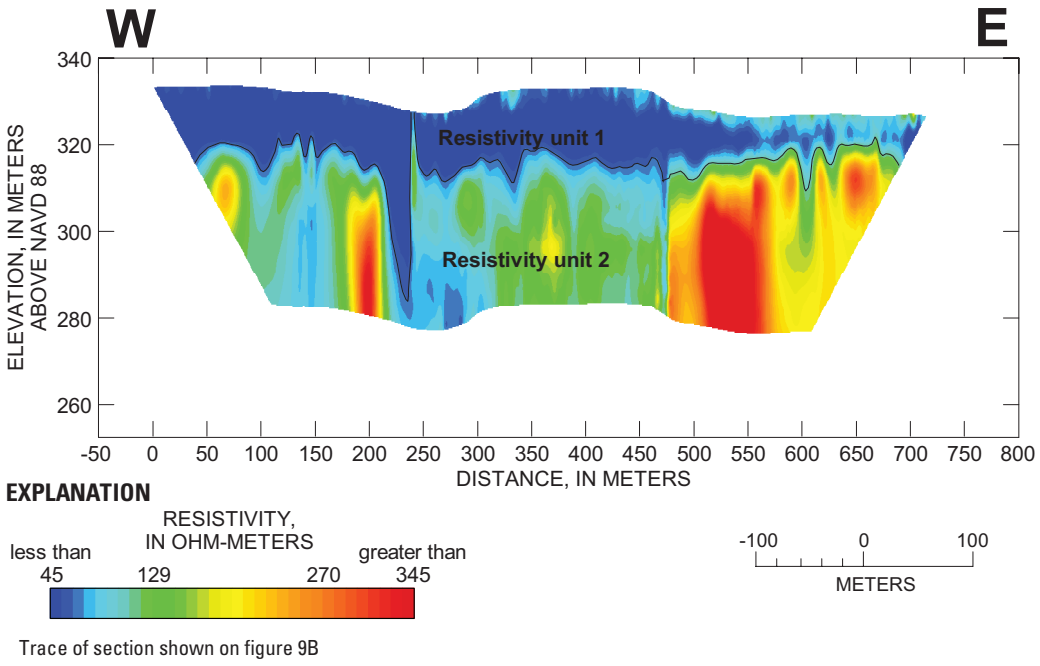


**Figure 10.** Continued.

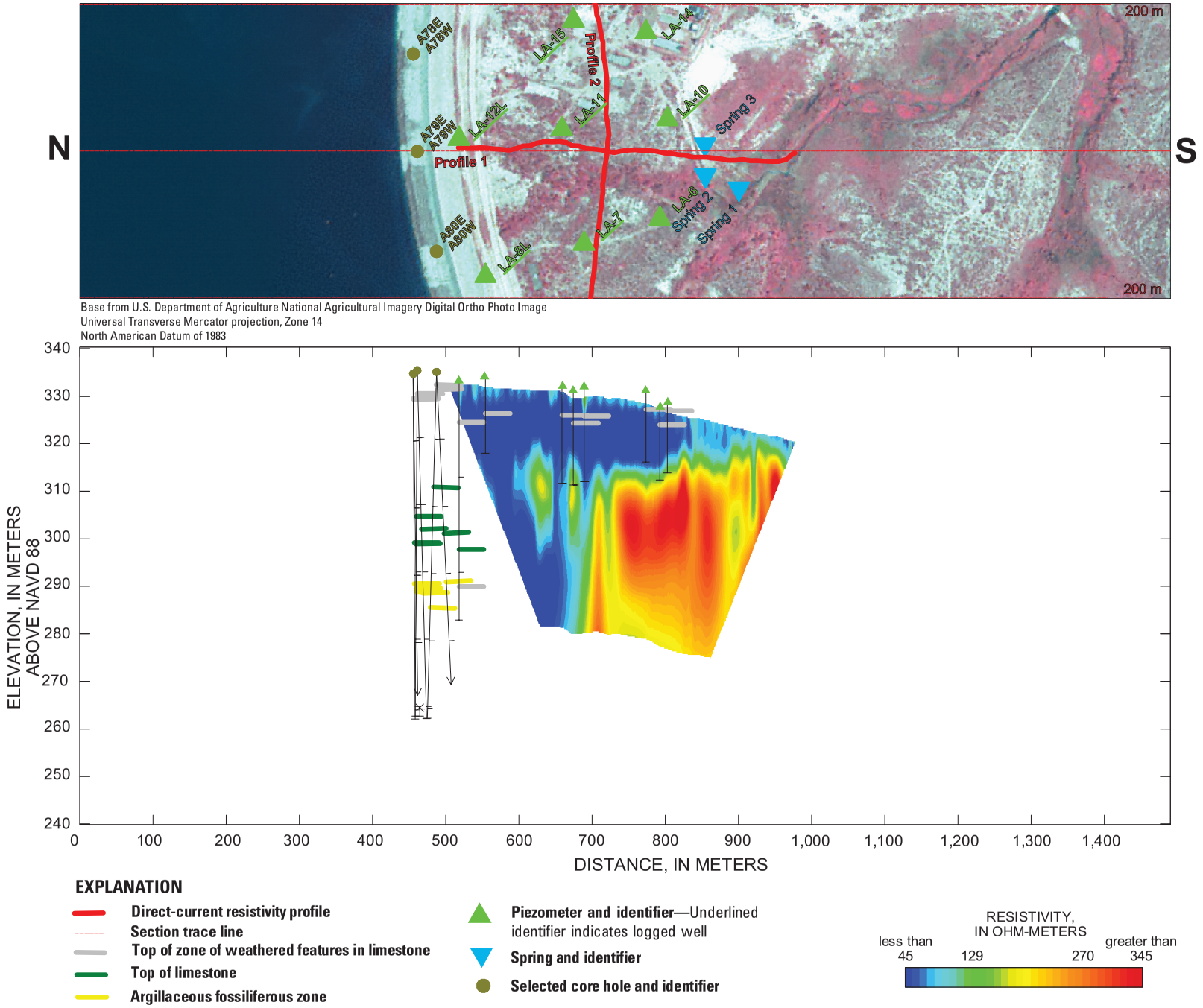


**Figure 11A.** Section showing lithologic tops from core holes and piezometers superimposed on direct-current resistivity profile 1 dipole-dipole array.

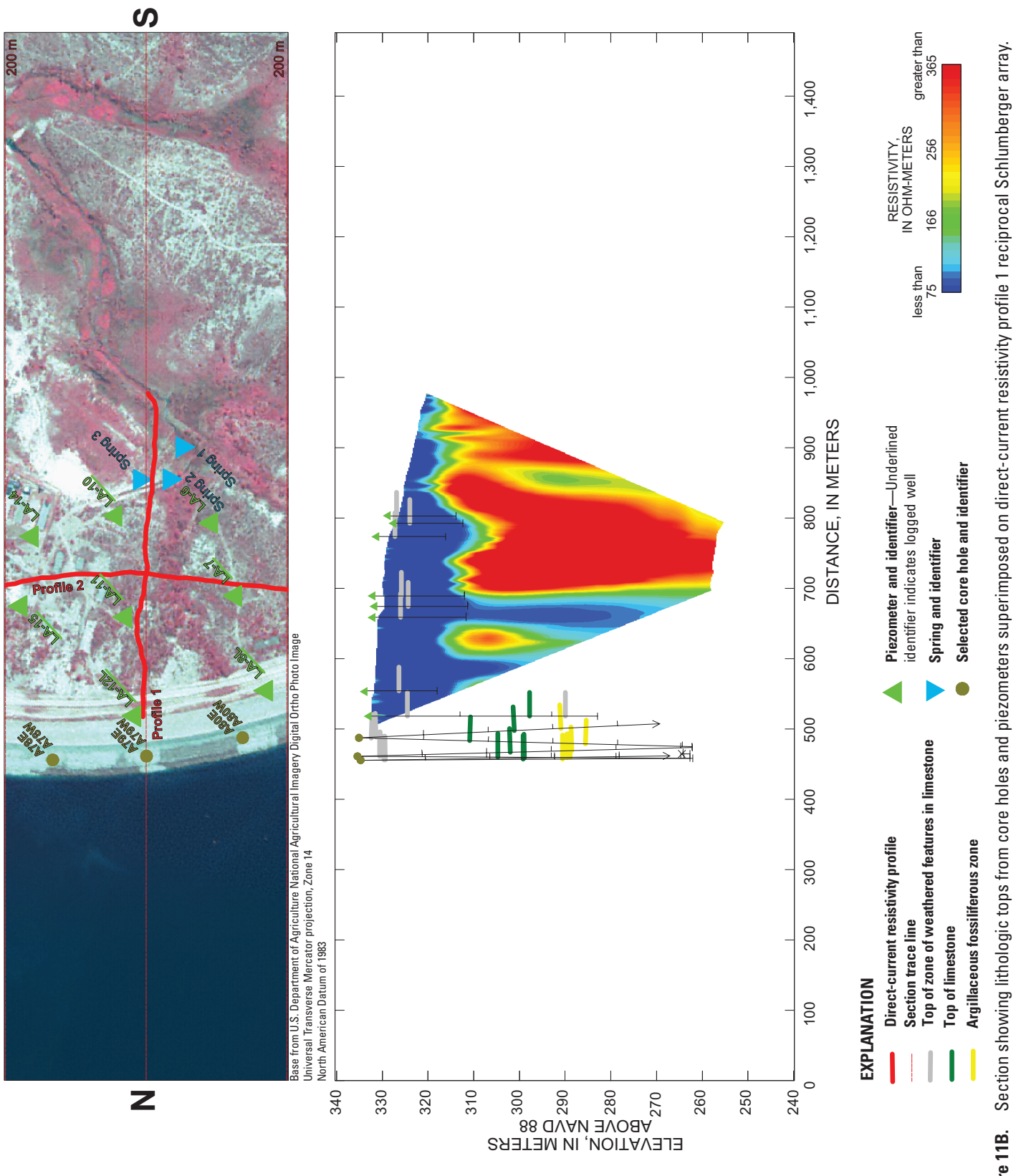


**Figure 11B.** Section showing lithologic tops from core holes and piezometers superimposed on direct-current resistivity profile 1 reciprocal Schlumberger array.

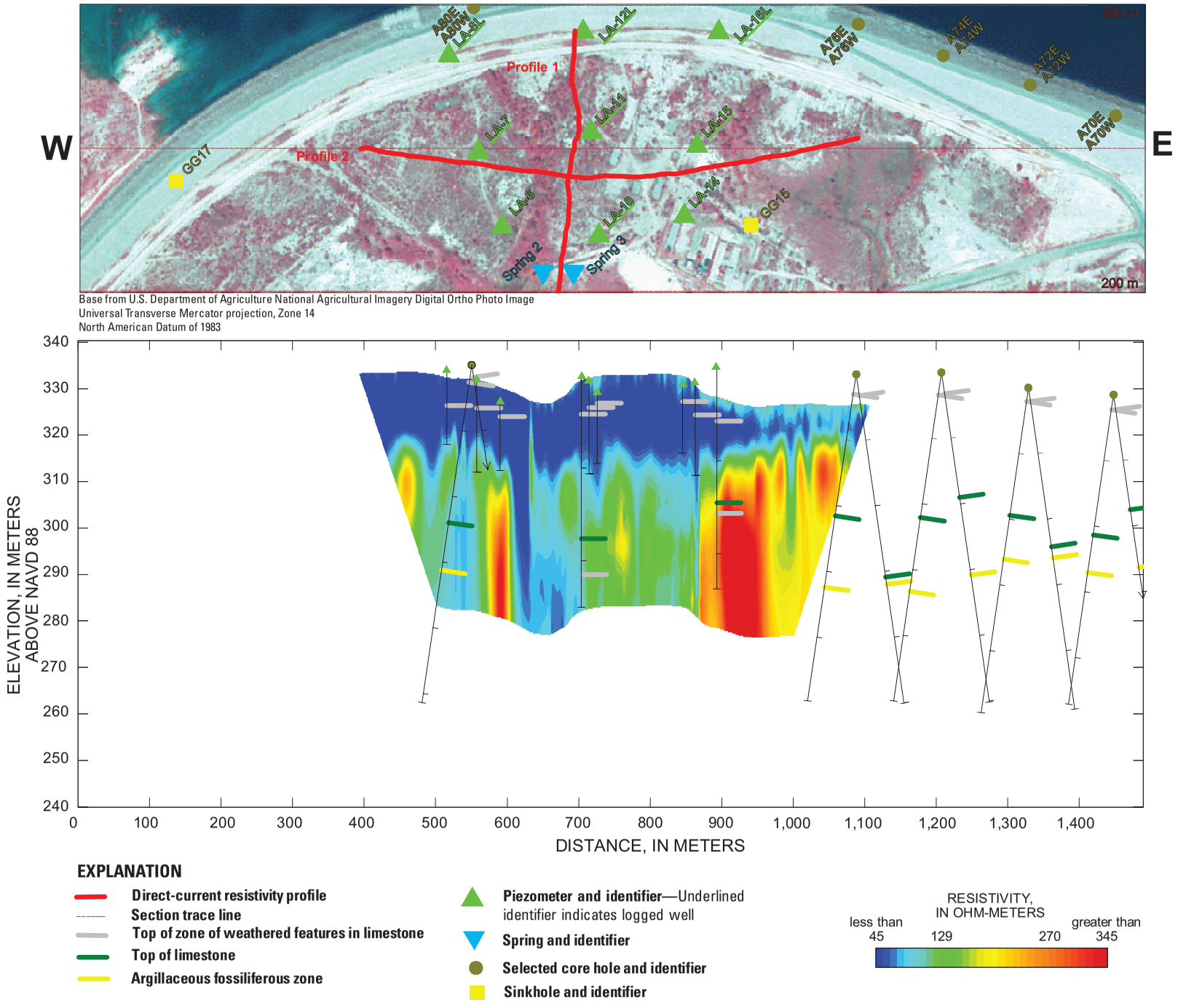


**Figure 11C.** Section showing lithologic tops from core holes and piezometers superimposed on direct-current resistivity profile 2 dipole-dipole array.

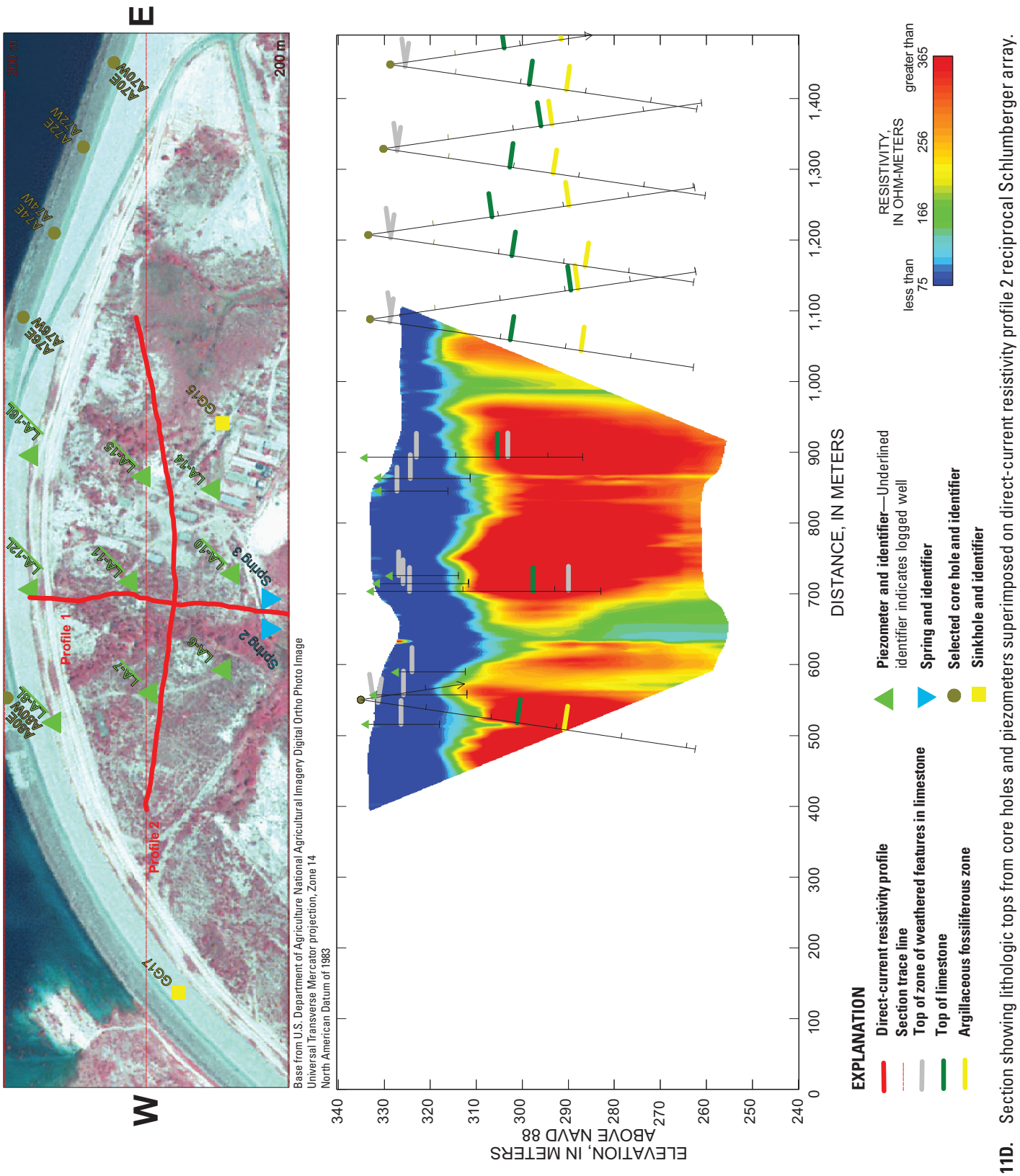


**Figure 11D.** Section showing lithologic tops from core holes and piezometers superimposed on direct-current resistivity profile 2 reciprocal Schlumberger array.

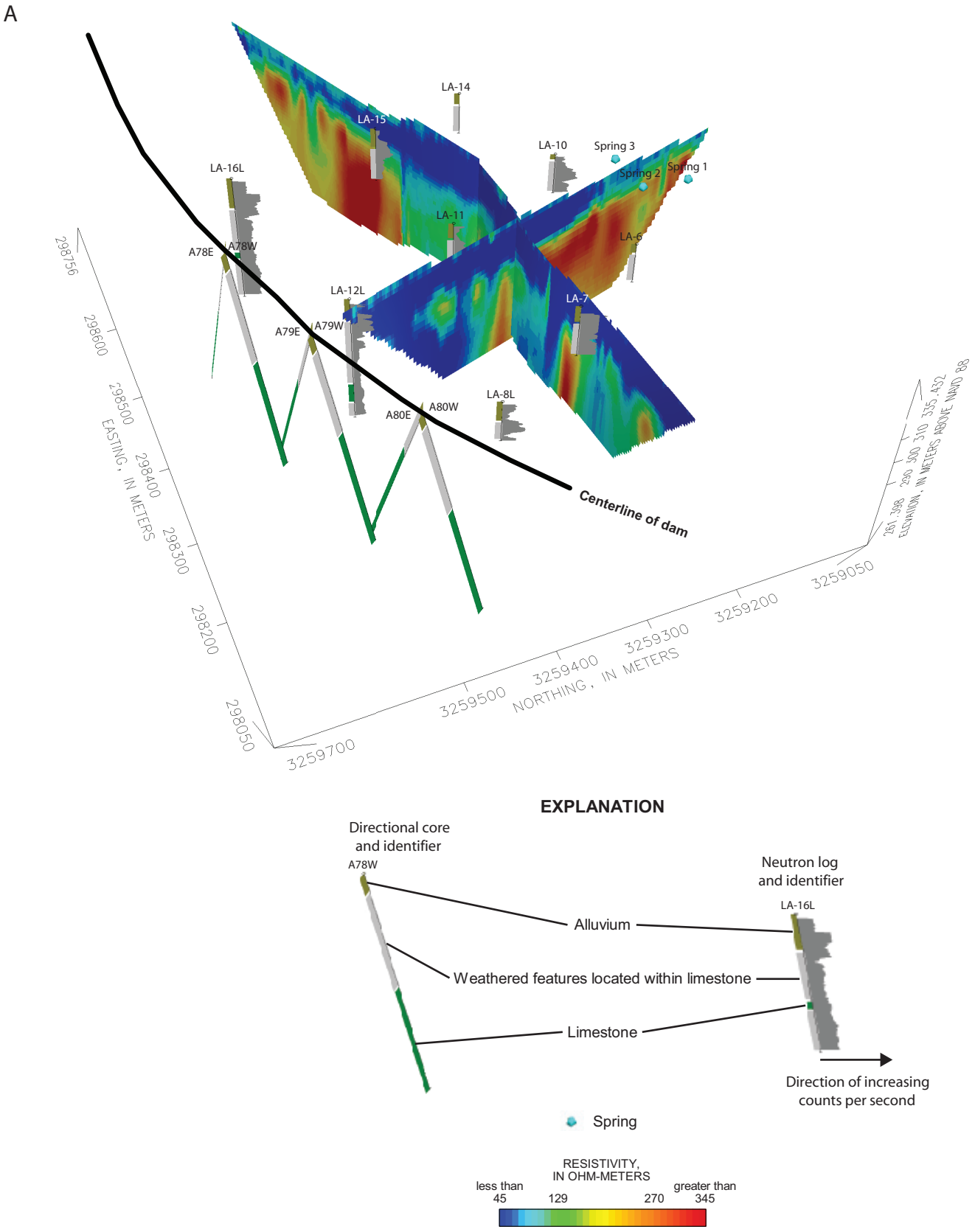


**Figure 12.** Three-dimensional image of merged dipole-dipole direct-current resistivity profile at western embankment study site, looking (A) southeast and (B) southwest.

B

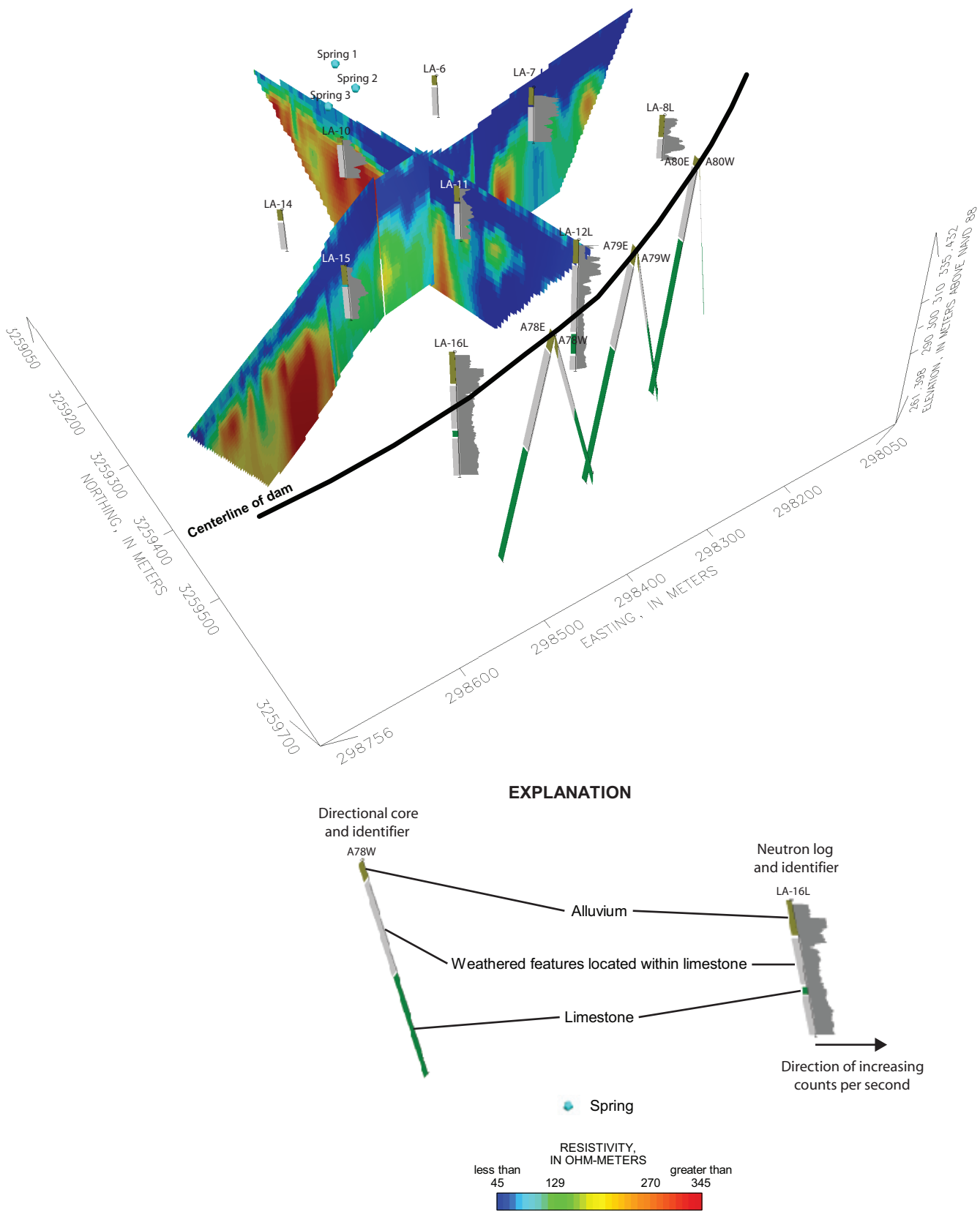


**Figure 12.** Continued.

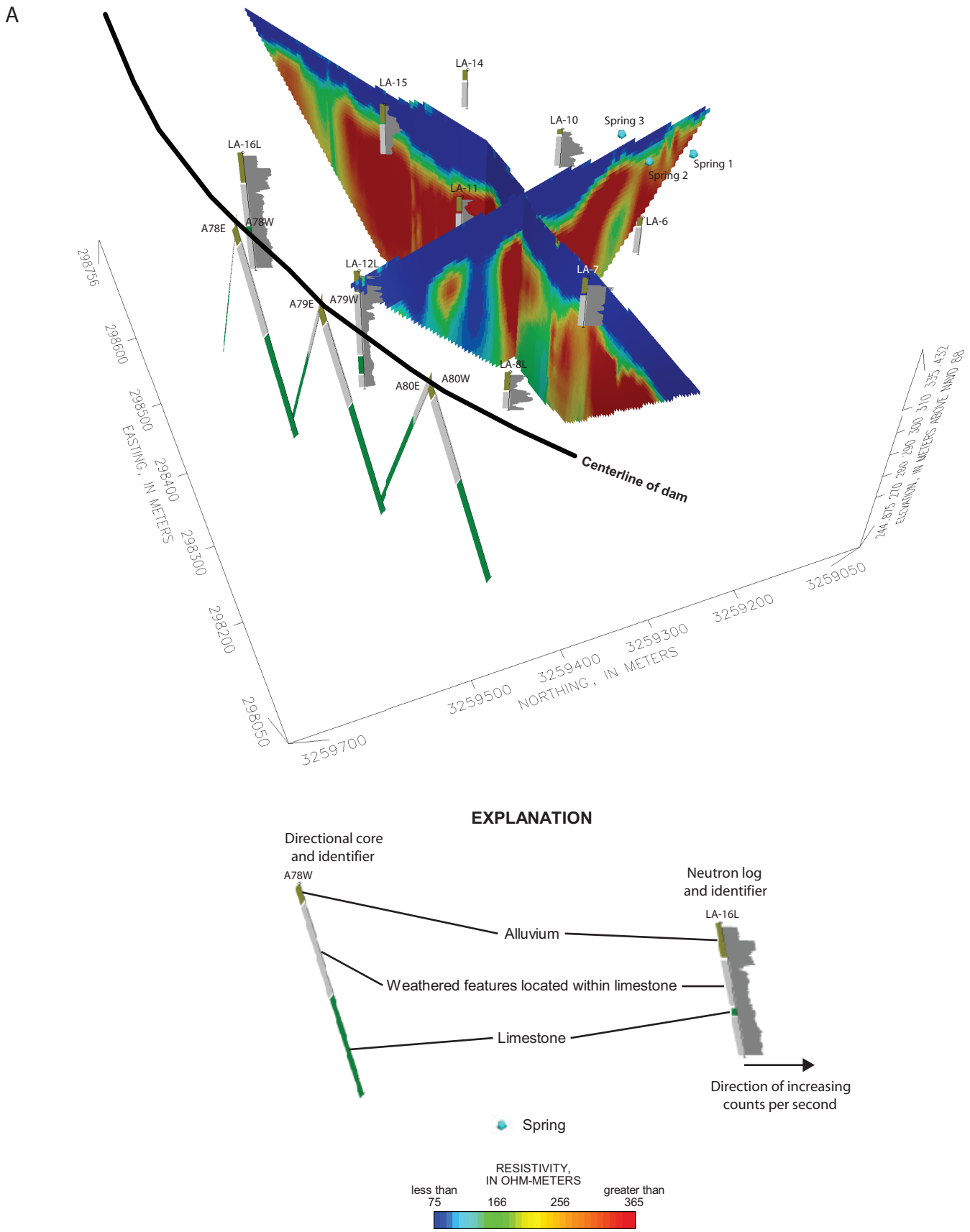


**Figure 13.** Three-dimensional image of merged reciprocal Schlumberger direct-current resistivity profile at western embankment study site, looking (A) southeast and (B) southwest.

B

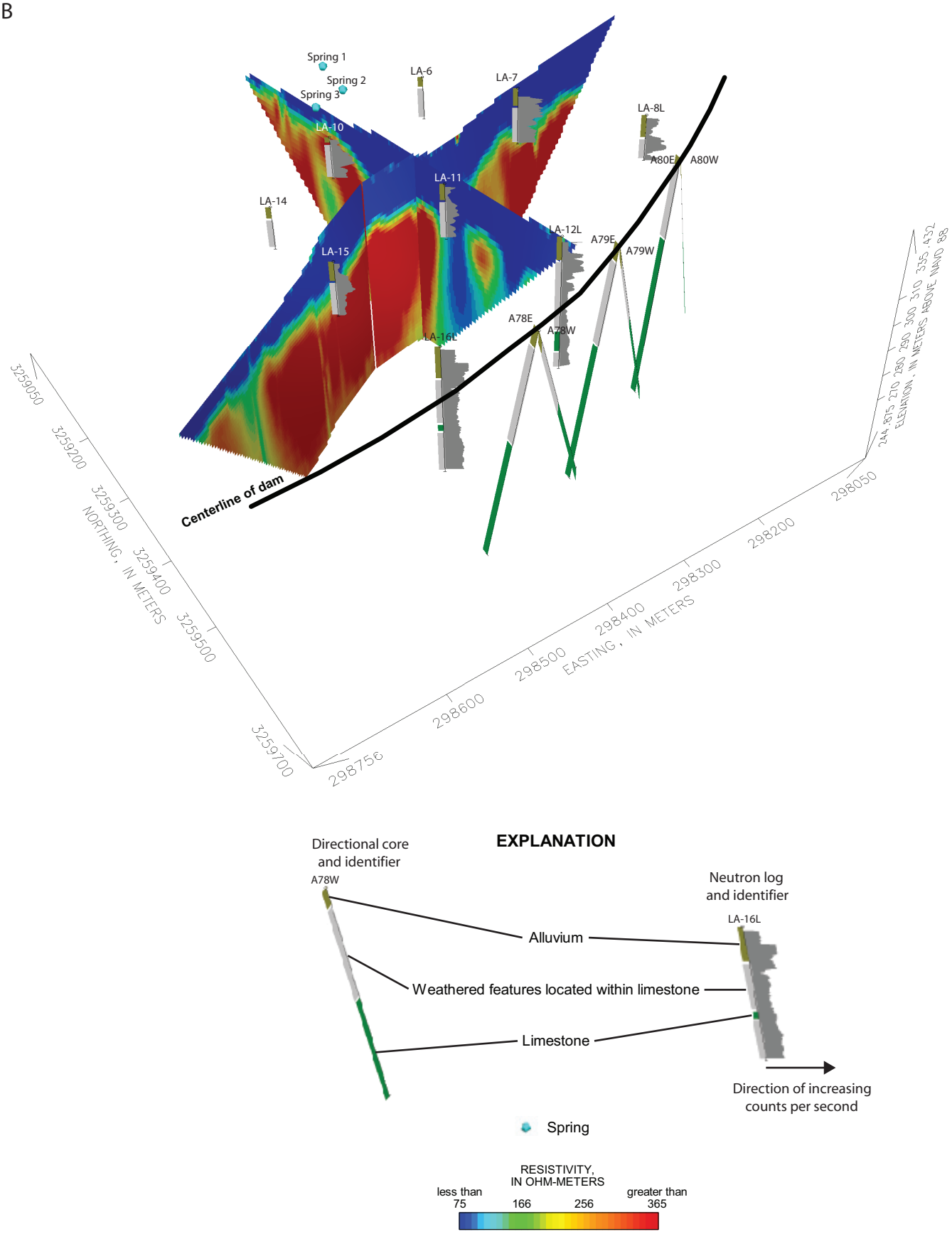


**Figure 13.** Continued.

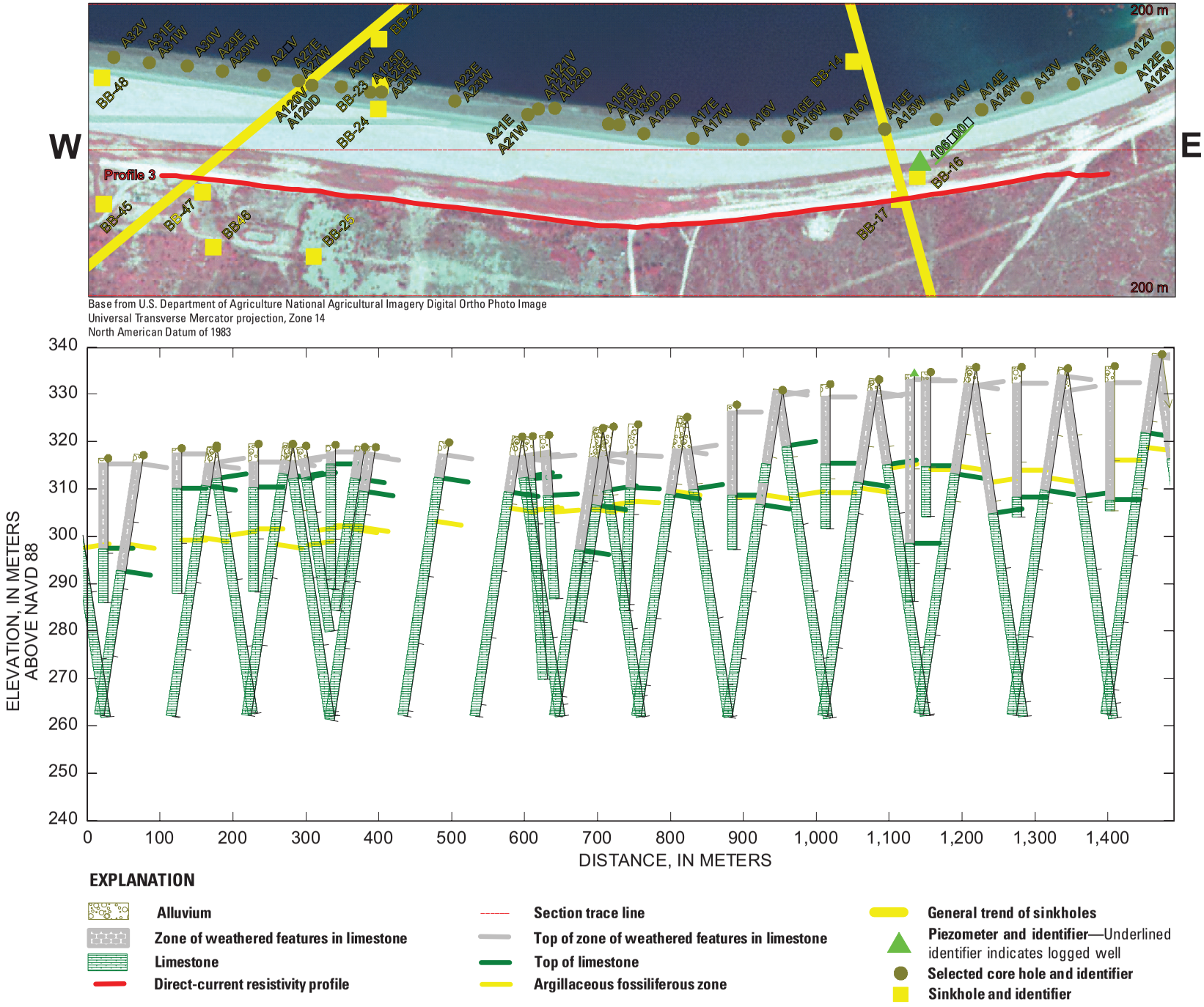

Base from U.S. Department of Agriculture National Agricultural Imagery Digital Ortho Photo Image
Universal Transverse Mercator projection, Zone 14
North American Datum of 1983

**Figure 14.** Section showing available lithologic data near direct-current resistivity profile 3.

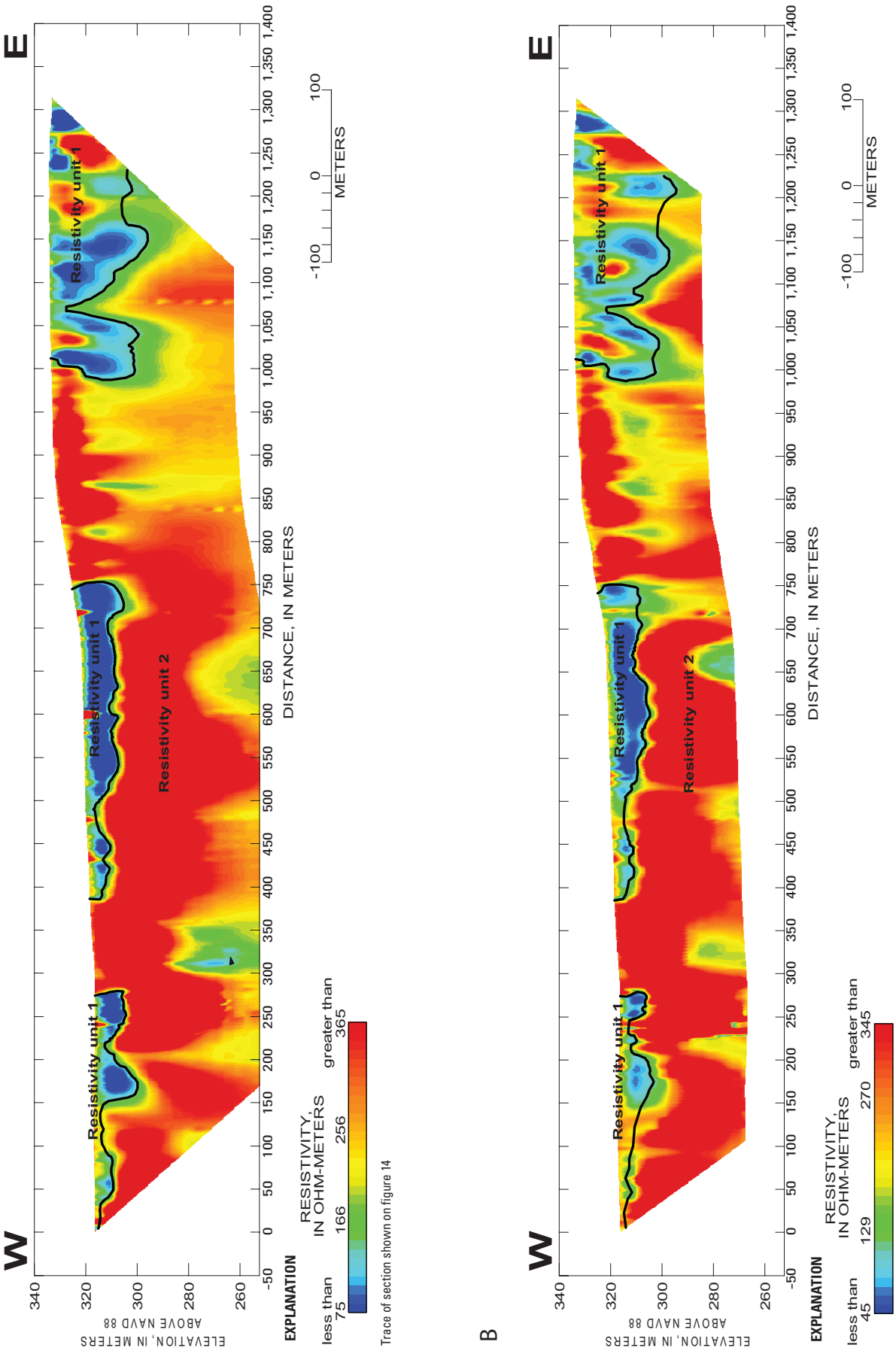


**Figure 15.** Robust inverse model results of direct-current resistivity profile 3 (A) reciprocal Schlumberger array and (B) dipole-dipole array.

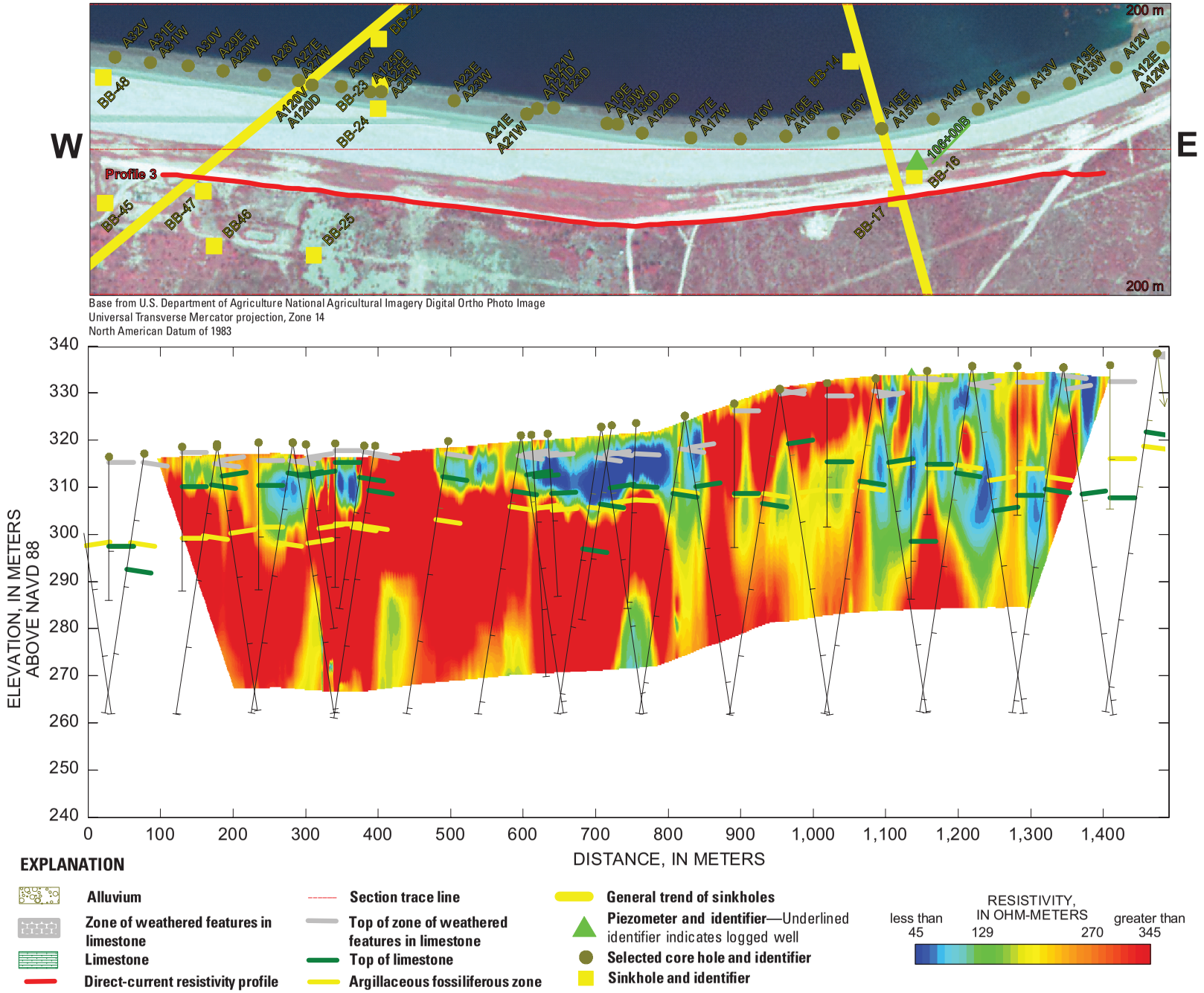


**Figure 16A.** Section showing lithologic tops from core holes and piezometers superimposed on direct-current resistivity profile 3 dipole-dipole array.

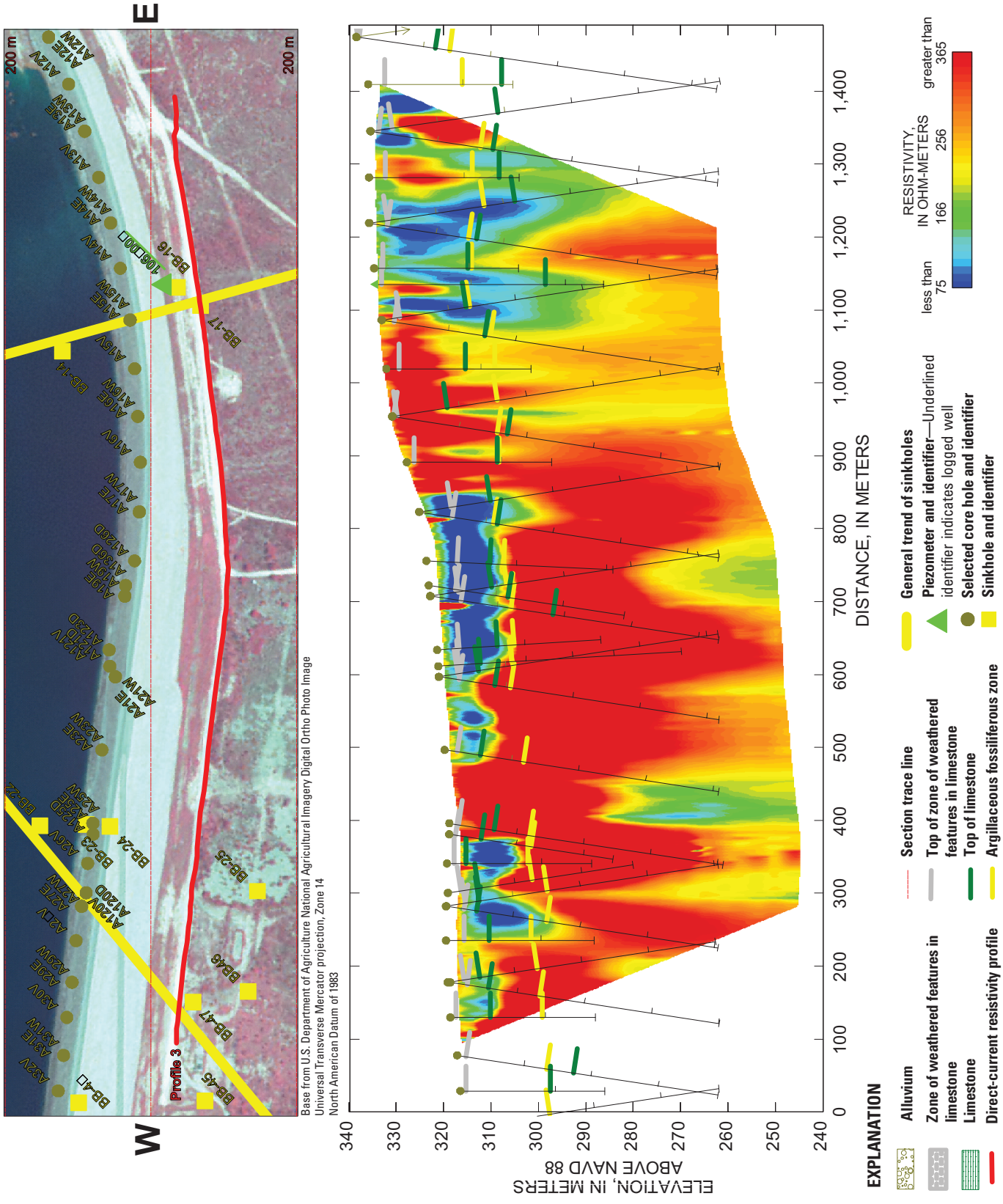


**Figure 16B.** Section showing lithologic tops from core holes and piezometers superimposed on direct-current resistivity profile 3 reciprocal Schlumberger array.

# Appendix 1—Detailed Descriptions of Borehole Geophysical Methods

Blank Page

## Electromagnetic Induction Logs

Electromagnetic (EM) induction probes measure conductivity in air- or water-filled holes and perform well in open holes or PVC cased holes. The measurement of conductivity commonly is reciprocated to provide logs with curves of both resistivity and conductivity (Keys, 1997), as are the logs contained in this report. Conductivity is affected by the salinity of borehole and formation fluids and the type of lithology encountered. Generally, pure carbonates, sands, and gravels have lower conductivity (thus higher resistivity) than clays or shales (Keys, 1997). A Geonics EM39 induction conductivity probe was used in all wells. The EM39 was calibrated twice daily using manufacturer's recommended procedures (Geonics Limited, 1992) at temperatures within the range expected in the boreholes. To attain a stable temperature, the probe was hung in a well for 20–30 minutes prior to calibration. During a two-point calibration process, the probe was calibrated (1) to a zero-conductivity environment and (2) to a calibration coil of known conductivity with the bottom of the probe at least 3 meters above land surface. The calibration also was checked periodically between calibrations. The EM induction conductivity measurements (commonly sensitive to metallic conductive objects) were affected at depths corresponding with metal objects such as centralizers and stainless steel screens.

## Natural Gamma Logs

Natural gamma logs provide a record of gamma radiation detected at depth in a borehole. Fine-grained sediments that contain abundant clay tend to be more radioactive than quartz-grain sandstones or carbonates (Keys, 1997). The natural gamma log was run in conjunction with the fluid resistivity log and was recorded in natural gamma counts per second simultaneously as the induction log was recorded in both cased and open boreholes. A Mount Sopris 2PGA-1000 natural gamma probe with a sodium iodide detector was used. The natural gamma probe is calibrated at the factory and does not require calibration in the field. The natural gamma and induction logs collectively can be useful to identify lithologies and contact depths of the strata penetrated in the borehole. Natural gamma count rates, which commonly will increase near clay and shale, could be slightly increased adjacent to any bentonite seals in the wells.

## Electric Logs

Electric logs use a series of electrodes mounted on the downhole probe and a surface electrode in the ground to measure potential (or voltage) that varies with the electrical properties of fluids and rock materials. Electric logs require an uncased, fluid-filled hole to allow the current to flow into the formation.

Normal resistivity methods actually measure apparent resistivity in ohm-meters using two current electrodes at each end of the tool and two potential electrodes at two different spacings, 16 inches (short normal) and 64 inches (long normal). A constant current is applied to the electrodes by the surface instrumentation regardless of the resistance of the formation. The current goes through the borehole fluid and into the formation, and the voltage is measured by the potential electrodes at the two spacings. Using Ohm's law, resistance is computed as resistance (ohms) equals the voltage measured by the potential electrodes divided by the constant current (amperes). A spatial component is introduced with the electrode spacing and ohm-meters are the resulting unit. About 50 percent of the signal is measured from a radius of investigation that is about twice the distance from the borehole as the electrode spacing. Consequently, the long normal measures a larger volume of the subsurface than the short normal. When estimating thickness of a lithologic unit, the normal resistivity-curve deflections are subject to error where the thickness of the unit is less than the distance of the 16- or 64-inch spacing for the short normal and long normal, respectively. The normal resistivity log curves are usually recorded on a logarithmic scale to minimize the high-resistivity values going off-scale yet providing detail at low-resistivity values. Generally, carbonate rocks have a higher resistivity than sandstone, and sandstone generally has higher resistivity than clay or shale. Therefore the normal resistivity logs are useful for determining and correlating various lithologies but also are affected by the resistivity of the fluids in the borehole and formation. The normal resistivity probe can be calibrated in the field using a special resistor box with various resistor switch positions and cables that connect to the electrodes. A detailed explanation of the theory of normal resistivity logging is in Keys (1997). A Century model 8044 multiparameter E-log probe was used to measure the normal resistivity and was calibrated prior to logging.

The lateral resistivity is measured with four electrodes as is the normal resistivity, but the electrodes are in a different configuration to focus the current flow away from the borehole into the rocks that surround the (Keys, 1990) borehole. The lateral resistivity is in a 48-inch-spacing configuration that actually measures a greater distance from the borehole than the 64-inch normal resistivity. The sheetlike current pattern of the lateral log increases the resolution and decreases the effect of adjacent beds in comparison with the normal resistivity logs (Keys, 1990). A Century model 8044 multiparameter E-log probe was used to measure the lateral resistivity and was calibrated in conjunction with the normal resistivity.

The spontaneous potential (SP) is one of the oldest logging techniques and uses a very simple method of measuring the potentials produced by various salinity conditions (Keys, 1990). SP is a function of the chemistry of fluids in the borehole

and adjacent rocks, the temperature, and the clay present and is not related directly to porosity and permeability (Keys, 1997). Electrochemical effects are the main source of natural spontaneous potentials in most boreholes and result from the migration of ions from concentrated to more dilute solutions (Keys, 1997). Clay or shale decreases the mobility of the ions. The SP log curve is scaled in millivolts of potential and deflects in a positive or negative direction as the salinity of the formation fluid or borehole changes vertically. When the borehole fluid column is fresher than the formation fluid, current flow is such that the SP curve deflects in a negative direction; when the borehole fluid column is more saline than the formation fluid, the current flow and curve deflection will be reversed (Keys, 1997). Rapid oscillations in a SP curve that is normally smooth are caused by streaming potentials that are commonly a result of water moving in or out of the borehole through a permeable media (Keys, 1997). SP logs are susceptible to extraneous effects from stray electrical currents and equipment problems. SP logs that are periodically rerun on the same well will most likely show a difference in log response because any changes of water contained in the borehole (drilling fluid or aquifer water), or its depth of invasion into the formation, can cause the log to change (Keys, 1997). A Century model 8044 multiparameter E-log probe was used to measure the SP values and was calibrated in conjunction with the normal resistivity.

## Caliper Logs

Caliper logs provide a measurement of the diameter of the borehole and are useful in determining changes in borehole diameter that can be related to drilling techniques, cavernous formations, lithology, and well construction. The Century model no. 7074 three-arm caliper probe used in this study records an average diameter measured by the three arms. The caliper is calibrated by performing a two-point calibration on short sections of pipe where diameters are larger and smaller than the borehole sizes that are expected to be encountered.

## Fluid Resistivity Logs

Fluid resistivity logs provide a record of the capacity of the borehole fluid to conduct electrical current (Keys, 1990). Changes in fluid resistivity are measured by ring electrodes inside a housing that allows borehole fluid to flow through it. Best fluid resistivity logging results are achieved when logging downward into boreholes containing ambient water that has had sufficient time to stabilize. Ideally, fluid resistivity logs are run as the first logging run to record the ambient conditions before other probes have passed through the borehole and vertically mixed the borehole fluid. Curve deflections on the fluid resistivity log can indicate horizontal or vertical flow, stratification of borehole fluid, or screened intervals in cased wells. The fluid resistivity values also can be used in calculations with other logs. The reciprocal of fluid resistivity, fluid conductivity, is shown on the logs in this study for comparison to specific conductance values collected at springs. The fluid conductivity values contained in the logs for this study are the values recorded at the ambient borehole temperature and are not corrected to a standard temperature. A Century model 8044 multiparameter E-log probe was used to log fluid resistivity on uncased (open) boreholes, and the Century model 9042 probe was used to measure fluid resistivity in cased wells. Calibration of the fluid resistivity logging probes was done with solutions of known conductivity in a two-point calibration.

## Acoustic Velocity Logs

Acoustic velocity logs record the travel time of pulsed acoustic waves from a transmitter to one or more receivers. The acoustic pulse travels through the fluid in the well and through the surrounding rock at a velocity that is related to the lithology and porosity of the rocks (Keys, 1997). Consequently, the well must be filled with mud or water to transmit the acoustic energy to the borehole wall. The acoustic velocity probe must be centered with bowspring or rubber centralizers to keep the travel path of the acoustic energy at a consistent length. The Century model 9320 acoustic probe uses a single transmitter and dual receiver system for recording the travel times through the formation. The receivers are spaced at 0.6 and 0.9 meter from the transmitter; therefore, a 0.3-meter calculation can be made to measure this interval transit time (delta-T) in microseconds per meter (or foot).

The acoustic wave train received by the two receivers can be divided into several components; the most important are the compressional (P) waves and shear (S) waves. P waves have particle movement in the direction of propagation and have a lower amplitude and higher velocity than S waves. S waves have particle movement perpendicular to the direction of propagation (Keys, 1997). S waves have a velocity about one-half of that of P waves (Keys, 1997). Generally, acoustic velocity logs record the travel time of the P waves, or the first arrival of amplitude. The Century acoustic logging system contains a full analog-to-digital conversion of the receiver signals. The processor then scans the sampled data for the first negative arrival below a preset threshold for each receiver and calculates the travel time in microseconds per meter (or foot) (Century Geophysical Corp., 2006). Acoustic logging data are subject to many sources of error such as large or irregular borehole diameter, poor centralization,

cycle skipping, and unsaturated or highly unconsolidated formation material. In cycle skipping, the waveform first arrival at the far receiver might be too weak to be detected, and the acquisition program triggers on a later cycle in the waveform. When this happens, the recorded travel time is greater by the amount of time between the first peak on the far waveform and the peak that is actually detected.

For rocks with uniformly distributed, intergranular-pore spaces, porosity can be derived from the Wylie time-average equation (Wylie, 1963) or the Raymer-Hunt Formula (Raymer and others, 1980). This is usually very difficult in fractured carbonate rock.

## Full-Waveform Logs

Full-waveform logs, which are sometimes collected simultaneously with acoustic velocity logs, show the waveform of the received acoustic signal. The most common presentation of the full-waveform log is the variable intensity log (VIL). On a VIL, the intensity of the trace is modulated with the acoustic signal so that a zero-amplitude signal shows a gray area on the log; a very strong negative signal shows a white area on the log, and a very strong positive signal shows a darker area on the log (Hearst and others, 2000). A common application of a VIL is a qualitative indicator of rock properties in the vicinity of the borehole (Hearst and others, 2000). In unfractured rock, this display represents the waveforms as a series of parallel wavefronts. The wavefronts become less distinctive for zones where seismic velocities vary. Nonvertical fractures intersecting the borehole produce large discontinuities for wave-energy propagation along the borehole (Paillet, 1991). Studies indicate that a relation exists between fracture permeability and attenuation of the part of the waveform with a velocity about equal to that of the fluid in the borehole (Paillet, 1991). Waveforms display several “modes” or propagation patterns; however the attenuation and permeability correlation primarily applies to the tube-wave mode (Paillet, 1991). The tube-wave is a guided-wave mode associated with the same interface mode of propagation as the Stoneley wave known to exist between a fluid and an elastic solid (Biot, 1952; Paillet, 1991).

## Acoustic Televiewer

The acoustic televiewer (ATV) is an oriented logging device that can provide a high-resolution, 360-degree image or “cylindrical picture” of the circumference of the borehole that can be used to evaluate secondary porosity features such as fractures and solution openings. The ATV image shows the borehole-fracture intersection by scattering acoustic energy such that the location of a fracture or other opening appears as a dark line on the ATV log display (Paillet, 1991). The vertical interval over which the fracture intersects the borehole is used to determine the orientation of a fracture, and the width of the fracture image in the ATV image is a qualitative indicator of fracture aperture (Paillet, 1991). Furthermore, the ATV image also can be used to calculate the strike and dip of planar features such as fractures and bedding planes (Keys, 1997); however, the depth of the fracture into the well bore cannot be determined using this method.

## Electromagnetic Flowmeter

The EM flowmeter measures the vertical flow rate and direction in a borehole using the principal of Faraday’s Law of EM Induction (Century Geophysical Corp., 2006). The EM flowmeter probe consists of an electromagnet and two electrodes 180 degrees apart and oriented 90 degrees to the magnetic field inside a hollow cylinder or tube. The voltage induced by a conductor moving at right angles through the magnetic field is directly proportional to the velocity of the conductor (water) through the field (Century Geophysical Corp., 2006). Generally, when using the tool to measure low-velocity flow, rubber diverters direct the water flow through the tube, which is open at both ends, instead of around the tool. Because the diameter of the tube and voltage response is calibrated, the volume of flow is instantaneously recorded. The direction of water flow is determined by the polarity of the response; upward flow is positive and downward flow is negative.

Blank Page

# Appendix 2—Detailed Descriptions of Geophysical Logs

Blank Page

## Western Embankment Piezometers

Seven piezometers along the western embankment (LA–12L, LA–11, LA–10, LA–16L, LA–15, LA–8L, and LA–7) were logged through casing using borehole geophysical methods in March 2006. The open boreholes were logged at the time of drilling in 1995 by the Mexico Section, International Boundary and Water Commission (MxIBWC). Selected logs run in open boreholes in 1995 were digitized and are presented with 2006 logs (appendix 3) as denoted in log headers of western embankment piezometers only.

### Piezometer LA–12L

Piezometer LA–12L is near the toe at of the dam on the western embankment (fig. 2A) and extends about 50 meters below land surface datum (LSD). The well is constructed of polyvinyl chloride (PVC) casing to a depth of 43 meters and is screened from about 44 to 50 meters below LSD. The log data collected on March 8, 2006, by the U.S. Geological Survey (USGS) include natural gamma, induction resistivity and conductivity, and fluid conductivity. Open borehole geophysical log data were collected in 1995 at the time of drilling by MxIBWC and include caliper, natural gamma, gamma-gamma (density), and neutron. The geophysical log plots for this well are in appendix 3 and include logs run in 2006 and 1995 and a lithologic description translated from the MxIBWC drilling logs (Paul Gibson, U.S. Section, International Boundary and Water Commission, written commun., 2006).

The natural gamma logs collected at the time of drilling in 1995 and the natural gamma log recorded through casing during this study are considerably different, probably because of bentonite or other clay material used in the well completion and grouting. The 2006 natural gamma shows a greater count rate than the log run in open hole in 1995 from near-surface to about 42.5 meters below LSD. However, the two natural gamma logs do show a correlation of clay or shale layers near 8, 12, 16, 21, 24.5-25, and 32 meters below LSD. The presence of clay material in the grout could have affected the induction conductivity and resistivity. Another log artifact derived from well construction is the slight deflection of induction conductivity/resistivity and fluid conductivity curves about every 3 meters throughout the well. This response likely is caused by conductive material (possibly pipe-thread compound) used in the joints of casing sections. The induction resistivity and conductivity logs show about 150 ohm-meters, except for the previously mentioned casing joints and shale zones at about 16 and 4–9 meters below LSD, which show slightly lower resistivity/higher conductivity measurements. The lack of deflection of resistivity and conductivity measurements deeper than 9 meters below LSD possibly could be caused by grout in the annular space shielding the formation.

The neutron log is an indicator of the presence of hydrogen (Keys, 1990), which absorbs neutrons and reduces the neutron count rate. The neutron log for LA–12L was run in open-hole conditions in 1995. Increased count rates are shown on the neutron log at 3–6, 7.5–8.5, and 18.5 meters below LSD because of shale beds at those depths. The neutron log shows relatively low count rates from 20 meters to the bottom of the borehole compared with the upper part of the borehole. However, slightly increased count rates are at 27–28, 29.5–32, 37–42, and 44.5–48.5 meters below LSD, which also is coincident with lower natural gamma responses, indicating a more pure limestone lithology at those depths. Possible zones of increased water content in the formation are at 24–27, 32–36.5, and 41–44 meters below LSD.

The fluid conductivity log (appendix 3) indicates a sharp increase in conductivity at 44.1 meters below LSD, indicating the screened interval from that depth to the deepest point reached during the 2006 logging at about 45.1 meters below LSD. The difference between the 2006 logged depth of 45.1 meters below LSD and the well completion record depth of 47 meters below LSD could indicate about 3 meters of fill in the bottom of the well.

### Piezometer LA–11

Piezometer LA–11 is about 141 meters southeast of piezometer LA–12L on the western embankment (fig. 2A) and extends about 20 meters below LSD. The well is constructed of PVC casing to a depth of 16.25 meters and is screened at about 16.25–18 meters below LSD. The log data collected on March 8, 2006, by USGS include natural gamma, induction resistivity and conductivity, and fluid conductivity. Open borehole geophysical log data were collected in 1995 at the time of drilling by MxIBWC and include caliper, natural gamma, gamma-gamma (density), and neutron. The geophysical log plots for this well are in appendix 3 and include logs run in 2006 and 1995 and a lithologic description translated from the MxIBWC drilling logs (Paul Gibson, U.S. Section, International Boundary and Water Commission, written commun., 2006).

Natural gamma log peaks generally correlate with shale and clay on the lithology log provided by MxIBWC (Paul Gibson, U.S. Section, International Boundary and Water Commission, written commun., 2006) and correlate well with the induction resistivity and conductivity logs and neutron log at 3.5–8 and 14.3–15.3 meters below LSD. Decreased neutron count rate and decreased natural gamma count rate at 8–9, 12–13, and 16.8–17.8 meters below LSD are interpreted as possible zones of increased water content in the formation.

The fluid conductivity log indicates a sharp increase in conductivity at 16.3 meters below LSD, indicating the screened interval from that depth to the deepest point reached during the 2006 logging at about 18.5 meters below LSD.

## Piezometer LA–10

Piezometer LA–10 is about 286 meters southeast of piezometer LA–12L on the western embankment (fig. 2A) and extends about 15 meters below LSD. The well is constructed of PVC casing to a depth of 12 meters and is screened at 12–14 meters below LSD. The log data collected by USGS include natural gamma and induction resistivity and conductivity. Open borehole log data were collected at the time of drilling in 1995 by MxIBWC and include caliper, natural gamma, gamma-gamma (density), and neutron. The geophysical log plots for this well are in appendix 3 and include logs run in 2006 and 1995 and a lithologic description translated from the MxIBWC drilling logs (Paul Gibson, U.S. Section, International Boundary and Water Commission, written commun., 2006).

The natural gamma log (2006) shows two zones of increased counts per second at 2.8–3.4 and 10.5–11 meters below LSD that correspond to shale beds in the lithologic descriptions and zones of decreased count rates on the neutron log. Neutron count rates also are decreased somewhat at 3.5–4.5 and 12.7–14 meters below LSD, intervals that correspond to weathered limestone zones. These intervals of decreased neutron count rates that likely contain higher amounts of hydrogen (Keys, 1990) also show decreased gamma count rates and are assumed to be water-bearing zones in the limestone. There is little resistivity variation on the induction resistivity log; most of the log shows greater than 100 ohm-meters except for the interbedded shale zone at 2.5–3.5 meters below LSD, where the resistivity decreases to less than 100 ohm-meters. The 2006 induction log also shows a slight deflection of induction conductivity/resistivity about every 3 meters throughout the well, which probably is an artifact of well construction. This response is similar to that in LA–12L and likely is caused by conductive material (possibly pipe-thread compound) used in the joints of casing sections. The 1995 caliper shows a constant diameter of about 6 centimeters in the initial borehole. The well currently (2006) has a screened interval at a depth of about 12–14 meters, as shown by the fluid conductivity log. The logging tools reached the deepest point at about 14 meters below LSD during the 2006 logging.

## Piezometer LA–16L

Piezometer LA–16L is about 189 meters east-northeast of piezometer LA–12L on the western embankment (fig. 2A) and extends about 47.5 meters below LSD. The well is constructed of PVC casing to a depth of 38.25 meters and is screened at 38.25–40.25 meters below LSD. The log data collected on March 9, 2006, by USGS include natural gamma, induction resistivity and conductivity, and fluid conductivity. Open borehole log data were collected at the time of drilling in 1995 by MxIBWC and include caliper, natural gamma, gamma-gamma (density), and neutron. The geophysical log plots for this well are in appendix 3 and include logs collected in 2006 and 1995 and a lithologic description from the MxIBWC drilling logs (Paul Gibson, U.S. Section, International Boundary and Water Commission, written commun., 2006).

The natural gamma logs collected at the time of drilling in 1995 and the natural gamma log recorded through casing during this study are considerably different, partly because of bentonite or other clay material used in the well completion and grouting. The open borehole (1995) natural gamma shows an overall lower count rate (less than 20 counts per second) than all of the other open hole natural gamma logs, the explanation for which is unknown but is likely caused by an equipment malfunction. However, both natural gamma logs show a correlation with clay and shale layers per the lithologic description (Paul Gibson, U.S. Section, International Boundary and Water Commission, written commun., 2006) from near-surface to 7.5 and about 16 meters below LSD. The presence of bentonite in the grout could have affected the induction conductivity and resistivity logs. Another log artifact of well construction is the slight deflection of induction conductivity and resistivity and fluid conductivity curves about every 3 meters throughout the well. This response likely is caused by conductive material (possibly pipe-thread compound) used in the joints of casing sections. The clay and shale layers at near-surface to 7.5 and about 16 meters below LSD also correlate with zones of decreased count rates on the neutron log. However, the shale layer described in the lithologic description (Paul Gibson, U.S. Section, International Boundary and Water Commission, written commun., 2006) at 7.5–11.5 meters below LSD corresponds with a very high neutron count rate (greater than 2,000 counts per second) and a low natural gamma count rate (in both the 1995 and 2006 logs), which are uncharacteristic of a shale lithology; but the induction conductivity log shows an increase in conductivity (and the resistivity log shows a decrease in resistivity), which indicates more clay or shale present. Below the shale layer at 15.5–16.5 meters below LSD, the neutron count rate is decreased at 21–28 and 28.5–30.5 meters below LSD, which reflects increased water content in the weathered limestone.

The fluid conductivity log indicates a sharp increase in conductivity at 38.25 meters below LSD, indicating the screened interval from that depth to the deepest point reached during the 2006 logging at about 40 meters below LSD.

## Piezometer LA–15

Piezometer LA–15 is about 225 meters south-southeast of piezometer LA–16L on the western embankment (fig. 2A) and extends about 20 meters below LSD. The well construction data contained in the drilling records indicate that LA–16L is constructed of PVC casing to a depth of 14 meters and is screened at 14–16 meters below LSD (appendix 3). The log data collected on March 10, 2006, by USGS include natural gamma, induction resistivity and conductivity, and fluid conductivity. Open borehole log data were collected at the time of drilling in 1995 by MxIBWC and include caliper, natural gamma, gamma-gamma (density), and neutron. The geophysical log plots for this well are in appendix 3 and include logs collected in 2006 and 1995 and a lithologic description translated from the MxIBWC drilling logs (Paul Gibson, U.S. Section, International Boundary and Water Commission, written commun., 2006).

The natural gamma log run in 2006 shows increased count rate at 1.75–4.5 and 11.3–12.3 meters below LSD, which correspond with shale layers on the lithology log (Paul Gibson, U.S. Section, International Boundary and Water Commission, written commun., 2006) along with increased conductivity and decreased resistivity at these depths. The increased natural gamma count rate extends from the base of the shale layer at about 12.3 meters below LSD into the top of weathered limestone above the screened interval at 13.2 meters below LSD. The neutron log (1995) shows decreased count rates in the shale layers. Below the shale layer at 11.3–12.3 meters below LSD, the neutron count rate decreases at 13.5–14.7 and 16–19 meters below LSD, indicating increased water content in the weathered limestone at these depths.

The fluid conductivity log indicates a sharp increase in conductivity at 14.8 meters below LSD, indicating the screened interval from that depth to the deepest point reached during the 2006 logging at about 16.5 meters below LSD. The screen interval indicated by the fluid conductivity log is about 0.8 meter deeper than the well completion information indicates.

## Piezometer LA–8L

Piezometer LA–8L is about 191 meters west-southwest of piezometer LA–12L on the western embankment (fig. 2A) and extends about 46.5 meters below LSD. The well is constructed of PVC casing to a depth of 40 meters and is screened at 40–42 meters below LSD. The log data collected on March 9, 2006, by USGS include natural gamma, induction resistivity and conductivity. Open borehole log data were collected at the time of drilling in 1995 by MxIBWC and include caliper, natural gamma, gamma-gamma (density), and neutron. The geophysical log plots for this well are in appendix 3 and include logs collected in 2006 and 1995 and a lithologic description from the MxIBWC drilling logs (Paul Gibson, U.S. Section, International Boundary and Water Commission, written commun., 2006).

The natural gamma log run in 2006 shows increased count rate at 10–12, 14–15.5, and 37.5–40 meters below LSD. The zone at 10–12 meters below LSD corresponds with a shale layer on the lithology log (Paul Gibson, U.S. Section, International Boundary and Water Commission, written commun., 2006). Other zones of natural gamma count rate increase do not correspond with shale layers on the lithology log (Paul Gibson, U.S. Section, International Boundary and Water Commission, written commun., 2006) and possibly could be caused by a clay-filled void (at 14–15.5 meters below LSD) and a bentonite seal (at 37.5–40 meters below LSD). The induction conductivity and resistivity logs both show erratic measurements at 14.2–15.1 meters below LSD, which probably are caused by some metal in the borehole or well construction. Another log artifact of well construction is the slight deflection of induction conductivity and resistivity logs about every 3 meters throughout the well. This response likely is caused by conductive material (possibly pipe-thread compound) used in the joints of casing sections. A zone of increased induction conductivity and decreased resistivity at 5–9 meters below LSD correlates with gravel, clay, and shale and with interbedded shale layers along with a zone of decreased neutron count rate. Other zones of decreased neutron count rate appear at 16.5–17.5, 22.4–23.5, 24.2–25.4, 28.8, and 31 meters below LSD and all occur in weathered limestone per the lithologic description (Paul Gibson, U.S. Section, International Boundary and Water Commission, written commun., 2006), which indicates possible water-bearing zones at these depths.

## Piezometer LA–7

Piezometer LA–7 is about 223 meters south-southeast of piezometer LA–8L on the western embankment (fig. 2A) and extends about 20 meters below LSD. The well is constructed of PVC casing to a depth of 14.5 meters and is screened at 14.5–16.5 meters below LSD. The log data collected on March 10, 2006, by USGS include natural gamma, induction resistivity and conductivity, and fluid conductivity. Open borehole log data were collected at the time of drilling in 1995 by MxIBWC and include caliper, natural gamma, gamma-gamma (density), and neutron. The geophysical log plots for this well are contained in appendix 3 and include logs collected in 2006 and 1995 and a lithologic description translated from the MxIBWC drilling logs (Paul Gibson, U.S. Section, International Boundary and Water Commission, written commun., 2006).

The natural gamma log run in 2006 shows increased count rate at 5–6, 7.7–8.6, and 13.2–14.5 meters below LSD, all of which correspond with shale layers on the lithology log (Paul Gibson, U.S. Section, International Boundary and Water Commission, written commun., 2006) and with increased conductivity and decreased resistivity at these intervals. The natural gamma log at 13.2–14.5 meters below LSD also is affected by the bentonite seal at that interval.

The caliper log shows increased borehole diameter at 3.5–6 and 16 meters below LSD and large and small diameter responses at 16.9–17.6 meters below LSD. These zones probably are related to karst openings or fractures in the weathered limestone. The zone at 16.9–17.6 meters below LSD is unique in that it shows an increase in borehole diameter above and below a 0.5-meter zone of borehole that is smaller than bit size. This smaller-diameter zone possibly indicates a swelling clay layer within a karst opening. The neutron-log count rate is drastically decreased in this zone, which also indicates clay or water-bearing media, or both.

## Eastern Embankment Piezometers

Geophysical logging of the eastern embankment piezometers occurred in March 2006 immediately after drilling was completed and before casing was set. One additional well on a nearby ranch was logged for a better understanding of the underlying hydrostratigraphy.

### Piezometer 105+90B

Piezometer 105+90B is the deepest of the 105+90 pair of piezometers (fig. 2B), extending about 36 meters below LSD. The borehole geophysics data collected in this well (appendix 3) include natural gamma, induction resistivity, 64N and 16N normal resistivity, lateral log, SP, caliper, casing collar locator (CCL), fluid conductivity, temperature, acoustic televiewer (ATV), and EM flowmeter measurements. Included in the well log is a 6-meter section of surface direct current (DC) resistivity for both the dipole-dipole array and reciprocal Schlumberger array. The CCL indicates that the bottom of the steel surface casing is at 3.75 m. Resistivity logs, including induction, normal, and lateral logs all show little variation in resistivity except for the zone at 16.5–21.5 meters below LSD. That zone is described as limestone and limey shale, which generally is less resistive than pure limestone. However, the natural gamma does not indicate an abundance of shale (no increased count rate) in this zone. Several zones of enlarged borehole diameter are evident on the caliper log, probably related to karstification or fracture openings in the limestone. These zones are centered at 6, 8, 12.2, 22.5, 24.5, 27.3, 27.8, and 30.5 meters below LSD. The natural gamma shows increased counts per second on all of these caliper enlargements. Increased counts probably are caused by the clay commonly contained in karst openings.

The ATV indicated several different rock units that are easily distinguished by texture. Many of these textural units correspond to the described lithologic units. Also visible in the borehole televiewer are some indications of open dissolution voids and bedding planes or low-angle fractures, many of which correspond with caliper enlargements. Some easily identifiable voids occur at 7.5–8.5, 12.2, 14.2–14.5, 15, 22.5, 24.5, 25, 27–28.7, 30.3–30.8 meters below LSD.

The EM flowmeter measurements indicate low upward (+) flow of about 0.006 liter per second (0.1 gallon per minute) over nearly the entire length of the borehole. Because the geophysical logging occurred shortly after the hole was drilled, the water level was still rising slightly during the EM flowmeter logging; however the largest increase in flow occurs at 35–33 meters below LSD (near bottom of borehole), where measurements indicate the beginning of upward flow at about 0.006 liter per second (0.1 gallon per minute). Because this flow rate appeared steady above the 35–33-meter interval, the conclusion is that the interval is contributing the flow into the borehole. The fluid conductivity curve indicates a slightly lower conductivity (fresher) fluid at the bottom of the hole, which probably is aquifer water entering the hole at the bottom and displacing slightly higher-conductivity fluid left in the hole from drilling. The temperature curve has a trend similar to that of fluid conductivity, showing a slightly lower temperature near the bottom of the borehole.

The 6-meter surface DC resistivity section superimposed on the resistivity logs indicates three discernible layers that can be observed in the dipole-dipole array. The resistivity characteristics of these layers are described in the “Eastern Embankment Investigation/Integration of Results” section of the report.

### Piezometer 105+90A

Piezometer 105+90A is about 10.7 meters below LSD and is a shallow companion to piezometer 105+90B, which is 3.5 meters southeast (fig. 2B) . The borehole was filled with fluid from the drill rig water tank to facilitate logging; however the water level could not be maintained so some logs were not run. The borehole geophysics data collected in this well include natural gamma, induction resistivity, caliper, CCL, fluid conductivity, and temperature (appendix 3). Included in the well log is a 6-meter section of surface DC resistivity for both the dipole-dipole array and reciprocal Schlumberger array. The CCL indicates

the bottom of steel surface casing at about 4 meters below LSD. The natural gamma and induction resistivity logs closely resemble those of piezometer 105+90B, showing similar natural gamma peaks at 3.3, 6, and 7.9 meters below LSD and similar induction resistivity peaks about 7–7.25 meters below LSD. The caliper log shows zones similar to those of 105+90B—increased borehole diameter at 6 and 8 meters below LSD, which indicates possible continuous openings at those depths between piezometers 105+90A and 105+90B. The coincidence of natural gamma peaks and caliper anomalies in the two wells indicates clay is present in the karst openings of both. The fluid conductivity log indicates increased conductivity of the borehole fluid compared to that of piezometer 105+90B; this likely is because the source of the borehole fluid in piezometer 105+90B was the drill rig water tank, which was filled from a local well. However, a decrease in fluid conductivity was noted at about 9 meters below LSD, which could indicate fresher inflow into the borehole from the aquifer. Both the dipole-dipole array and the reciprocal Schlumberger array for the surface DC resistivity show a single resistive layer near this well.

## Piezometer 106+00B

Piezometer 106+00B is the deepest of the 106+00 pair of piezometers and the deepest of the USGS-drilled wells, extending about 48 meters below LSD (fig. 2B). The borehole geophysics data collected in this well include natural gamma, induction resistivity, 64N and 16N normal resistivity, lateral, SP, caliper, CCL, fluid conductivity, temperature, acoustic velocity, full-waveform/variable intensity log (VIL), ATV, and EM flowmeter measurements (appendix 3). Included in the well log is a 6-meter section of surface DC resistivity for both the dipole-dipole array and reciprocal Schlumberger array. The CCL indicates that the bottom of the steel surface casing is at 4.5 meters below LSD.

Resistivity logs, including induction, normal, and lateral, all show little variation in resistivity except for the zones at 16.5–21 meters below LSD (similar to variation in logs of piezometer 105+90B) and at 10–12.5 meters below LSD, which show slight decreases in resistivity. The 64N resistivity log curve shows greater resistivity than the 16N and lateral log at the 10–12.5-meter zone, which indicates that the 16N and lateral log probably are being influenced by borehole fluid in the area of the formation closest to the borehole wall. The zone at 16.5–21 meters below LSD shows a smaller decrease in resistivity than the similarly located resistivity decrease in piezometer 105+90B, which is 3 meters from piezometer 106+00B. The lithologic description of this zone in well 106+00B does not note limey shale as does the description of the less resistant zone in piezometer 105+90B, but does note hard clay layers and a decrease in clay content with depth. The natural gamma does not indicate an abundance of shale or clay (no increased count rate) at 16.5–21 meters below LSD on either log.

A few zones of enlarged borehole diameter are evident on the caliper log, probably related to dissolution or fracture openings in the limestone. These zones are described in the “Eastern Embankment Investigation/Borehole Geophysical Log Analysis” section of the report.

The ambient EM flowmeter measurements indicate a consistent upward flow of about 0.006 liter per second (0.1 gallon per minute) from the bottom of the borehole to about 12.5 meters below LSD, where it decreases slightly. The presence of clay could be restricting flow through some of the openings.

Computer-generated virtual core analysis using the caliper and ATV data of zones not showing natural gamma peaks indicates several additional zones of fractures and or dissolution openings at 15–16, 19.7, 21–21.5, 22.5, 27.25, 34.5–35.5, 38–39, and 45.5–48 meters below LSD. The horizontal features intersecting the borehole at 22.5, 24.3, and 30.6 appear to produce discontinuities for acoustic wave-energy propagation along the borehole, creating a diagonal effect on the acoustic full-waveform VIL near these depths.

The surface DC resistivity sections superimposed on the piezometer 106+00B resistivity logs indicate three discernible layers that can be observed in the dipole-dipole array. The resistivity characteristics of these layers are described in the “Eastern Embankment Investigation/Integration of Results” section of the report.

## Piezometer 106+00A

Piezometer 106+00A is about 26 meters below LSD and is a shallow companion to piezometer 106+00B, which is 3.5 meters southeast (fig. 2B). The borehole geophysical data collected in this well include natural gamma, induction resistivity, 64N and 16N normal resistivity, lateral log, SP, caliper, CCL, temperature, acoustic velocity, full waveform/VIL, ATV, and EM flowmeter measurements (appendix 3). Fluid conductivity was not collected on this borehole because of tool malfunction. Included in the well log is a 6 meter section of surface DC resistivity for both the dipole-dipole array and reciprocal Schlumberger array. The CCL indicates that the bottom of the steel surface casing is at 4.5 m.

Resistivity logs, including induction, normal, and lateral, all show some variation in resistivity. The variations, and other characteristics of logs that provide subsurface information, are described in the “Eastern Embankment Investigation/Borehole Geophysical Log Analysis” section of the report.

Both the dipole-dipole array and the reciprocal Schlumberger array for the surface DC resistivity indicate a two-layer model near this well. The resistivity characteristics of the layers are described in the "Eastern Embankment Investigation/Integration of Results" section of the report.

## Piezometer 106+00C

Piezometer 106+00C is about 24 meters below LSD and is the third piezometer in the 106+00 transect. The well was installed 137 meters south of piezometers 106+00A and 106+00B, which are near the toe of the dam (fig. 2B). The log data include natural gamma, induction resistivity, 64N and 16N normal resistivity, lateral, SP, caliper, CCL, temperature, acoustic velocity, full-waveform/VIL, and ATV (appendix 3). Fluid conductivity was not collected on this borehole because of tool malfunction. The CCL indicates that the bottom of the steel surface casing is at 4.5 meters below LSD. This borehole was mostly dry immediately after drilling, so water was added to the borehole to facilitate logging. With water added, the borehole would only sustain a water level about 11.5 meters below LSD and would not fill above this level. Resistivity logs, including induction, normal and lateral logs all show some variation in resistivity, the most prominent of which was a decrease (in induction resistivity) at 10–13.5 meters below LSD and an increase (in 16N, 64N, and lateral log resistivity) at 13.5–16 meters below LSD.

At 10–12.5 meters below LSD, a decrease in induction resistivity and increase in natural gamma counts per second probably are associated with the large borehole diameter that likely is the result of a dissolution cavity that appears to be about 2 meters high, per the caliper log response. The increase in natural gamma counts per second from 10.5 to 12.5 meters below LSD probably is caused by the abundance of clay in the cavity, as noted in the lithologic description. This cavity also was the likely exit point of some water added to the borehole, as previously noted. The ATV shows an excellent image of the trace of the bottom of this cavity at 12.5 meters below LSD. A similar set of responses, although at a much smaller scale, occurs at 13–13.5 meters below LSD.

At 13.5–16 meters below LSD, the increases in resistivity, as shown on the 16N, 64N, and lateral logs probably are the result of unsaturated dense, limestone (as noted in the lithologic description). Immediately below the higher-resistivity zone at 16–16.4 meters below LSD, a natural gamma count increase appears to correspond to a dark trace on the ATV that probably is a horizontal opening that contains clay. This horizontal feature intersecting the borehole appears to produce discontinuities for acoustic wave-energy propagation along the borehole, creating a diagonal effect on the acoustic full-waveform VIL at 15.7–16.4 meters below LSD.

At 16.5–21 meters below LSD, the ATV image shows a vertical striped effect that possibly is the result of hammer-bit drilling impacts that caused some rugosity of the borehole wall. This borehole rugosity is a possible cause of the erratic delta-T fluctuations for acoustic velocity in this interval that likely are erroneous responses.

## Piezometer 106+00D

Piezometer 106+00D is about 21.6 meters below LSD and is the fourth piezometer in the 106+00 transect. The well was installed 275 meters south of piezometers 106+00A and 106+00B, which are near the toe of the dam (fig. 2B). The log data include natural gamma, induction resistivity, 64N and 16N normal resistivity, lateral, SP, caliper, CCL, temperature, full-waveform/VIL, and ATV (appendix 3). Fluid conductivity and acoustic velocity were not collected on this borehole because of tool malfunction. The CCL indicates that the bottom of the steel surface casing is at 4.5 meters below LSD. This borehole was mostly dry immediately after drilling, so water was added to the borehole to facilitate logging. With water added, the borehole would only sustain a water level about 13.5 meters below LSD and would not fill above this level. Resistivity logs, including induction, normal, and lateral, all show some variation in resistivity, the most prominent of which was a decrease (in induction resistivity) at 10–12 meters below LSD and an increase (in 16N, 64N, and lateral log resistivity) at 15–17 meters below LSD. The log responses from this well are very similar to those of piezometer 106+00C. The zones noted above correlate with similar zones and responses in piezometer 106+00C on the induction resistivity, 16N/64N/lateral log resistivity, natural gamma, caliper, ATV image, and VIL.

## Brite Well

The Brite well is 662 meters southwest of piezometer 106+00A and extends about 133 meters below LSD (fig. 2B). The well is cased with steel casing to a depth of 9 meters and is open to the formation below that depth. The log data collected on March 11, 2006, by USGS include natural gamma, induction resistivity, 16N/64N/lateral log resistivity, SP, caliper, acoustic travel time (delta-T), fluid conductivity, and ambient EM flowmeter measurements (appendix 3). The Brite well was drilled into the Salmon Peak and McKnight Formations in 1965 as a water well for stock use. IBWC water-level data indicate a water level of about 44 meters below LSD in July 1968, which rose to 2.71 meters below LSD in November 1969 in response to the

reservoir filling. At the time of logging on March 11, 2006, the well flowed at about 2.8 liters per second from the casing at land surface.

The natural gamma log indicates that most of the borehole is drilled through rocks containing very little shale or clay (low count rate) with the exception of scattered, thin shale layers at the following depths (in m) below LSD showing greater count rates: 5.8–6.6 (probably clay), 10.3, 25.7, 28.7, 32.3, 35, 36.2, 40–41, 44.8, 50.4, 51.6, 53.7, 56, 57.5, 69.9–76.5 (interbedded shale), 79, 80.5, 82.7, 85.7, 92.7, 94–94.5, 101–104, 106, and 113. The induction resistivity and 16N/64N/lateral log resistivity logs show slight decreases in resistivity associated with most of these shale layers. The upper McKnight Formation generally contains anhydrites, fecal pelleted packstone and organic-rich, laminated mudstone with thin layers of oyster shells, all of which can increase the natural gamma count rate. Increased count rates on the natural gamma occurred at depths below the top of the McKnight at 118.5 meters below LSD continuing to the bottom of the hole at 134 meters below LSD. The acoustic travel time (delta-T) was post-processed to reduce cycle skips and mostly varies between 147 and 197 microseconds per meter (45 and 60 microseconds per foot), which is consistent with limestone of low porosity. The acoustic velocity tool could not be lowered into the borehole past 109 meters below LSD because of an obstruction.

The caliper log shows casing to be about 17 centimeters in diameter and the bottom of casing at 9 meters below LSD. Below the bottom of casing in the Salmon Peak Formation, the diameter generally is representative of bit size, which appears to be about 22 centimeters. An interval of variable and irregularly increased borehole diameter, which probably is associated with karst evaporite dissolution or fracture-related openings, occurs in the McKnight Formation below 119 meters below LSD. Consequently, most of the flow that is moving up the borehole originates from the McKnight Formation as evident on the ambient EM flowmeter measurements, which increase from about 0.22 liter per second (upward) at 126 and 128 meters below LSD to greater than 3 liters per second (48 gallons per minute) (upward) at 121.5 meters below LSD. Also, the fluid conductivity shows a greater variability in salinity in the McKnight Formation with fluid conductivity ranging from about 1,160 to 1,190 microseimens per centimeter, possibly indicating a mixing of various sources of water in the borehole.

Blank Page

# Appendix 3—Borehole Geophysical Logs

Blank Page

Appendix 3 contains borehole geophysical logs collected March 8, 9, 11, 19, and 22, 2006, in Val Verde County, Tex., and Coahuila, Mexico. The logs collected in Coahuilla also contain some log data collected in 1995 (as marked on logs).

The log data identifiers are located at the top and bottom of each log as follows:

GAM(NAT)—natural gamma
SP—spontaneous potential
BHC-DELT—acoustic travel time or delta-T
DT—acoustic travel time or delta-T
CALIPER—borehole diameter
CCL—casing collar locator
FLUID COND—fluid conductivity at borehole temperature
TEMP—borehole temperature
Ambient flow—vertical flow in the borehole (+, upward; -, downward)
RES(16N) —16-inch normal resistivity (short normal)
RES(64N)—64-inch normal resistivity (long normal)
LATERAL—lateral resistivity
I. Res.—induction resistivity
AMP(F) (MV)—variability intensity log of acoustic amplitude of the far detector (in millivolts)
Acoustic Televiewer—acoustic televiewer (ATV) image
D-C Resistivity, dipole-dipole—surface geophysical DC resistivity (dipole-dipole array)
D-C Resistivity, rec. schl.—surface geophysical DC resistivity (reciprocal Schlumberger array)

**NOTE: All borehole geophysical logs available at** *http://pubs.usgs.gov/sir/2007/5143/5143-app.html*

Blank Page

# Appendix 4—Online Positioning User System (OPUS) Solutions of Global Positioning System Data

Blank Page

## 4–1. OPUS Base 1

```
FILE: 18200700.dat 000446317

                            NGS OPUS SOLUTION REPORT
                            ========================

      USER: U.S. Geological Survey                  DATE: March 13, 2006
RINEX FILE: 1820070u.06o                            TIME: 02:46:57 UTC


  SOFTWARE: page5  0601.10 master30.pl            START: 2006/03/11  20:13:00
 EPHEMERIS: igr13656.eph [rapid]                   STOP: 2006/03/11  23:26:30
  NAV FILE: brdc0700.06n                       OBS USED:  8000 /  8164   :  98%
  ANT NAME: TRM5800         NONE              # FIXED AMB:    42 /    42   : 100%
ARP HEIGHT: 2.250                            OVERALL RMS: 0.016(m)


 REF FRAME: ITRF00(EPOCH:2004.0000)            ITRF00 (EPOCH:2006.1915)

         X:     -1068140.677(m)   0.016(m)          -1068140.707(m)   0.016(m)
         Y:     -5455267.761(m)   0.033(m)          -5455267.763(m)   0.033(m)
         Z:      3117407.122(m)   0.012(m)           3117407.110(m)   0.012(m)

       LAT:   29 26 53.46040      0.009(m)        29 26 53.45994      0.009(m)
     E LON:  258 55 17.93172      0.010(m)       258 55 17.93064      0.010(m)
     W LON:  101  4 42.06828      0.010(m)       101  4 42.06936      0.010(m)
    EL HGT:          310.363(m)   0.035(m)               310.364(m)   0.035(m)

                        UTM COORDINATES
                         UTM (Zone 14)
Northing (Y) [meters]     3259440.074
Easting (X)  [meters]      298425.036
Convergence  [degrees]    -1.02213848
Point Scale                1.00010139
Combined Factor            0.99962747

                               BASE STATIONS USED
PID       DESIGNATION                        LATITUDE    LONGITUDE DISTANCE(m)
DH3844 TXSN SANDERSON CORS ARP             N300909.264 W1022434.121  150536.6
DG6566 TXDR DEL RIO CORS ARP               N292151.860 W1005358.200   19686.2
DH3842 TXFR FREDERICKSBURG CORS ARP        N301445.496 W0985048.428  233068.3

This position and the above vector components were computed without any
knowledge by the Instituto de Estadistica, Geografia e Informatica (INEGI)
and the National Geodetic Survey (NGS) regarding the equipment or field
operating procedures used.
```

## 4–2. OPUS Base 2

```
FILE: 59980701.dat 000446316

                            NGS OPUS SOLUTION REPORT
                            ========================

      USER: U.S. Geological Survey                  DATE: March 13, 2006
RINEX FILE: 5998070t.06o                            TIME: 02:46:41 UTC


  SOFTWARE: page5  0601.10 master28.pl             START: 2006/03/11  19:52:00
 EPHEMERIS: igr13656.eph [rapid]                    STOP: 2006/03/11  23:19:30
  NAV FILE: brdc0700.06n                        OBS USED:  8625 /  8733   :  99%
  ANT NAME: TRM5800         NONE              # FIXED AMB:    36 /    36   : 100%
ARP HEIGHT: 1.669                             OVERALL RMS: 0.016(m)


 REF FRAME: ITRF00(EPOCH:2004.0000)            ITRF00 (EPOCH:2006.1915)

         X:     -1068306.719(m)   0.014(m)          -1068306.749(m)   0.014(m)
         Y:     -5455307.685(m)   0.029(m)          -5455307.687(m)   0.029(m)
         Z:      3117277.762(m)   0.008(m)           3117277.750(m)   0.008(m)

       LAT:   29 26 48.66697      0.010(m)        29 26 48.66651      0.010(m)
     E LON:  258 55 12.17016      0.008(m)       258 55 12.16909      0.008(m)
     W LON:  101  4 47.82984      0.008(m)       101  4 47.83091      0.008(m)
    EL HGT:          308.670(m)   0.030(m)               308.671(m)   0.030(m)

                        UTM COORDINATES
                         UTM (Zone 14)
Northing (Y) [meters]     3259295.265
Easting (X)  [meters]      298267.143
Convergence  [degrees]    -1.02288401
Point Scale                1.00010218
Combined Factor            0.99958509

                               BASE STATIONS USED
PID       DESIGNATION                         LATITUDE    LONGITUDE DISTANCE(m)
DH3844 TXSN SANDERSON CORS ARP             N300909.264 W1022434.121  150481.7
DG6566 TXDR DEL RIO CORS ARP               N292151.860 W1005358.200   19754.7
DH3842 TXFR FREDERICKSBURG CORS ARP        N301445.496 W0985048.428  233268.7

This position and the above vector components were computed without any
knowledge by the Instituto de Estadistica, Geografia e Informatica (INEGI)
and the National Geodetic Survey (NGS) regarding the equipment or field
operating procedures used.
```

# Appendix 5—Parameters Used for Inversion Process of Direct-Current Resistivity Data

Blank Page

```
[Startup]
Xpos=-4
Ypos=-4
Width=1288
Height=1002
State=2
FontName=Times New Roman
FontSize=10
LastProjDir=S:\Projects\CG600_Amistad\Data\DCRes_Geophysical_Data\Processed_Data\EarthImager_110106\Line1\rSch
LastLineDir=S:\Projects\CG600_Amistad\Data\DCRes_Geophysical_Data\Processed_Data\EarthImager_110106\Line1\rSch\L1_rS_r0
LastTrialDir=S:\Projects\CG600_Amistad\Data\DCRes_Geophysical_Data\Processed_Data\EarthImager_110106\Line1\rSch\L1_rS_r0\trial1
LastDataFile=S:\Projects\CG600_Amistad\Data\DCRes_Geophysical_Data\Processed_Data\EarthImager_110106\Line1\rSch\L1_rS_r0.dat
MetersFeet=Meters
JobCodeK=Job Code
ProjSiteK=Project Site
ApprovedByK=Approved By
SurveyDateK=Survey Date
InstrumentK=Instrument
InvSoftwareK=Software
DataFileK=Data File
EmployerName=U.S. Geological Survey
JobCode=CG602
ProjSite=Amistad
ApprovedBy=Wade H. Kress
Instrument=Syscal Pro
IPUnit=0
[Initial]
MinVoltage=1
MinVoverI=1E-5
MinAppRes=1
MaxAppRes=100000
MaxRepeatErr=3
MaxRecipErr=5
RemoveNegERT=0
KeepAllData=1
ExcludeEdges=0
InvMethod=2
VerticalAxis=0
YAxis=0
MinElecSepX=0.01
MinElecSepZ=0.01
ContourLines=0
BlnAspectRatio=1
[Forward]
ForwModMeth=1
ForwSolver=0
BCType=1
ForwAccuracy=1
Anisotropy=1
ElemDivision=2
ThickFactor=1.1
DepthFactor=1.1
ForwCGIter=100
ForwCGResid=1E-6
[ResInv]
```

```
MaxNumInvIter=10
MaxRMSRes=1
MinErrReduction=5
StopOnMaxIter=1
StopOnMaxRMS=1
StopOnMinErrDiff=1
DataReweight=0
UseRecipErr=0
StopOnL2Norm=1
Lagrange=10
RoughConditioner=0.2
ResStartID=0
StartRes=97.21
MinResis=1
MaxResis=100000
ParameterWidth=1
ParameterHeight=1
HVRoughRatio=0.5
ResNoisePC=3
MaxNumIterInvCG=10
DampFactorRes=10
EpsilonD=1
EpsilonM=1
QuasiNewton=20
[IPInv]
IPInvMethod=0
MaxNumInvIterIP=8
MaxRMSIP=3
MinErrReductionIP=5
StopOnMaxIterIP=1
StopOnMaxRMSIP=1
StopOnMinErrDiffIP=0
DataReweightIP=1
StopOnL2NormIP=1
MinIP=-0.2
MaxIP=0.5
IPNoisePC=3
IPNoiseMin=-0.2
IPNoiseMax=0.5
MinIPCorr=0.5
RemoveNegIP=0
Positivity=0
LagrangeIP=10
DampFactorIP=10
IPWinStart=1
IPWinEnd=6
IPStartID=1
StartIP=0.01
[Terrain]
MeshXformMethod=0
```

Prepared by the USGS Lafayette Publishing Service Center.

Information regarding water resources in Texas is available at
http: //tx.usgs.gov/